DESIGN, FABRICATION, AND CHARACTERIZATION OF A SHAPE MEMORY POLYMER EMBOLIC DEVICE

A Dissertation

by

WON JUN HWANG

Submitted to the Office of Graduate and Professional Studies of
Texas A&M University
in partial fulfillment of the requirements for the degree of

DOCTOR OF PHILOSOPHY

Chair of Committee, Duncan J. Maitland
Committee Members, John C. Criscione
Matthew W. Miller
Roland R. Kaunas
Head of Department, Gerard L. Coté

August 2014

Major Subject: Biomedical Engineering

ABSTRACT

Shape memory polymers (SMPs) are a unique class of smart materials that can remember two shapes, and can be remotely actuated to achieve a predefined shape by application of thermal energy. Porous scaffold of SMP foams enable high volume change up to 70 times. Use of these SMP foams in a minimally invasive treatment of cerebral aneurysms is of significant interest in the biomedical community.

In the application of treating aneurysms, a spheroid SMP foam is envisioned to be compressed to a rod-like cylindrical secondary shape. The device in this secondary shape can then be delivered through a catheter to the aneurysm site and, once in the aneurysm, can be actuated to recover the primary shape to fill the aneurysmal protuberance. Blood is expected to infiltrate and clot within the porous internal structure of the expanded SMP foam, ultimately leading to complete isolation of the aneurysm from the parent artery through tissue healing.

This study reports the functional characterization of SMP foam with respect to the design and the fabrication of the prototype embolic device for treatment of cerebral aneurysms. The pressure exerted by the expanding SMP foam on the aneurysms wall during the occlusion is estimated. Frictional loads between SMP foam and a catheter pathway are investigated. This is a critical factor in the feasibility of transcatheter delivery of a SMP foam device. Porcine *in vitro* and *in vivo* aneurysm models are used to test and validate the deployment process of the proposed device. Important aspects are studied and discussed, such as deliverability through a catheter, recovery of the primary

shape by thermal actuation, and fluoroscopic visualization of the device during the delivery.

Finally, the performance of SMP embolic device, which is the endovascular delivery and the occlusion of porcine aneurysms, are compared to performance of Guglielmi Detachable Coil that is considered as the standard treatment. 90 and 180 days follow-up studies present promising healing responses of the SMP treated aneurysm. This study forms an important step towards the realization of these devices in clinical practice.

DEDICATION

To my parents, Sang-Yeol Hwang and Jung-Rye Lee

To my wife, Hyunsoo Lee and my lovely daughter, Abigail Y. Hwang

ACKNOWLEDGEMENTS

I would like to express my utmost gratitude to my PhD advisor, Dr. Duncan Maitland, for his guidance, mentorship, and patience. He gave me the opportunity to keep pursuing my dream in medical device. He allowed me to research with freedom, to find clues about problems with his patience, and grow tremendously as a scientist. I will forever be grateful to him for that.

I would like to thank my committee chair, Dr. John Criscione, Dr. Matthew Miller, and Dr. Roland Kaunas, for their guidance and support throughout the course of this research. Additionally, I would also like to thank Dr. Thomas Wilson, Dr. Jonathan Hartman, and Dr. Egemen Tuzun, Their feedback toward my research was priceless.

Thanks also go to my friends and colleagues and the department faculty and staff for making my time at Texas A&M University a great experience. I also want to extend my gratitude to the National Institutes of Health/National Institute of Biomedical Imaging and Bioengineering Grant R01EB000462.

Finally, thanks to my mother and father for their support and encouragement, to my wife for her patience and love, and my lovely daughter.

NOMENCLATURE

SMA	Shape Memory Alloy
SMP	Shape Memory Polymer
CCA	Common Carotid Artery
LCCA	Left Common Carotid Artery
RCCA	Right Common Carotid Artery
GDC	Guglielmi Detachable Coil
SAH	Sub-Arachnoid Hemorrhage
SS	Stainless Steel
CNC	Computer Numerical Control
FDM	Fused Deposition Modeling
STL	Standard Tessellation Language
TIPS	Texas Institute for Preclinical Studies
FDA	Food and Drug Administration

TABLE OF CONTENTS

LIST OF FIGURES

Page

LIST OF TABLES

Page

CHAPTER I

INTRODUCTION AND LITERATURE REVIEW

1.1 Introduction

This study proposes to develop a shape memory polymer (SMP) interventional device for treating intracranial saccular aneurysms that pose a significant threat of morbidity and mortality from subarachnoid hemorrhage by rupture. Even with recent advances in interventional techniques, the risk of rupture is still substantial.

Recently, SMPs have been proposed as an alternative material with higher strain recovery and good biocompatibility for applications of medical devices (Metcalfe et al. 2003, Maitland et al. 2007). Another type of active material, shape memory alloys (SMAs) have been broadly used in medical devices such as vascular stent and embolic coils, during the last two decades. SMAs present good biocompatibility and better stress recovery. SMPs are able to be deformed, frozen into a secondary shape, and then activated (e.g., thermally) back to the primary shape. For the application of treating saccular aneurysms, the primary shape of the SMP is a machined spheroid. The crimped secondary shape is delivered to the lesion and is then thermally actuated into its primary shape. Thus, the aneurysm is filled with open celled foam that presents a scaffold for blood clot formation. *In vivo* results (Rodriguez et al. 2014) from our group on surgically implanted foams show that the clotted foam is fully endothelialized across the neck of the treated aneurysm and that the clot on the interior of the foam is remodeled by

collagenous tissue. These preliminary *in vivo* results were observed at 30 and 90 days post implant.

This study proposes to build on the surgically implanted foam results by designing, developing and testing the first catheter delivered foam occlusion device.

The main goal of this research is to deliver a SMP embolic device into a necked swine aneurysm model. The following aims will serve to develop a pre-clinical prototype for such a device.

1. Measure two critical factors needed for the foam deployment system design: foam generated wall stresses and friction of foam in catheter.
2. Design and fabricate a SMP embolic device system. The device design will include foam mounting, heating systems, and release mechanism for the SMP foam. This aim will include an *in-vitro* test module and demonstrate the delivery and embolization of a SMP foam device in a saccular aneurysm model in all flow conditions
3. Perform animal studies by delivering and deploying SMP embolic device in the porcine animal model. This functional animal study will be supported by a follow-up study of the vasculature in the region the device deployment.

1.2 Literature review

1.2.1 Neurovascular aneurysms

Cerebral aneurysm rupture occurs in approximately 30,000 people per year in the United States, with devastating consequences. Three-fourths of patients will either die or become neurologically debilitated. The primary motivation to treat brain aneurysms is prevention of new or recurrent intracranial hemorrhage. Cerebral aneurysms account for roughly 5% of all strokes (Bederson et al. 2000, Rinkel et al. 1998, George J. Hademenos 1998, Wardlaw and White 2000). The 30-day mortality rate after hemorrhage is about 45%, with about half the survivors sustaining permanent brain damage. Some 30,000 Americans per year will suffer aneurysmal sub-arachnoid hemorrhage (SAH) (Harrod et al. 2005). Fusiform aneurysms account for approximately 10% of the SAH and large and small neck saccular aneurysms account for 50% and 40% respectively (Murayama et al. 1999a).

Cerebral aneurysms are sac like focal dilatations of the arterial wall typically found in or near the circle of Willis, the major network of arteries supplying blood to brain. A common feature of intracranial aneurysms is a significantly fragmented or degraded elastic lamina and muscular media (Toth et al. 1998, Zhang et al. 2003). However, the exact cause is still a subject of debate as the lack of cerebral elastic lamina and supporting perivascular tissue along with sparse medial elastin and structural irregularities at the apex of bifurcations are thought to render the cerebral arteries susceptible to the development of aneurysms (Finlay et al. 1998, Stehbens 1990).

Genetic factors and habits like cigarette smoking, alcohol consumption, long term analgesics and oral contraceptive might also have a role in their development (Investigators 1998, Kilic et al. 2005, Mitchell et al. 2004).

While most studies establish the rupture potential on the maximum dimension or size of the aneurysms (Ujiie et al. 1993, Wiebers et al. 2003), there is no consistent or definitive criterion to predict the rupture of aneurysms. The location of the lesion relative to the inlet flow stream seems to play an important role as it directly affects the hemodynamics and the associated mechanobiological responses of within the aneurysms (Hassan et al. 2005). These effects can directly affect the collagen production and thus wall strength (Rodriguez-Feo et al. 2005).

It is thought that an initial "insult" (i.e. damage of elastin) leads to a cascade of local restructuring via collagen turnover and deposition. The region at this time is found to experience low wall shear stresses (lower than the normal values for that region), which are thought to increase the residence time of the necrotic factors and particles that degrade the wall making it weaker and susceptible to further growth and rupture (Acevedo-Bolton et al. 2006). These growths and remodeling processes aide in lowering the stresses to near homeostatic values via changing the structure and material properties in the arterial wall (Humphrey and Taylor 2008).

1.2.2 Existing aneurysm treatments

Sub-arrachnoid hemorrhages from aneurysm rupture are a significant cause of morbidity and mortality. To prevent potential risk of subarachnoid hemorrhages from these aneurysms, neurosurgeons used to clip the neck of aneurysm micro-surgically. Walter Dandy reported the first successful surgical clipping of the neck of aneurysms in 1937 (Dandy 1938) (see Fig. 1. (a) (Brisman et al. 2006)). This technique, however, is a very invasive surgical opening through the skull and is associated with neurologic risk and prolonged recovery. In addition, there are limitations of difficulty to access aneurysm and high risk of vessels damage near aneurysm.

In the early 1970, a Russian neurosurgeon, Fedor Serbinenko, first described endovascular treatment of intracranial aneurysm (Serbinenko 1971, 1974). He used implantable latex balloons to occlude or deconstruct the parent vessel and aneurysm. The lack of manufacturing technology for mirco-guidewire made accessing the aneurysm lesion via a catheter a challenge. In addition, incomplete conformation to the irregular shape of aneurysms did not result in full occlusion of the aneurysm and thus led to a "water-hammer effect" of pulsating blood flow on the aneurysm-balloon system (Kwan et al. 1991). Because of recent technological advances, the detachable silicone balloon system took off market in 2003.

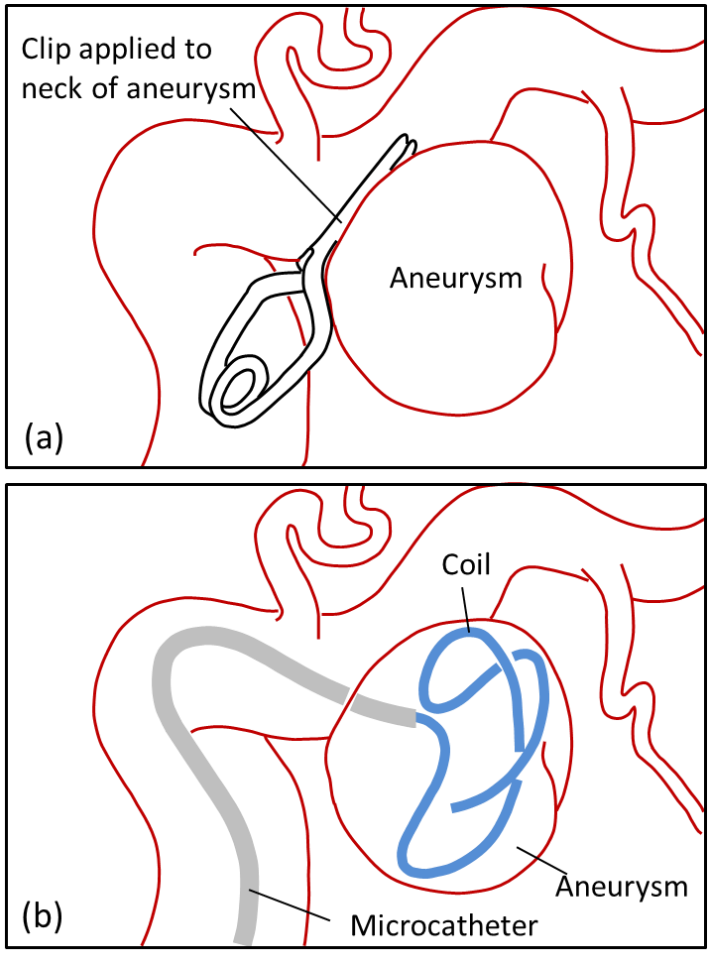

Figure 1 Aneurysm treatments (a) the application of the clip blade to the neck of the aneurysm. (b) the beginning of the coil deployment in the aneurysm. Adapted from Brisman et al. (Brisman et al. 2006)

In the 1991, Guido Gulielmi, a neurosurgeon from Italy, and Ivan Septka, an engineer at Target Therapeutics, Inc, and BOSTON Scientific, developed endovascular coil embolization with "pushable" platinum coils called Guglielmi detachable coils (GDCs) (Guglielmi et al. 1991a, Guglielmi et al. 1991b) (See Fig. 1. (b)(Brisman et al. 2006)). After FDA approval of GDCs in 1995, endovascular coiling treatments became more common and significantly improved the treatment of intracranial aneurysms. A variety of modified coils and other novel devices and treatments have been proposed since the FDA decision (Ahuja et al. 1993, Kallmes et al. 1998a, Murayama et al. 1999b, Murayama et al. 2002, Tamatani et al. 1997), such as the balloon-assisted coil, flow-diversion devices (Kallmes et al. 2007, Lylyk et al. 2009, Szikora et al. 2010, Fiorella et al. 2008, Fiorella et al. 2009, Leonardi et al. 2008, Appelboom et al. 2010), open- and closed-cell stent designs (Ionita et al. 2008, Ionita et al. 2009, Biondi et al. 2007, Liang et al. 2010, Lubicz et al. 2009, Fiorella et al. 2006), bioactive and coated coils (Gunnarsson et al. 2009, Gaba et al. 2006, Geyik et al. 2010, Bendszus et al. 2007, Veznedaroglu et al. 2008, Wakhloo et al. 2007, Hirsch et al. 2007) and embolic materials (Piske et al. 2009, Molyneux et al. 2004, Cekirge et al. 2006).

Although coiling methods have improved the available treatment options on intracranial aneurysms, some limitations have been reported. For instance, based on the coil delivery technique, there is approximately 1–5% chance of intraprocedural rupture (i.e., the rupture of aneurysms during endovascular coil embolization) (Brisman et al. 2006, Murayama et al. 2003, Tummala et al. 2001, Cloft and Kallmes 2002, Brisman et al. 2005, Henkes et al. 2004, Brilstra et al. 1999). In addition, the occlusion of less than

50% of the aneurysm volume (Horowitz et al. 1997, Kallmes et al. 1998b), coil compaction, shifting, and possible migration of the coil out of the aneurysm can cause risks of aneurysm re-growth, rupture, or stroke (Choudhari et al. 2007, Willinsky 1999).

1.2.3 Shape memory polymer foams

Shape memory polymers (SMPs) are a class of polymeric materials that can be formed into a specific primary shape, deformed into a stable secondary shape, and then controllably actuated (e.g., via temperature) to recover the primary shape. SMPs have recently demonstrated significant potential to medical devices and applications (Lendlein and Langer 2002, Maitland et al. 2009, Liu 2003, Bertmer et al. 2005, Maitland et al. 2007, Small et al. 2007, Small et al. 2010). In 2009, U.S. Food and Drug Administration (FDA) approved the first SMP-based medical device (SMP shoulder suture anchor), developed by MedShape Solutions (Melkerson 2009).

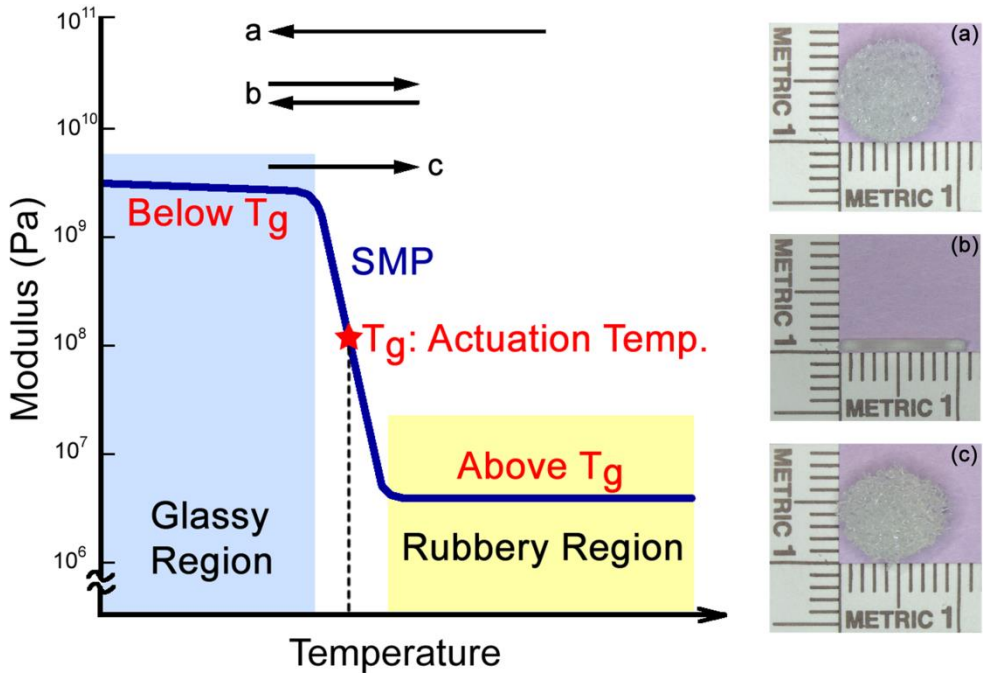

Figure 2 Description of the thermally actuated shape memory behavior in SMP foam. The foam is first fabricated into (a) its primary shape (e.g., 8-mm-diameter sphere) and then crimped, above the actuation temperature (i.e., the glass transition temperature *T*g), into (b) its temporary shape (e.g., 1-mm-diameter cylinder). The foam is cooled to below the *T*g to lock in the crimped configuration. Upon again heating through the *T*g, the foam returns to (c) the original, primary shape. Reprinted with kind permission from Springer Science + Business Media: Biomechanics and modeling in mechanobiology, Estimation of aneurysm wall stresses created by treatment with a shape memory polymer foam device, Volume 11, 2012, Page 715-29, Hwang, W., Volk, B.K., Akberali, F., Singhal, P., Criscione, J.C., Maitland, D.J., 1, © Springer-Verlag 2011

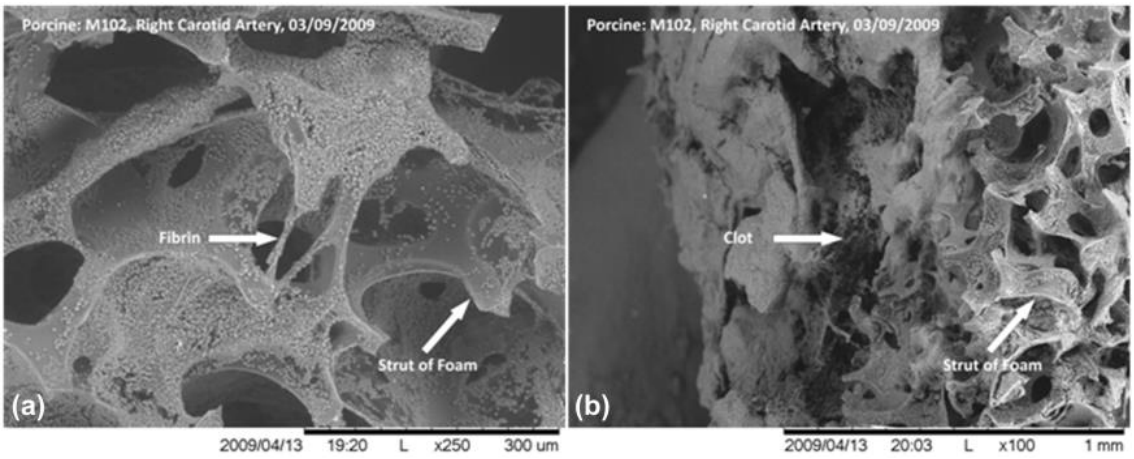

Figure 3 SEM Images of SMP foam interfaced with blood in porcine vein-pouch aneurysm (Maitland et al. 2009). (a) Blood and foam interface, 250X magnification. Red blood cells are adhered over the surface of the SMP. (b) foam and clot interface, 100X magnification. SEM Images of SMP foam interfaced with blood in porcine vein-pouch aneurysm. Maitland, D.J., Small IV, W., Singhal, P., Hwang, W., Rodriguez, J.N., Clubb, F., Wilson, T.S., Design and Realization of Biomedical Devices Based on Shape Memory Polymers, Material Research Society Symposium, Volume 1190, Issue NN06, Page 11, reproduced with permission.

Low-density open cell structured SMP foams (Metcalfe et al. 2003, Wilson 2005) are being investigated as an alternative to embolic device of aneurysm treatments (Wilson 2005, Maitland et al. 2007). The functionality of these foams is a result of their shape memory behavior, which is broadly summarized in Fig. 2. The shape memory characteristic of the foams allows them to be crimped to a small size, delivered endovascularly, and then thermally expanded to achieve complete occlusion of the aneurysm. After the occlusion of the aneurysm, blood percolating through the porous structure produces a blood clot and foreign body reaction, which then leads to fibrosis and eventual isolation of the aneurysm from the parent vessel. Figure 3 (a) shows SMP foam promoting thromogenesis at the site of the aneurysm and Fig. 3 (b) shows blood penetrating into the foam (Maitland et al. 2009).

This dissertation aims to develop (design, fabricate, and characterize) a prototype SMP embolic device and validate the device in an animal model.

CHAPTER II

ESTIMATION OF ANEURYSM WALL STRESSES CREATED BY TREATMENT WITH A SHAPE MEMORY POLYMER FOAM DEVICE*

2.1 Introduction

Intracranial saccular aneurysms pose a significant threat of morbidity and mortality from subarachnoid hemorrhage by rupture (Schievink 1997, Wijdicks et al. 2005); thus, many research efforts aim to better understand the aneurysm's behavior and material properties (David and Humphrey 2003, Shah and Humphrey 1999, Kyriacou and Humphrey 1996, Dandy 1938, Akkas 1990, Austin et al. 1989, Hung and Botwin 1975, Simkins 1973, Ferguson 1972, Scott et al. 1972, Suzuki and Ohara 1978, Steiger et al. 1989, Abruzzo et al. 1998). These aneurysms are sac-like focal dilatations of the arterial wall that are commonly found in or near the circle of Willis, which are the major network of arteries that supplies blood to brain.

To prevent potential risk of subarachnoid hemorrhage from a rupture of one of these aneurysms, treatment methods that surgeons employ is to clip the neck of the aneurysm micro-surgically or embolize it with Guglielmi detachable coils (GDCs). After FDA approval of GDCs in 1995, endovascular coiling treatments have become more common and have significantly improved the treatment for intracranial aneurysms. A variety of modified coils have been proposed since the FDA approval (Ahuja et al. 1993,

* Reprinted with kind permission from Springer Science + Business Media: Biomechanics and modeling in mechanobiology, Estimation of aneurysm wall stresses created by treatment with a shape memory polymer foam device, Volume 11, 2012, Page715-29, Hwang, W., Volk, B.K., Akberali, F., Singhal, P., Criscione, J.C., Maitland, D.J., © Springer-Verlag 2011

Kallmes et al. 1998a, Murayama et al. 1999b, Tamatani et al. 1997). Recently, novel devices and treatments have been proposed, such as balloon-assisted coils, flow-diversion devices (Kallmes et al. 2007, Lylyk et al. 2009, Szikora et al. 2010, Fiorella et al. 2008, Fiorella et al. 2009, Leonardi et al. 2008, Appelboom et al. 2010), open- and closed-cell stent designs (Ionita et al. 2008, Ionita et al. 2009, Biondi et al. 2007, Liang et al. 2010, Lubicz et al. 2009, Fiorella et al. 2006), bioactive and coated coils (Gunnarsson et al. 2009, Gaba et al. 2006, Geyik et al. 2010, Bendszus et al. 2007, Veznedaroglu et al. 2008, Wakhloo et al. 2007, Hirsch et al. 2007), and embolic materials (Cekirge et al. 2006, Molyneux et al. 2004, Piske et al. 2009).

Although coiling methods have improved the available treatment options on intracranial aneurysms, some limitations still exist. For instance, dependent on the coil delivery technique, there is approximately 1–5% chance of intraprocedural rupture (i.e., the rupture of aneurysms during endovascular coil embolization) (Brisman et al. 2006, Murayama et al. 2003, Tummala et al. 2001, Cloft and Kallmes 2002, Brisman et al. 2005, Henkes et al. 2004, Brilstra et al. 1999). In addition, the occlusion of less than 50% of the aneurysm volume (Horowitz et al. 1997, Kallmes et al. 1998b), coil compaction, shifting, and possible migration of the coil out of the aneurysm can cause risks of aneurysm re-growth, rupture, or stroke (Choudhari et al. 2007, Willinsky 1999).

Shape memory polymer (SMP) foams are being investigated as an alternative to coils (Maitland et al. 2007). The functionality of these foams is a result of their shape memory behavior, which is broadly summarized in Fig. 2. The shape memory characteristic of the foams allows them to be crimped to a small size, delivered

endovascularly, and then thermally expanded to achieve complete occlusion of the aneurysm. The SMP foam used in this study is a polyurethane. Polyurethanes are generally considered to have good biocompatibility and are widely used in the implantable medical devices. The biocompatibility of the neat form of our materials has also been previously reported (Cabanlit et al. 2007). Volumetric expansion ratios of SMP foams up to 60X have been reported (Small et al. 2007). Tailored foams can completely fill the geometry of the aneurysm, and blood percolating through the porous structure produces a blood clot and foreign body reaction, which then leads to fibrosis and thus isolation of the aneurysm from the vascular lumen due to endothelialization at the base of the aneurysm neck similar to a successful GDC deployment case.

A critical factor in the feasibility of these foams as a treatment option is the pressure exerted by the expanding SMP foam on the aneurysm wall during deployment. Considering the aneurysm wall strength has been reported to be in the range of 700–5,000kPa (Humphrey and Na 2002; MacDonald et al. 2000), it is not expected that rupture will occur due to foam expansion (Ortega et al. 2007). As a result, SMP foams have potential to improve the treatment for aneurysms.

This work establishes a method for estimating the stresses exerted on the aneurismal wall by the expanding foam and thus assessing the possibility of aneurysm rupture during treatment. To estimate these stresses, a series of experiments are performed on an idealized cylindrical aneurysm model, and finite element simulations are performed to predict the stresses that would be experienced in an aneurysm wall during treatment. Figure 4 presents the simplification of an intracranial aneurysm to an

idealized cylindrical model. Simplification of the aneurysm allows for applying cylindrical, thin-walled pressure vessel theory to estimate the stresses.

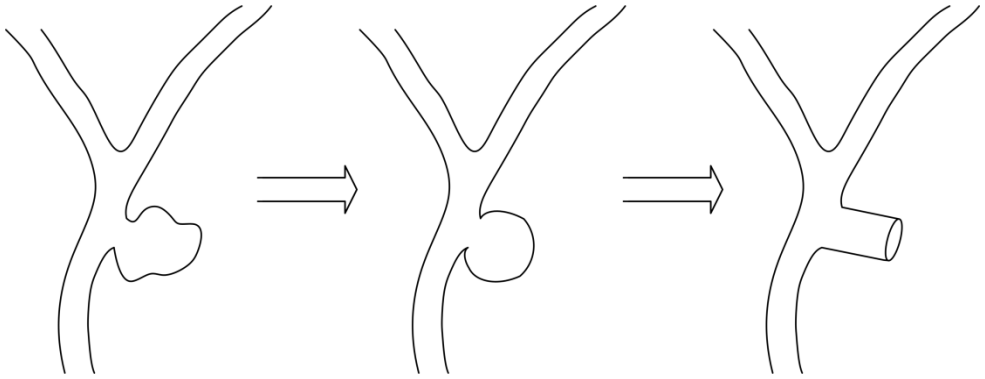

Figure 4 Schematic diagram of a saccular aneurysm near the bifurcation of an artery in the circle of Wills. Pictured is the idealization of the aneurysm into spherical and cylindrical shapes. The cylindrical model is used in the experiments and simulations performed in this work. Our cylindrical model ignores the boundary effect of distal end of the saccular aneurysm.

Due to the low modulus of the SMP foam, the cylindrical aneurysm model is fabricated using latex, which is a compliant material that can conform to the expanding foam. Oversized SMP foams are then deployed to completely fill the latex model. A pattern of makers are placed on the outer surface of the latex aneurysm model. These markers are then monitored and used to estimate the circumferential stress.

The stresses exerted by SMP foam expansion in the latex aneurysm model are not expected to be the same as in the human aneurysm model due to the difference in material properties. Before we estimate the stresses of the cylindrical human aneurysm models, mechanical and analytical solutions are used to validate the latex aneurysm finite element simulations performed using ABAQUS®. The latex material properties are obtained by performing tensile tests on dogbone specimens, and the displacement of the latex during mechanical expansion is used as input. The resulting pressure the foam exerts on the latex, calculated by ABAQUS, combined with the modulus of the aneurysm tissue is subsequently used to predict the stress that would result from deploying the foam in a cylindrical human intracranial aneurysm.

2.2 Materials

2.2.1 Shape Memory Polymer foam

The shape memory polymer (SMP) foam used in this study was composed of hexamethylene diisocyanate (HDI), N,N,N',N'-tetrakis (2-hydroxypropyl) ethylenediamine (HPED), and triethanolamine (TEA) (Wilson et al. 2007). The SMP foam, which had a glass transition temperature (*Tg)* of approximately 60°C, was cut using a biopsy punch (Sklar Tru-punchTM, Sklar Instruments) into 10-mm-long cylinders that had diameters of 8 and 6mm. Because the SMP foam has been observed to exhibit a loss of 7% in the expanded diameter during the first thermal actuation cycle (Maitland et al. 2009), it was preconditioned by performing one cycle of crimping and thermal expansion. The SMP foam was then threaded coaxially over a 0.38-mm-diameter nitinol guidewire (GUIDE-BB-10, Memry Corporation) and crimped (SC150-42, Machine Solutions, Inc.) for 10 min at 95◦C *(*±1°C*)*. This crimping process reduced the foam diameter to 1.38 ± 0.01mm for 3 samples that had an initial diameter of 8mm and a final diameter of 1.15 ± 0.01mm for 3 samples that had an initial diameter of 6mm. After crimping the foam, the temperature of the stent crimper was reduced by blowing dry house air into the machine for 2 hours. This constrained cooling process allowed the SMP foam to cool to room temperature (23 ± 1°C) and thus 'freeze' the foam in its crimped state. The crimped foam was then placed in a 6 Fr catheter, as shown in Fig. 5, in preparation for deployment in the latex model.

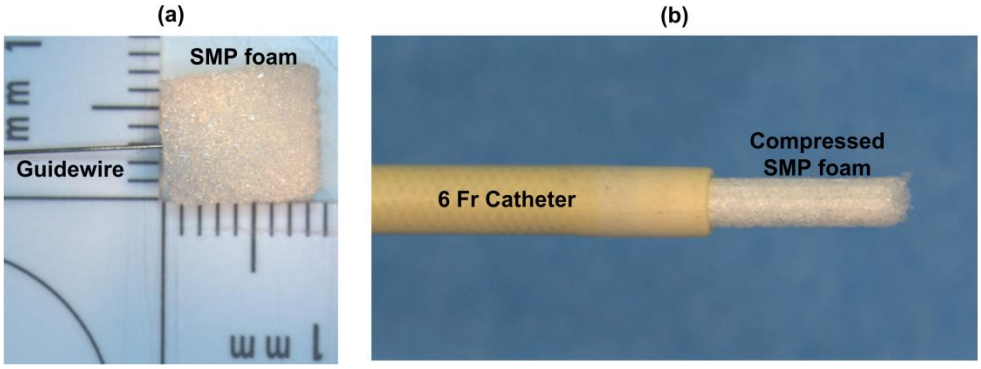

Figure 5 Photograph of the SMP foam and the corresponding delivery device. Pictured are an a 8mm diameter of cylindrical SMP foam sample with a guidewire and a b compressed SMP foam that has been passed through a 6 Fr catheter (ID=1.78mm, OD=2.00mm).

2.2.2 Latex

High ammonia natural rubber latex (Vytex®, Vystar Corporation) was used to make the aneurysm models. The liquid latex was filtered through a cone-shaped plastic mesh into a 2-oz-round glass bottle to remove all coagulation. The latex was then vortex-mixed (VM-3000, VWR International LLC) for 15–30 s, sonicated (Bransonic® 2510, Branson Ultrasonic Corporation) for 1 min, and then degassed in a desiccator (Pyrex®, Corning, Inc.) using a rotary vacuum pump (RV8 195, Labconco Corporation). The steps for preparing the liquid latex were performed at room temperature (23°C). The latex bath was then used to create both the thin-walled, cylindrical aneurysm models and the dogbone specimens for tensile testing.

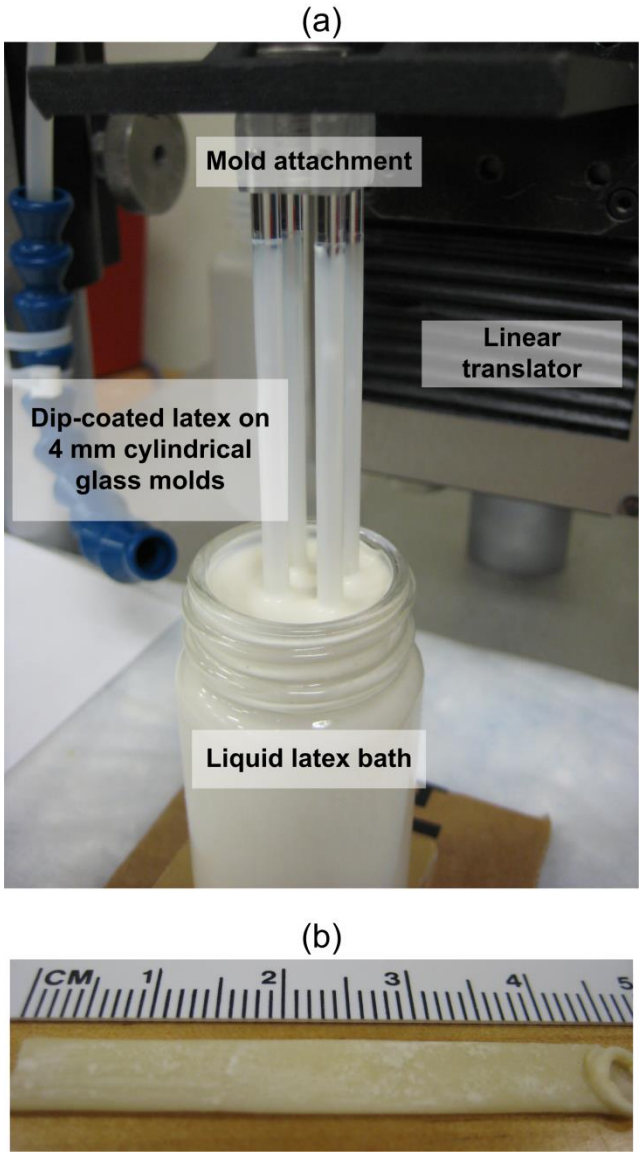

Figure 6 Photographs of a the liquid latex dip-coating system and b a resulting natural rubber latex tube. The primary components of the dip-coating system are four 4-mm glass molds, the attachment to connect the rods to the moveable platform, the linear translator, and the latex bath. A thin-walled latex tube that has been removed from the glass rod is pictured.

2.2.3 Thin-walled, cylindrical aneurysm model

The fabrication of the latex tubes (i.e., thin-walled, cylindrical aneurysm model) was based on the dip-coating technique of Neves-Junior et al. (Neves-Junior et al. 2006). Four 4-mm- cylindrical glass rods (McMaster-Carr Supply, Co.) were cleaned and dried with acetone, alcohol, distilled water, and high pressure air. The rods were then mounted in a custom-made fixture that was attached to a steel linear stage (UTM-50CC1DD, Newport Corporation). The linear stage was then translated with a motion controller (ESP3000, Newport Corporation, Irvine, California) such that the glass molds were vertically introduced into the latex bath at a constant speed of 50 mm/min, as shown in Fig. 6 (a). After dwelling in the latex bath for 30 s, the glass rods were removed at the same speed to ensure a uniform distribution of latex. The dip-coated glass rods were then air-dried for 1–2 min and subsequently cured at 50°C for 20min in an oven (1510, VWR International LLC). To increase the thickness of the latex tube, this procedure was repeated 4 more times with a minimum of 20 min provided for curing between each repetition. Before each coating, the latex bath was checked for bubbles and surface coagulations. After the fifth coat was applied, the dip-coated glass rods were cured at room temperature for 24 h.

To neutralize the tacky surfaces of the latex tube, corn starch powder was applied to the cured tube with a soft brush. The tube was then gently removed by hand from the glass rod. Care was taken to prevent excessive stretching of the latex tube and thus maintain the mechanical integrity. After 1mm of the tube was displaced from the glass rod, the removed section was coated with cornstarch to prevent the tube from sticking to

itself. This process continued until the entire inner surface of the tube was coated and removed from the glass mold. The bottom end of the tube where excess latex collected, as shown in Fig. 6 (b), was removed.

2.2.4 Dogbone specimens

In addition to forming the cylindrical aneurysm models, the latex was used to fabricate dogbone specimens for characterizing the material properties. First, a polytetrafluorethlylene (PTFE) block (McMaster-Carr Supply, Co.) was machined using a rapid prototyping mill (MDX-540SA, Roland DGA Corporation) to have a cavity of 180mm (L)×100mm (W)×1mm (D). The filtered liquid latex was then cast into the PTFE mold and cured in the oven for 24 h at room temperature. After curing, corn starch powder was applied on the surface of the latex sheet. Dogbone specimens were cut using a die (ASTM D-638 Type IV, Pionner-Dietecs Corporation).

2.3 Experimental procedures

2.3.1 Expansion of the SMP foam in the latex aneurysm model

2.3.1.1 Experimental setup

Figure 7 (a) shows the setup for the latex aneurysm model, which was placed on barbed connectors on each end. The latex tube was secured in place with non-sterile braided silk sutures (DEKNATEL® 2, Teleflex Medical, Inc.). The length of the latex tube between the barbed connections was 35mm, which was the same value for each experiment. Deionized water was injected via a syringe through the aneurysm model to verify there were no leaks and to remove the cornstarch from the inner lining of the latex tube. The cornstarch residue on the outer surface of the latex tube was removed by lightly applying water and then gently wiping with a wet tissue (Kimwipe®, Kimberly-Clark Corporation,). A micropipette (1B200-6, World Precision Instruments, Inc.) was drawn to a fine-tip through which extracted ink out of a black Sharpie® marker was used to apply the marks used for displacement tracking on the latex aneurysm model. Five groups of dots were applied on the top and along the centerline of the latex tube, as shown in Fig. 7 (b). Each group of dots consisted of five dots in a square 1-mm grid. The movement of these dots was captured on a camera (ProgRes® CF scan, Jenoptik Optical Systems, Inc.) and microscope (MX16, Leica Microsystems, Inc.), which allowed for calculating the 2D displacements of the dots.

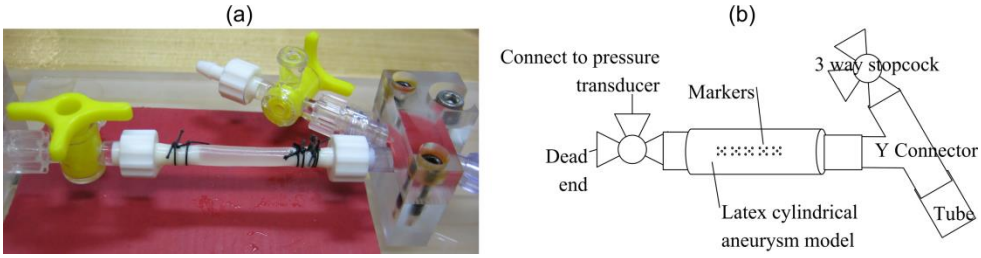

Figure 7 The cylindrical latex aneurysm model mounting stage. a Photograph of the latex aneurysm model secured to the connectors with sutures. b Schematic diagram of major components of the stage, including the connections to the pressure transducers and tubing, the latex tube, and the markers on the surface of the latex tube.

The entire aneurysm model experimental setup is shown in Fig. 8. The aneurysm chamber included the platform for the aneurysm model and the necessary connections. A y-connector was attached to one end of the platform. The y-connector allowed for both controlling the water input and also creating a pathway for the deployment of the compressed foam, which was delivered using a guiding catheter (ENVOY XB 6 Fr, Cordis Neurovascular, Inc.). The other end of the platform was connected to a pressure transducer (PX429-2.5G5V, OMEGADYNE Inc.) that correlated water reservoir height to a measure of the pressure. The water was heated to a temperature of 60°C using a water heater and pump (Tempette Junior TE-8J, Techne, Inc.), and the heated water was responsible for inducing the shape recovery of the SMP foam.

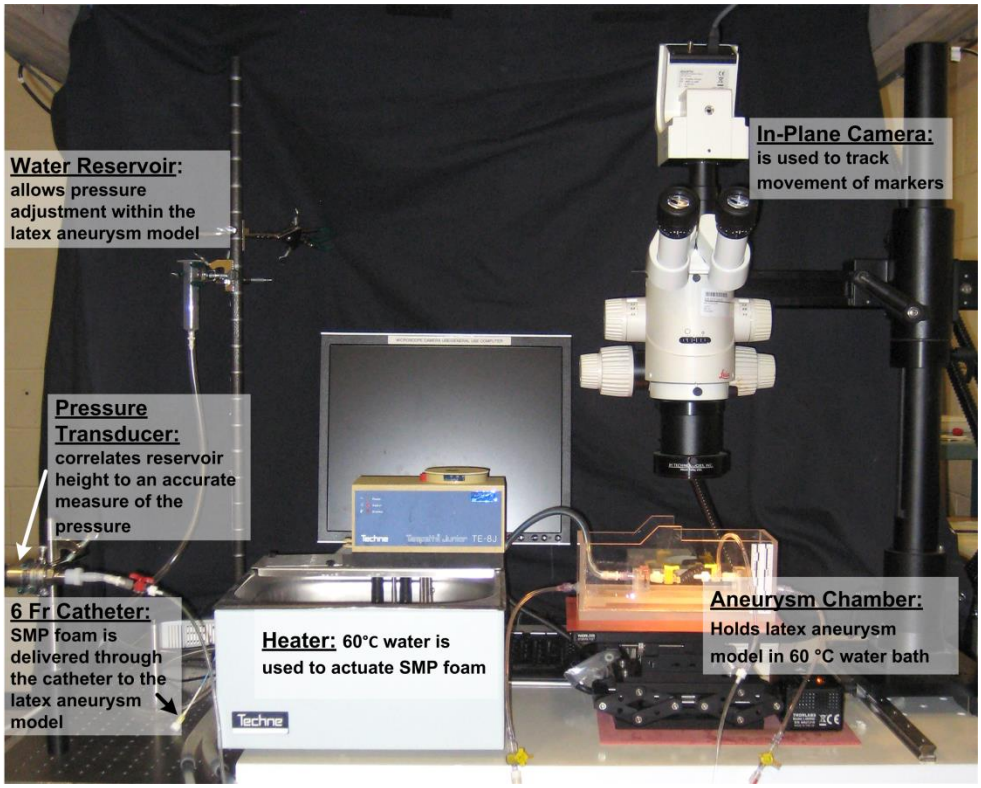

Figure 8 A photograph of the primary components of the experimental system, which consists of: a temperature-controlled aneurysm chamber, a distension system including a static water reservoir, pathways for a 6 Fr catheter pathway and a pressure transducer, and a video system for tracking the motion of markers on the surface of the latex aneurysm model.

2.3.1.2 Protocol for the deployment of the SMP foam

After the temperature of the water in the aneurysm chamber reached 60°C, the aneurysm model was pressurized by slowly increasing the height of the water reservoir that was connected to the pressure transducer. As a result, the pressure in the aneurysm model increased by increments of 3.0–3.8mmHg.To precondition the aneurysm model, the pressure was increased from 0mmHg to ~30 mmHg and then back to 0mmHg. This pressure cycle was repeated ten times. The temperature of the water in the aneurysm chamber was decreased to room temperature (23°C), and then the crimped SMP foam, attached to a guidewire (Fig. 5), was delivered through the catheter pathway to the center of the aneurysm model. The temperature of the water in the chamber was increased to 60°C, approximately the T_g of the SMP, and the SMP foam attempted to expand to its original shape, which was either 6 or 8mm diameter. Due to the constraints imposed by the latex aneurysm model, the final diameter of the foam and latex model was less than that of the original, expanded foam. After expansion was complete, the dots were again imaged to determine the resultant displacements from a single image.

2.3.1.3 Calculation of the strain in the latex aneurysm model

The tracking markers on the surface of the inflating latex aneurysm model were used to calculate the local displacement gradients and in-plane Green strain. As shown in Fig. 9, each set of five dots was decomposed into four similar triangles (Heistand et al. 2005, Humphrey 2002). The 2D deformation gradient tensor **F** was calculated using Eq. 1 (Lai 1993, Heistand et al. 2005) for each triplet by comparing the position vectors in

the current (deformed) configuration to the position vectors in the reference (undeformed) configuration. As shown in Fig. 9, the corners of the triplets were labeled with a, b, and c in the current configuration and A, B, and C in the reference configuration. The markers of the triplet were assumed to be close enough to approximate the deformation as homogenous within each marker triplet.

$$\begin{bmatrix} \Delta x_1^{(1)} & \Delta x_1^{(2)} \\ \Delta x_2^{(1)} & \Delta x_2^{(2)} \end{bmatrix} = \begin{bmatrix} F_{11} & F_{12} \\ F_{21} & F_{22} \end{bmatrix} \begin{bmatrix} \Delta X_1^{(1)} & \Delta X_1^{(2)} \\ \Delta X_2^{(1)} & \Delta X_2^{(2)} \end{bmatrix} \qquad (1)$$

where $\Delta x^{(1)}$ and $\Delta x^{(2)}$ were the differences in the current configuration positions of *a* and *b* ($x_b - x_a$) and a and c ($x_c - x_a$), respectively, and $\Delta X^{(1)}$ and $\Delta X^{(2)}$ were the differences in the reference configuration positions of a and b ($X_b - X_a$)and a and c ($X_c - X_a$), respectively. For each triplet, points A and a were taken to coincide with the vertex at the center of the five dots. After calculating the deformation gradient for each triplet, the finite 2D Green strain tensor **E** was calculated using Eq. 2 (Lai 1993),

$$\begin{bmatrix} E_{11} & E_{12} \\ E_{21} & E_{22} \end{bmatrix} = \frac{1}{2} \left\{ \begin{bmatrix} F_{11} & F_{12} \\ F_{21} & F_{22} \end{bmatrix}^{\mathrm{T}} \begin{bmatrix} F_{11} & F_{12} \\ F_{21} & F_{22} \end{bmatrix} - \begin{bmatrix} 1 & 0 \\ 0 & 1 \end{bmatrix} \right\} \qquad (2)$$

where *E*11 and *E*22 were the axial and circumferential components, respectively, and *E*12 and *E*21 were the shear components of the Green strain.

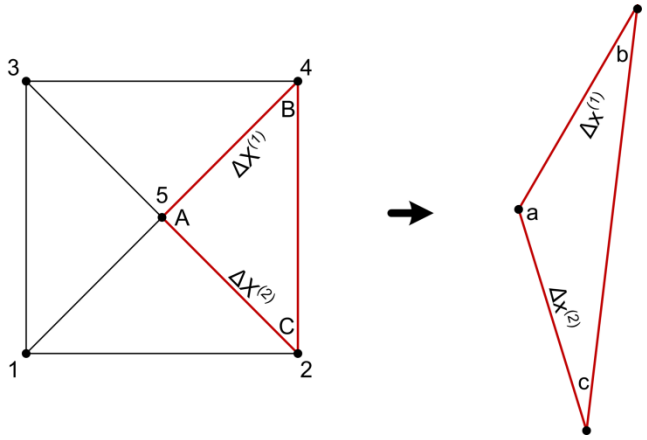

Figure 9 A set consist of 5 markers subdivided into four triplets (nodes 215, 135, 345, and 425 (highlighted)). The resulting deformation gradients are obtained from the difference of position vectors between the reference and current configurations. For each triplet, points A and a are selected to be at the center of the five-dot system. Adapted from Heistand et al (Heistand et al. 2005).

2.3.1.4 Estimation of the stress in the latex aneurysm model

The stress was estimated using 3 different methods: (1) physical, experimental estimate, (2) analytical solution, and (3) computational model. In all three methods, the deformation of the latex tube after foam deployment was the independent variable, and the stress required to produce the latex deformation was sought. For the experimental estimate, the latex tube was pressurized incrementally from 0 to 30mmHg, and Green strains were calculated from the measured deformations. Using a second-degree polynomial fit to the data, the pressures associated with the deformations of the foam deployments were estimated. The pressure values were then used to estimate the circumferential stress (hoop stress), σ_c, of the latex aneurysm model using the thin-walled, cylindrical pressure vessel formula in Eq. (3),

$$\sigma_c = \frac{pr}{t} \qquad (3)$$

where p was the pressure estimated from the regression curve, r was the inner radius of the cylindrical aneurysm model, and t was the wall thickness of the latex model.

2.3.1.5 Constitutive relation for latex model and dogbone tests

For the analytical solution and the computation model, the constitutive relation for latex was needed. We used a Mooney-Rivlin constitutive model with strain energy function:

$$W = C_{10}(I_C - 3) + C_{01}(II_C - 3) \quad (4)$$

where C_{10} and C_{01} were material-specific coefficients that were estimated from uniaxial testing of the dogbones, I_C and II_C were the first and second invariants of **C** in Eq. (5), and the material was assumed to be incompressible.

$$\begin{aligned} \mathrm{I}_C &= tr\mathbf{C} \\ \mathrm{II}_C &= \left(tr\mathbf{C}\right)^2 - tr\mathbf{C}^2 \end{aligned} \qquad (5)$$

The latex dogbones were submerged in a water bath (89032-216, VWR International LLC) at 60°C for 1 h. Each dogbone was stretched up to 150% of its original length. The preconditioning stretching was repeated ten times to simulate the preconditioning of the cylindrical samples. Tensile tests were performed on the latex dogbones to obtain the material properties that were used in the analytical solution and the finite element simulations. The experiments were performed on a single column, screw-driven, electromechanical tensile tester (Synergie 400, MTS Systems Corporation), which was accessorized with a 50N load cell (SMT1-50N-166, Interface, Inc.) and 10N spring action grips (100-033-242, MTS Systems Corporation). The tests were conducted with the specimen and grips inside a water bath (BionixMini Bath 685.07, MTS Systems Corporation) that was equipped with an additional coil heater to aid in achieving the desired temperature. The procedure for testing each of the three dogbone samples was:

- Set the load and strain to zero and mount the specimen in the grips.
- Fill the water bath and raise the temperature to 60°C. The temperature was measured by a thermocouple that was placed near the center of the latex specimen.

• Strain the specimen at a displacement rate of 50mm/min, which corresponded to the ASTM D638 standard for nonrigid polymers (ASTM Standard D638 2003).

2.3.2 Analytical solution of the stress in the latex aneurysm model

The inflation and extension of the circular tube with assumed incompressibility was a tractable boundary problem (Humphrey 2002). This problem was solved using the position vectors, in cylindrical coordinates, of the cylindrical tube in the reference (R, Θ, Z) and current (r, θ, z) configurations.

$$r = r(R),\ \theta = \Theta,\ z = \Lambda Z \qquad (6)$$

where Λ was the longitudinal stretch per unit unloaded length.

The deformation gradient tensor **F** for pure inflation and extension is

$$\mathbf{F} = \begin{pmatrix} \frac{\partial r}{\partial R} & 0 & 0 \\ 0 & \frac{r}{R} & 0 \\ 0 & 0 & \Lambda \end{pmatrix} \qquad (7)$$

Enforcing the incompressibility assumption $J = \det \mathbf{F} \equiv 1$ led to:

$$r^2 - r_i^2 = \frac{1}{\Lambda}(R^2 - R_i^2) \qquad (8)$$

where, *r* and *R* were radii in the loaded configuration and the unloaded configuration, respectively, and subscript *i* represented values corresponding to the inner-wall. The right and left Cauchy-Green strain tensors ($\mathbf{C} = \mathbf{F}^{\mathbf{T}}\mathbf{F}$ and $\mathbf{B} = \mathbf{F}\mathbf{F}^{\mathbf{T}}$,

respectively) were identical for the diagonal deformation gradient considered, and the result is presented in Eq. (9).

$$\mathbf{C} = \mathbf{B} = \begin{pmatrix} \frac{R^2}{\Lambda^2 r^2} & 0 & 0 \\ 0 & \frac{r^2}{R^2} & 0 \\ 0 & 0 & \Lambda^2 \end{pmatrix} \qquad (9)$$

The Cauchy stress was then calculated using Eq. (10).

$$\mathbf{t} = -p^* \mathbf{I} + 2\frac{\partial W}{\partial I_{\mathbf{C}}}\mathbf{B} - 2\frac{\partial W}{\partial II_{\mathbf{C}}}\mathbf{B}^{-1} \qquad (10)$$

where p^* was the Lagrange multiplier determined from boundary conditions and equilibrium in Eq. (11).

$$\begin{aligned} p^* = & \int_{r_{in}}^{r_{out}} \left(\left(\frac{2C_{10}r^2}{R^2} - \frac{2C_{01}R^2}{r^2} \right) - \left(\frac{2C_{10}R^2}{\Lambda^2 r^2} - \frac{2C_{01}\Lambda^2 r^2}{R^2} \right) \right) \frac{1}{r} dr \\ & + \left(\frac{2C_{10}R^2}{\Lambda^2 r^2} - \frac{2C_{01}\Lambda^2 r^2}{R^2} \right) \\ & - \int_{r_i}^{r} \left(\frac{2C_{10}r^2}{R^2} - \frac{2C_{01}R^2}{r^2} \right) \frac{1}{r} dr + \int_{r_i}^{r} \left(\frac{2C_{10}R^2}{\Lambda^2 r^2} - \frac{2C_{01}\Lambda^2 r^2}{R^2} \right) \frac{1}{r} dr \end{aligned} \qquad (11)$$

The material properties and values of deformation used as inputs for the analytical equations were obtained from the dogbone tensile tests and cylindrical expansion experiments, respectively. The longitudinal stretch, Λ, was obtained by

calculating the change of axial lengths in unloaded and loaded configurations. Table 1 summarizes the values of deformation used as input to the analytical equations. After solving for the Cauchy stress **t** with deformation values in Table 1 and the parameters in the Mooney-Rivlin coefficients in Table 2, the first Piola-Kirchhoff stress **P**, which was a 3D generalization of engineering stress, was calculated using Eq. (12).

$$\mathbf{P} = \det(\mathbf{F})\mathbf{F}^{-1}\mathbf{t} \qquad (12)$$

Table 1 Input parameters used to calculate the analytical solutions.

Analytical solution	Inner radius, initial (mm)	Outer radius, initial (mm)	Inner radius, final (mm)	Outer radius, final (mm)	Average axial stretch, Λ
1	2.151	2.21	2.304	2.36	0.9925
2	2.201	2.26	2.598	2.65	0.9660
3	2.211	2.27	2.384	2.44	0.9756
4	2.151	2.21	2.407	2.46	0.9925
5	2.186	2.245	2.568	2.62	0.9660
6	2.106	2.165	2.299	2.335	0.9716
7	2.151	2.21	2.209	2.265	1.0191
8	2.026	2.085	2.083	2.14	1.0021

C_{10} and C_{01} will be addressed in Table 2

Table 2 Material properties and geometries considered for the cylindrical aneurysm finite element model.

Cylindrical latex aneurysm model		Cylindrical human aneurysm		Foam	
Length	20 mm	Length	20 mm	Length	10 mm
Thickness	0.118 mm	Thickness[a]	0.0278 mm	Outer radius, initial	2 mm
Mooney-Rivlin coefficients		Elastic modulus[b]	1700 kPa	Elastic modulus	750 kPa
C_{10}	-28.97 kPa				
C_{01}	109.35 kPa				

a (Kyriacou and Humphrey 1996)
b (Steiger et al. 1989)

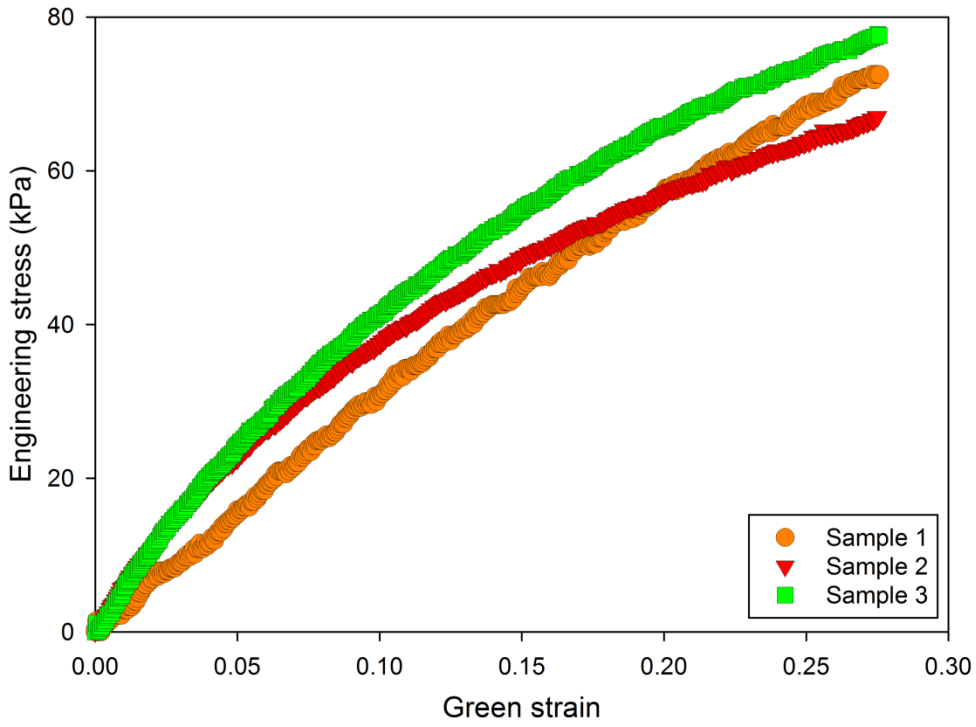

Figure 10 Stress versus Green strain (up to 0.5) for the three latex dogbone samples tested uniaxially while submerged in water at 60 ℃. The material response is observed to be repeatable between the three samples to approximately 0.20.

2.3.3 Finite element modeling of the cylindrical aneurysm

The simulations in this work were performed using ABAQUS® 6.9-EF1 finite element software. The geometry of the model was assumed to be an idealization of the experimental setup. The latex was modeled as an isotropic, 2D cylindrical shell with a length of 20mm. The thickness of the shell was chosen to be 0.118mm, which was an average of the thicknesses of the latex samples in the experimental procedure. The material properties of the latex were calculated from the tensile tests performed on the latex dogbones, of which the results were presented in Fig. 10. Using the ABAQUS® material evaluator, the average Mooney-Rivlin coefficients C_{10} and C_{01} were −28.97 and 109.35kPa.

The foam was modeled as an isotropic, solid cylinder 10mm in length and 2mm in initial outer radius. The expansion of the foam was modeled as a uniform radial displacement imposed on the boundary. This radial displacement was approximated using the outer radius of the latex, measured experimentally, before and after the expansion of the foam. Because the stress in the latex model (and not the foam) was the quantity of interest, the foam was arbitrarily modeled as a linear elastic material with an elastic modulus of 75kPa.

The latex was modeled using 2D, linear, reduced integration elements (S4R), and the foam was modeled using 3D, linear, hybrid brick elements (C3D8H). The element seed size was selected to be 0.1 for both the latex and the foam, resulting in approximately 3500 and 18000 elements, respectively. The foam was assumed to be at the center of the latex, of which the edges were assumed to be pinned. The nonlinear

geometry feature was enabled for the simulation, and the general contact feature was used to accommodate the resulting contact between the foam and the latex. Using symmetrical boundary conditions in each of the three principal directions, only 1/8th of the aneurysm model was simulated.

The finite element model was used to simulate the smallest and largest expansion cases in the 8-mm foam experiments as well as the median expansion cases for each of the four 8-mm foam experiments and the two 6-mm foam experiments. Tables 2 and 3 summarize the parameters for the finite element simulations. Table 2 presents the model geometries and material properties for the cylindrical latex and human aneurysm models. Table 3 presents the experimentally measured outer diameters before and after expansion and the resulting radial displacements for the foam for each case considered.

Table 3 Boundary conditions used as input to the finite element simulations.

Simulation	Outer radius (latex), initial (mm)	Outer radius (foam + latex), final (mm)	Radial displacement, foam (mm)	Equivalent contact pressure (kPa)[a]
1	2.21	2.36	0.242	1.9
2	2.26	2.65	0.532	3.53
3	2.27	2.44	0.322	1.95
4	2.21	2.46	0.342	2.75
5	2.245	2.62	0.502	3.5
6	2.165	2.335	0.237	2.3
7	2.21	2.265	0.147	0.75
8	2.085	2.14	0.022	0.82

[a] The equivalent contact pressure is the pressure the foam exets on the latex aneurysm model, and these values are used as input to the human aneurysm model

After simulating the foam expansion experiments in the latex system, the finite element model was used to predict the stresses that would result upon deployment of the shape memory polymer foam inside a human aneurysm. The initial radius of the simplified cylindrical aneurysm was assumed to be equal to that of the latex system (2mm), but the thickness was modified to be 0.0278mm, which was assumed to be a reasonable minimum value for a saccular aneurysm (Kyriacou and Humphrey 1996; Scott et al. 1972; Stehbens 1990; Suzuki and Ohara 1978). The aneurysmwas then modeled as a linear elastic material with a modulus of 1700kPa, which is an average value for the elastic modulus at the aneurysm fundus (Steiger et al. 1989). Rather than using the radial expansion of the foam measured in the latex experiments, the foam expansion was simulated as an applied pressure. The pressures used for these predictions were the contact pressures calculated in the foam and latex simulations. The contact pressure was the pressure that the foam exerted on the latex during expansion and was assumed to be a representation of the tendency of the foam to return to its original, expanded shape. As a result, the contact pressure was assumed to be the same value for both the latex or aneurysm systems and considered to be a more reasonable input to the aneurysm model predictions than the radial displacements measured in the latex experiments, which were dependent on the compliance and thickness of the cylindrical shell. The pressure values used for each of the eight predictions are presented as the equivalent contact pressure in Table 3.

2.4 Results

2.4.1 Calibration of pressure versus strain

Figure 11 presents the results for a test in which the latex model was inflated to pressures of 0 to 30mmHg for five cycles. The data shown represent one triplet of the center of the five groups (five nodes/marks per group). After preconditioning the sample (inflation and deflation) ten times, no correlation of the calculated circumferential strains with the cycle number is observed. Figure 11 indicates that the Green strain of a particular marker triplet is repeatable for each of the five cycles. The standard deviation of the circumferential strain varies exponentially from 0.001 at 0mmHg to 0.033 at 30mmHg for each nominal value of pressure.

2.4.2 Estimation of the stress in the latex aneurysm model

Cylindrical SMP foams, with original (uncrimped) diameters of 6 and 8mm, were deployed inside a latex aneurysm model that had an initial inner diameter of 4mm. As the water was heated to 60◦C to deploy the foam, the latex tube was also heated and became more compliant, which allowed the latex to better conform to the shape of the expanding foam. Figure 12 presents the Green strains and estimated circumferential stresses, using thin-walled, cylindrical pressure theory, for six experiments. Experiments 1–4 correspond to SMP foam samples with uncrimped diameters of 8mm, and experiments 5–6 correspond to SMP foam samples with uncrimped diameters of 6mm.

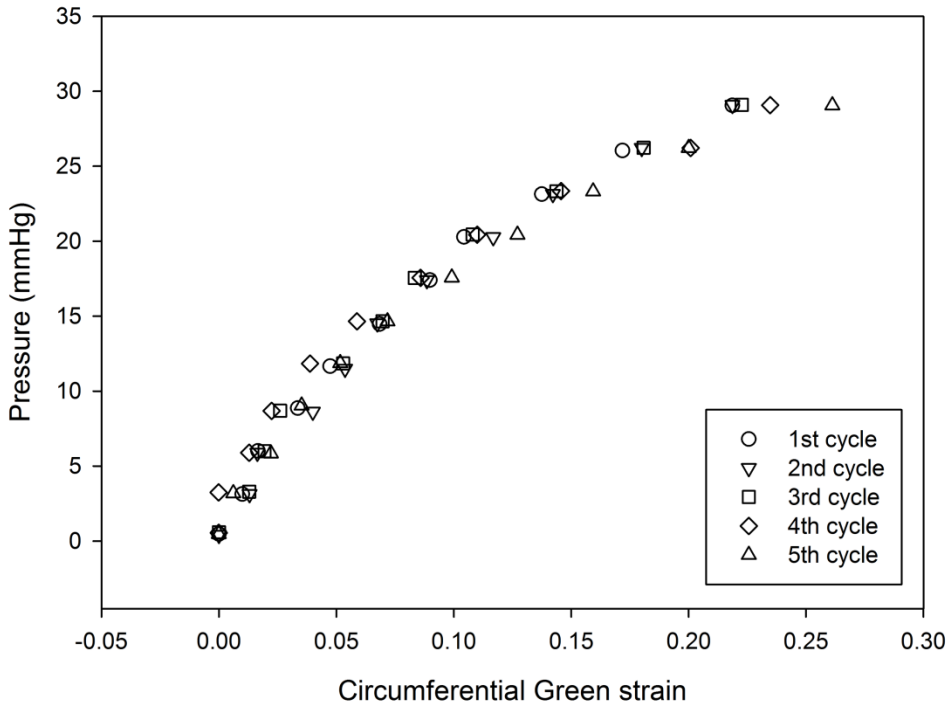

Figure 11 Five inflation cycles of a preconditioned latex aneurysm mode. The pressure versus Green strain in the circumferential direction is presented for each inflation cycle.

With the exception of experiment 2, the data from each experiment show no correlation of the pressure and strain with the location of marker sets. The maximum stress from experiments 1, 3, and 4 is 67.3 kPa at a strain of 0.22 and minimum stress is 26.04 kPa at a strain of 0.07. In these three experiments, all markers were located in the middle of the foam expansion region. Experiment 2, on the other hand, analyzed the circumferential strains near one end of expanded SMP foam, and the maximum stress is 45.59 kPa at a strain of 0.14. The minimum stress is 15.38 kPa at a strain of 0.03. For the 6mm SMP foams (experiments 5 and 6), the maximum stress is 24.3 kPa at a strain of 0.04 and the minimum stress is 2.15 kPa at a strain of 0.004. For all 6- and 8-mm foams, the pressure resulting from the expansion of foams is measured experimentally to be less than 10mmHg (6-mm foams) to 30mmHg (8-mm foams).

The difference in the stress and strain values for SMP foam samples of the same size is likely due to the heterogeneity of the foam (e.g., difference in pore cell sizes, anisotropy, etc.). As a result, the SMP foams may not be expanded uniformly inside of the latex aneurysm model, and thus, the stress distribution in each experiment might vary between each contact point (marker set) between the SMP foams and the latex aneurysm model.

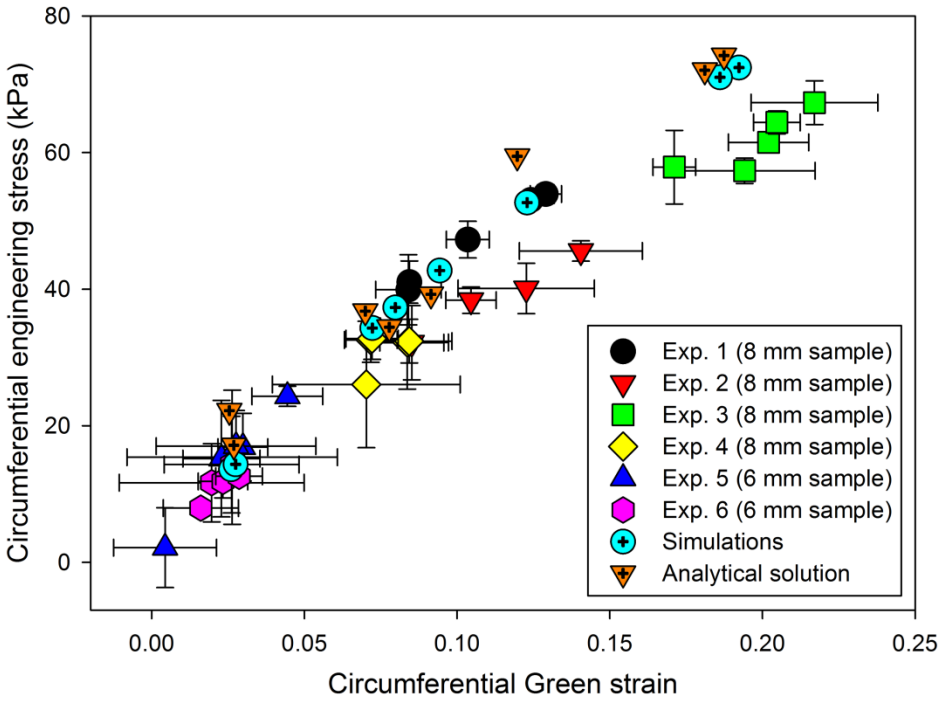

Figure 12 Circumferential stress versus circumferential strain for the analytical theory, simulations, and experimental data.

2.4.3 Analytical solution of the stress in the latex aneurysm model

The results from analytical solution for the stress exerted by the foam expansion in the latex aneurysm model are presented in Fig. 12. In this figure, the circumferential stresses are presented for the smallest and largest strains in the 8-mm foam expansion experiments as well as the median strain cases for each of the 6- and 8-mm experiments. The difference in the stresses estimated using thin-walled, cylindrical pressure theory and the analytical equations is due to the Poisson effect, which becomes non-negligible for large expansions, and is captured by the analytical solution but not by the thin-walled, cylindrical pressure theory. Specifically, for expansions resulting in large circumferential strains, the contraction of the aneurysm in the longitudinal direction results in an increase in the circumferential stress, which is captured in the analytical solutions through the variable Λ.

2.4.4 Finite element modeling

2.4.4.1 Cylindrical latex aneurysm experiments simulations

The results from simulating the foam expansion in the latex aneurysm model are presented in Fig. 12. In this figure, the circumferential stress values are presented for the smallest and largest strains in the 8-mm foam expansion experiments as well as the median strain cases for each of the 6- and 8-mm experiments. The results for the circumferential stress in the shell are compared to the stresses estimated from the experiments. It is observed that the finite element simulations have reasonable

agreement with the values calculated from both the thin-walled, cylindrical pressure theory and the analytical solutions and capture well the nonlinear stress versus strain behavior. The differences between the finite element simulations and the analytical solutions in the circumferential stresses and circumferential Green strains are 2.311 ± 4.175 (kPa) and 0.003 ± 0.002, respectively. The slight differences are primarily a result of the differences in input parameters to the analytical equations and finite element simulations. In the analytical solutions, both the longitudinal stretch and change in outer diameter, estimated from the experimentally acquired images, are used as inputs. On the other hand, the finite element simulations use the change in the final outer diameter as input and the longitudinal stretch is handled through the incompressibility condition.

2.4.4.2 Cylindrical human aneurysm predictions

In Figs. 13, 14, and 15, the predictions for the stress and strain of a cylindrical human aneurysm with reasonable material properties are presented. In Fig. 13, the stress versus strain behavior is presented for the range of pressures corresponding to the 6- and 8-mm foam expansion experiments. The stresses predicted for the human aneurysm are higher than those simulated for the latex aneurysm model because the human aneurysm has a smaller thickness (0.0278mm) compared to the latex (0.118mm) and because the linear elastic modulus of the human aneurysm is higher than the modulus of the latex. In addition, Fig. 14 presents the contour plots for the two 6-mm foam expansion cases. The maximum circumferential stress is observed in the larger expansion case (right), and the maximum value is approximately 65kPa. In Fig. 15, the smallest, median, and largest 8-

mm foam expansion cases in the first, second, and third columns, respectively. The hoop stresses, axial stresses, and resulting von Mises stresses in the cylindrical aneurysm are presented in the first, second, and third rows, respectively.

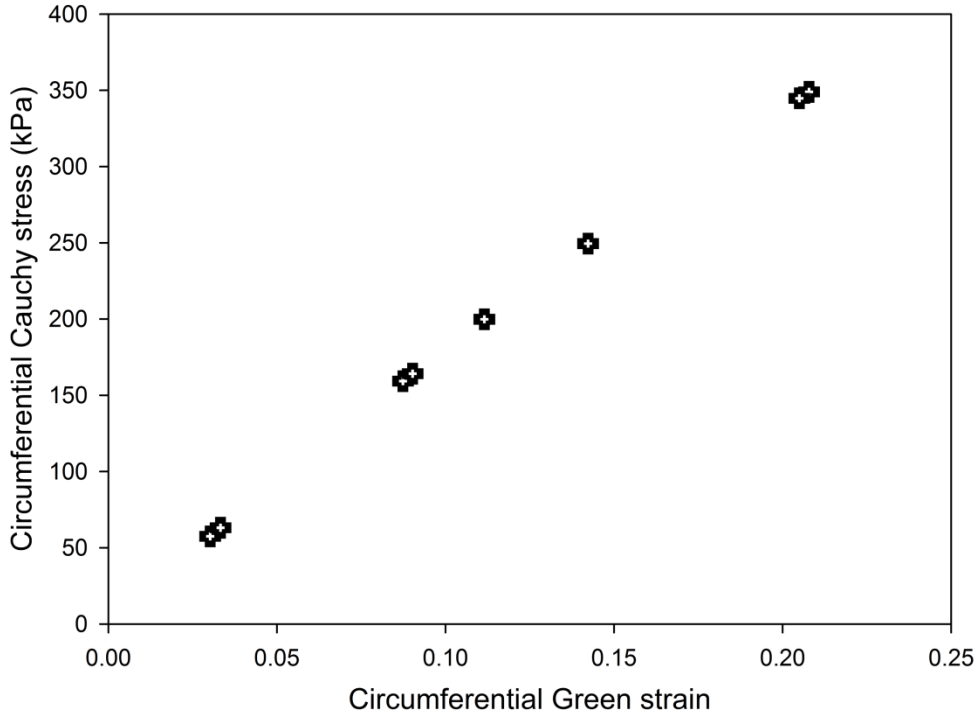

Figure 13 Finite element predictions for the cylindrical stress versus cylindrical strain in a cylindrical human aneurysm that has a thickness of 0.0278mm and an elastic modulus of 1700kPa. The input pressures used in these simulations are the results of the latex simulations shown in Fig. 12.

In addition, the spatial variation of the stresses with respect to position can be obtained from the finite element analyses. In Fig. 16 (a), (b), the circumferential stresses and von Mises stresses are presented, respectively, with respect to the longitudinal position for the largest 8-mmfoam, the smallest8-mm foam, and the larger 6-mm foam. In these analyses, the cylindrical aneurysm was longitudinally and radially constrained at 0mm, the symmetrical boundary conditions were applied at 10mm, and the equivalent pressure used to model the foam expansion was radially applied from 5mm to 10mm. From Fig. 16, it is observed the stresses are at a maximum from approximately 7–10mm—the central portions of the foam expansion. The stresses then decrease near the edge of the foam expansion, with the circumferential stress decreasing to approximately zero at a position of 3mm, and the von Mises stress reaching an approximately constant value at 4mm. This constant value ranges from 15 to 80 kPa for the larger 6-mm foam and the largest 8-mm foam cases, respectively, and is primarily a result of stretching in the longitudinal direction.

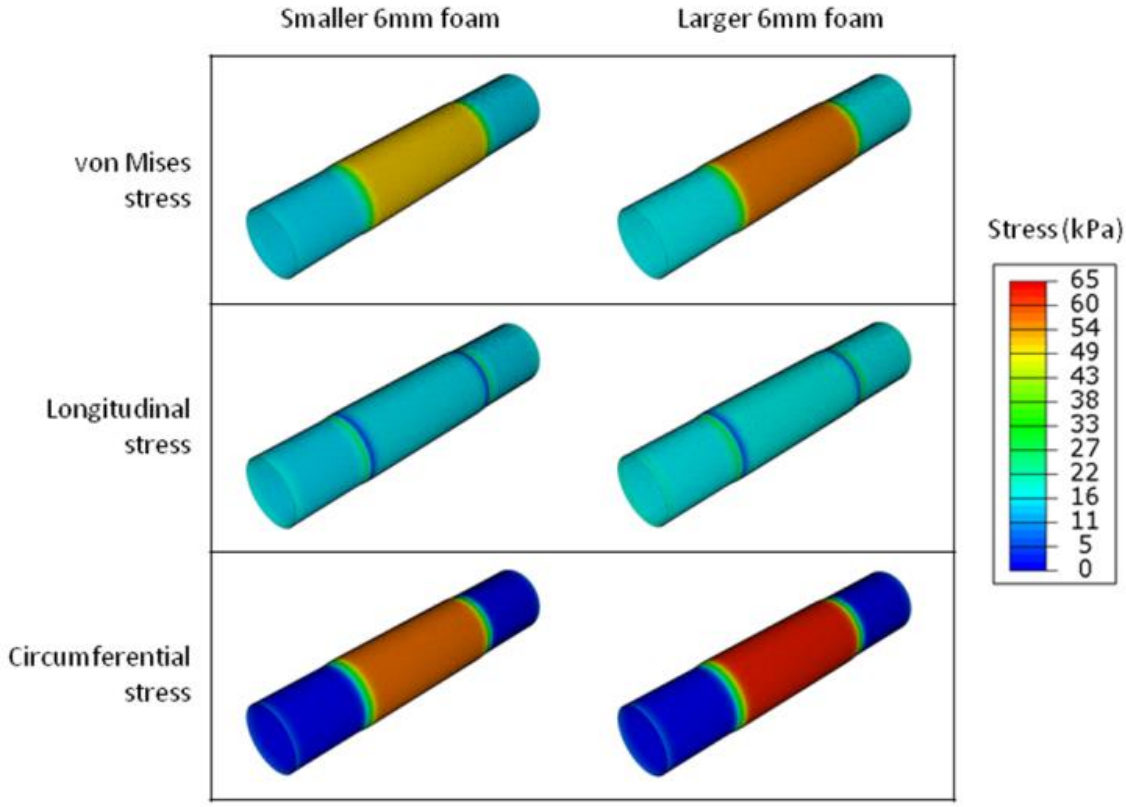

Figure 14 Predictions in the aneurysm wall for the stresses in the two 6-mm foam expansion cases. The smaller and larger of the two expansions are presented in the *left* and *right columns*, respectively. The von Mises, longitudinal, and ircumferential stresses are presented in the *first, second, and third rows*, respectively. All contours are presented with respect to the same scale, which has a maximum of 65kPa.

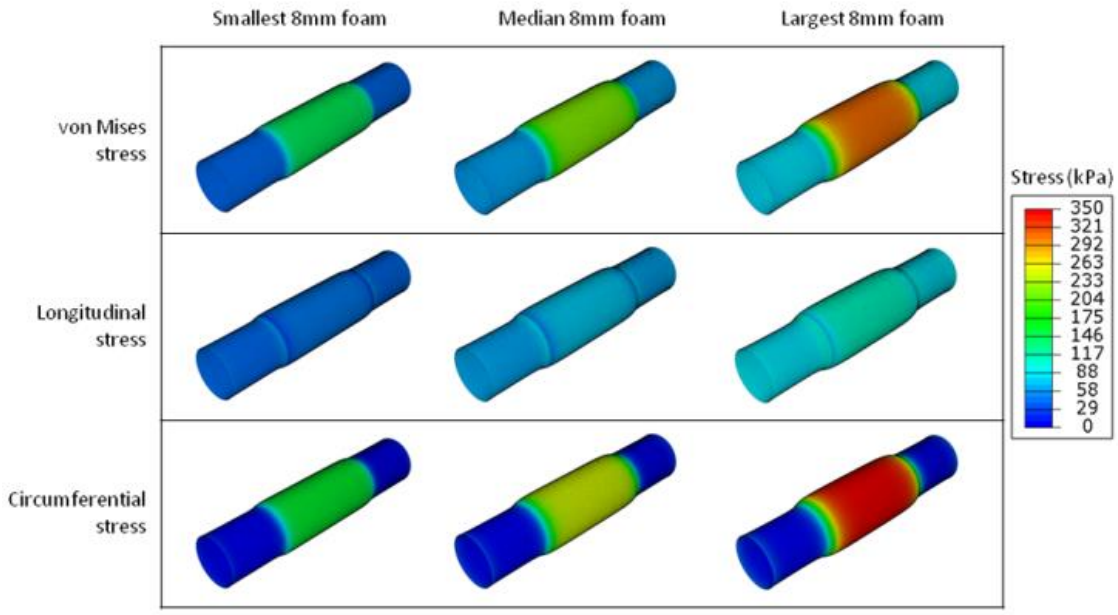

Figure 15 Predictions in the aneurysm wall for the stresses in three 8-mm foam expansions. The smallest, median, and largest 8-mm foam deployments are presented in the *first, second, and third columns*, respectively. The von Mises, longitudinal, and circumferential stresses are presented in the *first, second, and third rows*, respectively. All contours are presented with respect to the same scale, which has a maximum of 350kPa.

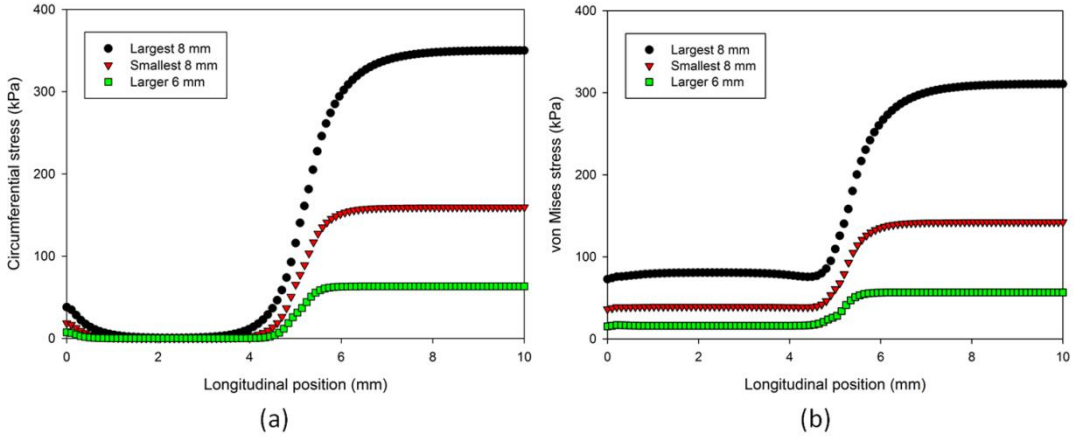

Figure 16 Predictions of the a circumferential and b von Mises stresses in a cylindrical human aneurysm for the largest 8-mm foam, the smallest 8-mm foam, and the larger 6-mm foam cases. The foam expansion is modeled as an equivalent radial pressure, applied from a longitudinal position of 5–10mm. The aneurysm is constrained longitudinally and radially at 0mm and symmetrical boundary conditions are enforced at 10mm.

2.5 Discussion

This study presented a deployment of oversized SMP foam to embolize an aneurysm. The foam, either 150 or 200% oversized compared to the diameter of the latex aneurysm model, was deployed *in-vitro*, and the displacements of the applied marker dots were used to estimate the strains in the latex, which was 0.118mm thick.

The stresses in the latex resulting from the foam expansion, estimated using thin-walled, cylindrical pressure theory, an analytical solution, and finite element simulations were all in good agreement with each other. The finite element model extended to predict the stresses in a human aneurysm considered a worst case scenario of an aneurysm wall with a reasonable minimum thickness, 1.5 and 2 times oversized embolization, and linear elastic material properties for the aneurysm wall. The maximum circumferential stress predicted in these simulations was 350kPa at a circumferential Green strain of 0.21, which was still well below threshold wall breaking stress the minimum wall breaking stresses of 700kPa (Humphrey and Na 2002, MacDonald et al. 2000).

A Mooney-Rivlin material model is ill-conceived for the determination of material response functions for latex because of a degeneracy, wherein there are many representations with the same response (Criscione 2003). However, the degeneracy of representations based on $W(I_1, I_2)$ is inconsequential for our application, a forward solution. This material model is well-recognized as one that gives accurate results for the stresses in rubber-like materials undergoing moderate strain.

It is noteworthy that this study uses a cylindrical aneurysm model instead of a spherical model, which is considered a better representation of the real human aneurysm. While providing for a simplification in the study, the cylindrical model also allows for the worst case for the circumferential stresses generated in the model from the expanding foam. The circumferential stresses of a spherical latex aneurysm using the thin-walled spherical pressure vessel can be written as $\sigma_s = \frac{pr}{2t}$, where, p is pressure, r is radius, and t is thickness. From Eq. 3, σ_s for a spherical geometry is a half of the circumferential stresses of a cylindrical latex aneurysm. Therefore, for the same pressure exerted by the expanding foam, circumferential stresses generated in the cylindrical geometry will be higher than the spherical, giving the worst case for aneurysm rupture in cylindrical model. Human aneurysms however are generally of very complex geometries ranging from small spherical to large fusiform shapes. For better estimation of biomechanics of human aneurysm in future studies, it may be useful to consider both multiaxial mechanical data of real aneurysm tissue and a realistic geometry in modeling.

The results here indicate that SMP foam samples 1.5–2 times the size of aneurysm can be safely implanted in the aneurysm without a risk of rupture, thereby providing a high packing volume in the treatment. While this result is promising in itself, there are several other details for an effective translation of this concept into clinical practice that are worth discussing:

Foam shape If a SMP foam is deployed in an aneurysm, there is a possibility of the SMP to protrude into the vessel lumen. There are two general ways to overcome this risk: constrain the foam geometry and constrain expansion. Constraining geometry refers

to limiting the foams geometry such that it does not expand into the parent vessel. One example of geometry constraint is mounting the foam on a wire or coil backbone similar to current embolic coil designs. If the foam is limited to radial expand by 1mm, placing the hybrid device in an aneurysm with a 2-mm-long neck would minimize the risk of the foam protruding into the parent vessel. A second example of geometric constraint would be to produce foam spheroids with machined concave indentations that would limit foam expansion into the parent vessel. Constrained expansion is the use of a temporary or permanent mechanical constraint to limit the foam protrusion into the parent vessel. Placing the foam through a stent wall would result in the stent constraining the foam expansion. The use of stent-assisted SMP foam device has been reported in an earlier study for a fusiform aneurysm model (Small et al. 2007). Even though an oversized packing with SMP foam was not performed in the former study, a neurovascular stent-assisted SMP foam deployment may be possible for treating wide neck or fusiform aneurysms.

Flexibility It is a challenge for the embolic device (crimped SMP foam and delivery device) to be navigated through tortuous vascular pathways such as the carotid siphon. For this reason, a 3-point bending experiment was run to measure the flexural moduli (moduli of elasticity in bending) of the crimped SMP foam (1.15±0.05mm diameter), 5 Fr guiding catheter (ENVOY 5 Fr, Cordis Neurovascular, Inc., Miami Lakes, Florida), and 1.7 Fr micro catheter (PROWLER-10, Cordis Neurovascular, Inc., Miami Lakes, Florida), and the results were 79.60 ± 26.90, 182.78 ± 16.16, and 76.65 ± 5.95MPa, respectively (n = 5 in all cases). Because the modulus of the crimped SMP

foam is less than half of the 5 Fr guiding catheter, the SMP foam will be easy to navigate within the catheter. Even if the modulus of the microcatheter is similar to that of the crimped SMP, we believe that less material volume and a surface modification of the crimped SMP foam will allow flexibility in navigating tortuous pathways.

Actuation These thermally actuated shape memory foams require heat energy to come to their expanded primary shape from a crimped secondary shape. In this study, we use 60◦C water as a thermal source because latex is an elastomer whose mechanical properties can get changed with temperature changes, and with a uniform water bath, it was possible to characterize the mechanical properties of latex repeatably under this condition. In clinical practice, a radiative energy source at the distal end of the delivery device could be used to actuate the SMP to the primary, recovered shape (Maitland et al. 2007, Ortega et al. 2007).

2.6 Conclusion

This study established an experimental method of estimating the forces applied by a low-modulus SMP foam on the aneurysm wall during expansion. Thin-walled, cylindrical latex models custom-made via dip coating were used for allowing measurement of low strains from the foams, and calculation of stresses was done using the thin wall pressure vessel theory, an analytical solution, and finite element modeling. The experimental results were used with finite element modeling to predict stresses generated in a human aneurysm in the worst case scenario of a minimum thickness, 1.5 and 2 times oversized embolization, and linear elastic material properties for the cylindrical aneurysm wall.

It is predicted that a 1.5 times oversized foam (e.g., 6-mm foam in a 4-mm aneurysm) can be deployed and result in a maximum circumferential stress of 65 kPa, which is less than 1/10th of the minimum wall breaking stress of 700kPa. In addition, the expansion of 6-mm foam is measured to exert a pressure of less than 10mmHg, which is not expected to pose a significant additional risk to the existing physiological condition of patients.

In conclusion, the use of oversized SMP foam as embolic devices can promote a more complete filling of an aneurysm while generating stresses that are well below the threshold that may cause the aneurysm wall to break. Thus, these foams may present reduced risk of rupture resulting from the embolic implant compared to microcoils.

CHAPTER III

FRICTIONAL LOAD OF A SHAPE MEMORY POLYMER FOAM DEVICES DELIVERED VIA A SIMULATED PATHWAY USING CATHETER

3.1 Introduction

Shape memory polymer (SMP) foams are being actively considered for embolic biomedical applications (Maitland et al. 2007). Our group has applied this material to treat aneurysms. For this application, a SMP foam can be cut in an original shape to fill the void of aneurysm bulge, which is a focal dilation at a susceptible area of cerebral artery wall. The foam can be programed in a compressed shape, which is able to be actuated by application of thermal energy, to pass through a catheter.

Studies towards realization of this SMP foam device in clinical practice are being addressed. Recently, we reported that 50% oversized SMP foams may be used to fill the aneurysmal cavity while still keeping the stresses exerted during device actuation significantly below the aneurysm wall breaking stress (Hwang et al. 2012). And we presented the transcatheter delivery of the compressed SMP device to the aneurysm site (Hwang et al. 2013).

Even though the SMP device could be delivered using a catheter within a limited time, the compressed SMP showed unintended actuation under moisture exposures in an extended time. This premature actuation of the compressed SMP was due to a depression of the glass transition temperature of the SMP (Yang et al. 2004, Yu et al. 2011). Once the compressed foam started the premature actuation during the delivery through a

catheter, the friction between a SMP device and a catheter was dramatically increased and could result in failure to deliver the device to the aneurysm.

In hydrogel coated embolic coil of using a polymer (Kallmes and Fujiwara 2002), working time existed for a delivery of the device to an aneurysm. The dried hydrogel device started to be swollen after contacting with saline or blood. Within 10 minutes, the device was able to be deployed to a target through a catheter. For the clinical application of SMP foam, the working time can be re-defined as the available period of SMP device delivery through a catheter without the complication: unreasonable high friction comparing to clinical devices, detachment of SMP foam from a delivery device, and damage of SMP foam during the delivery.

With respect to the working time of SMP device, our group reported controlling the actuation rate of SMP foam by varying the hydrophobicity of the SMP (Singhal et al. 2013). However, friction between the SMP and a catheter at 37°C aqueous solution has not been reported previously.

To quantify the friction of varied SMP compositions and dimensions delivered through a catheter, we standardized and fabricated a 3-D curved pathway with respect to previous studies (Schroder 1993a, b, Ogata et al. 1997, Zoarski et al. 1998, Konings et al. 2003, Nelken et al. 2005, Patriciu et al. 2005, Alderliesten et al. 2007, Schmidt et al. 2009).

In addition to presenting an experimental setup for measuring the friction between SMP foams and a catheter, this paper shows a relationship between premature actuations and SMP compositions. Choosing a proper SMP composition is an important

for the design of delivery device to achieve catheter based delivery of these devices in animal models. Researching the working time of the SMP foam should be necessary to apply SMP material as aneurysm treatment solution in clinic.

3.2 Materials

3.2.1 SMP synthesis

Varied hydrophobicity polyurethane SMP foams were prepared in this study by previously reported methods. H60 was hydrophilic foam, which was composed of N,N,N',N'-Tetrakis(2-hydroxypropyl)ethylenediamine (HPED), 2,2',2"-nitrilotriethanol (TEA), 1,6-diisocyanatohexane (HDI) (Singhal et al. 2012). TM series were hydrophobic foam, which were composed of HPED, TEA, HDI, and 1,6-diisocyanattrimethylhexane, 2,2,4- and 2,4,4- mixture (TMHDI) (Singhal et al. 2013). 40TM, 60TM, 80TM, and 100TM presented more hydrophobic characteristic, respectively (Singhal et al. 2013). Glass transitional temperatures of H60, 40TM, 60TM, 80TM, and 100TM were 61°C, 68°C, 69°C, 71°C, and 75°C, respectively (Singhal et al. 2012, Singhal et al. 2013).

3.2.2 SMP foam preparation

3.2.2.1 Foam cutting

Bulk foam was cut into a block, 4 cm (width) X 8 cm (length) X ~1.5 cm (height). The block was placed into a custom holder and the holder was mounted in the

rotary axis of a micro CNC milling machine (MDX-540SA , Roland DGA Corporation). Spheroid SMP foams of 4, 6, and 8 mm diameters were cut. The supporting areas were trimmed by scissors.

3.2.2.2 Post conditioning

To remove retained membranes, which is thin layer among polymer struts, of the foams, the foams were post processed by the previously reported method (Singhal et al. 2013). The cut foams were radially compressed by a stent crimper (SC150, Machine Solutions, Inc.) and returned to original shape by hot air blower (210A, Beahm Designs, Inc.). SMP foams were etched in hydrochloric acid (0.1N) for 2 hours in sonication, and cleaned with 80-20 volume% reverse osmosis (RO) water/contrad solution and RO water under sonication. Then, the foams were dried overnight under vacuum at 50°C.

3.2.3 SMP foam density

According to the ASTM standard D-3574, core densities of foams were measured in bulk and post conditioned foams. Five samples of each SMP composition were measured to estimate the variation in densities. Foam samples were cut into a cube geometry for volume measurement and any samples deformed due to post processing were re-cut into a cube by scalpel.

3.3 Methods

3.3.1 SMP foam crimping

Pre-conditioned SMP foam was threaded through a core wire for foam self-actuation test and two types of delivery devices for frictional load test. The foam was placed into the stent crimper (SC150, Machine Solutions, Inc.), which was heated at 97°C. The SMP foam was allowed to equilibrate to temperature for 5 minutes in the crimper. The foam was radially compressed. After 5 minutes, the compressed SMP foam was cooled down to room temperature over 2 hours. The compressed foam on a core wire was stored in a plastic bag with dry agent (McMaster-Carr Supply, Co.) before a test. The compressed diameters were measured using a digital caliper (797B, The L.S. Starrett Company).

3.3.2 Foam self-actuation test

Three samples of each 4, 6, and 8 mm diameters of spheroid SMP foams of each composition were threaded over 0.13 diameter mm of nitinol wire (Nitinol Devices & Components, Inc.). The samples were compressed by the stent crimper. The nitinol wire holding the compressed SMP foams were strung across an aluminum fixture and the assembly was submerged in 37°C water bath. Image of the samples were taken at 1 to 5 minutes intervals during 30 minutes. Figure 17 presented the experimental setup and progress of the self-actuation. Image J (nih.gov) was used to measure the diameter and

the length of the foams in the water bath. Measurements were normalized by the pre-compressed diameter of each sample.

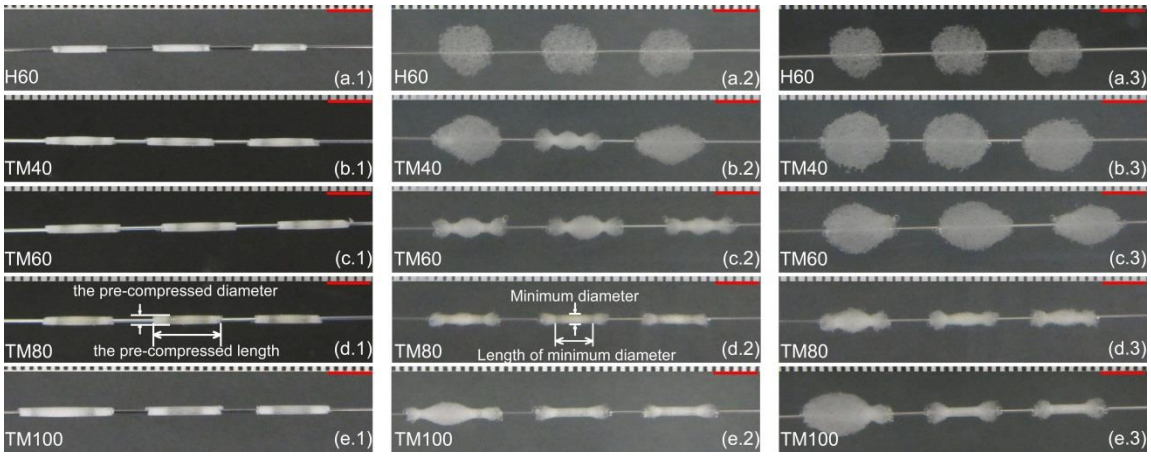

Figure 17 Passive actuation of SMP foam compositions. The panels of first, the second, and the third columns are the samples at 0 min, 5 min, and 14 min, respectively. Rows from top to bottom are (a) H60, (b) 40TM, (c) 60TM, (d) 80TM, and (e) 100TM, respectively. The middle sample of d.1 panel presents the original diameter and the original length. The sample of d.2 panel shows the minimum diameter and the length of minimum diameter. The length of the red bar in each panel presents 5 mm.

3.3.3 Frictional load test

3.3.3.1 Test environmental setup

The experimental setup was shown in Fig. 18 (a). An electro-mechanical tensile tester (Synergie 400, MTS Systems Corporation) was used for vertical movement of the samples. A 2N load cell (ULC-2N, Interface, Inc.), a data acquisition system (NI9237 and NI cDAQ-9174, National Instruments Corp.), and LabVIEW™ (National Instruments Corp.) measured and recorded frictional loads between the pathway and the catheter. An environmental chamber (Bionic Mini Bath 985.07, MTS Systems Corporation) and immersion heater (297-2, George Ulanet Co.) held 37±1°C RO water and simulated the pathway under body temperature condition.

Standardized 3D pathway was designed to measure frictional loads between SMP foams and a 6 Fr catheter (Envoy guiding catheter: OD 2.0 mm, ID 1.8 mm). The pathway was modeled using SolidWorks® and built by 3D printer (Fortus 360mc, Stratasys). The pathway has 2 two straight lines of 120 mm length and 60 mm length and two half circles with 30 mm diameter. The catheter, which was cut to the same length of the pathway, was inserted into the 3D pathway. Figure 2 (b) presents the standardized 3D pathway. The pathway was mounted in the environmental chamber and the lumen of the pathway was filled with water using a syringe.

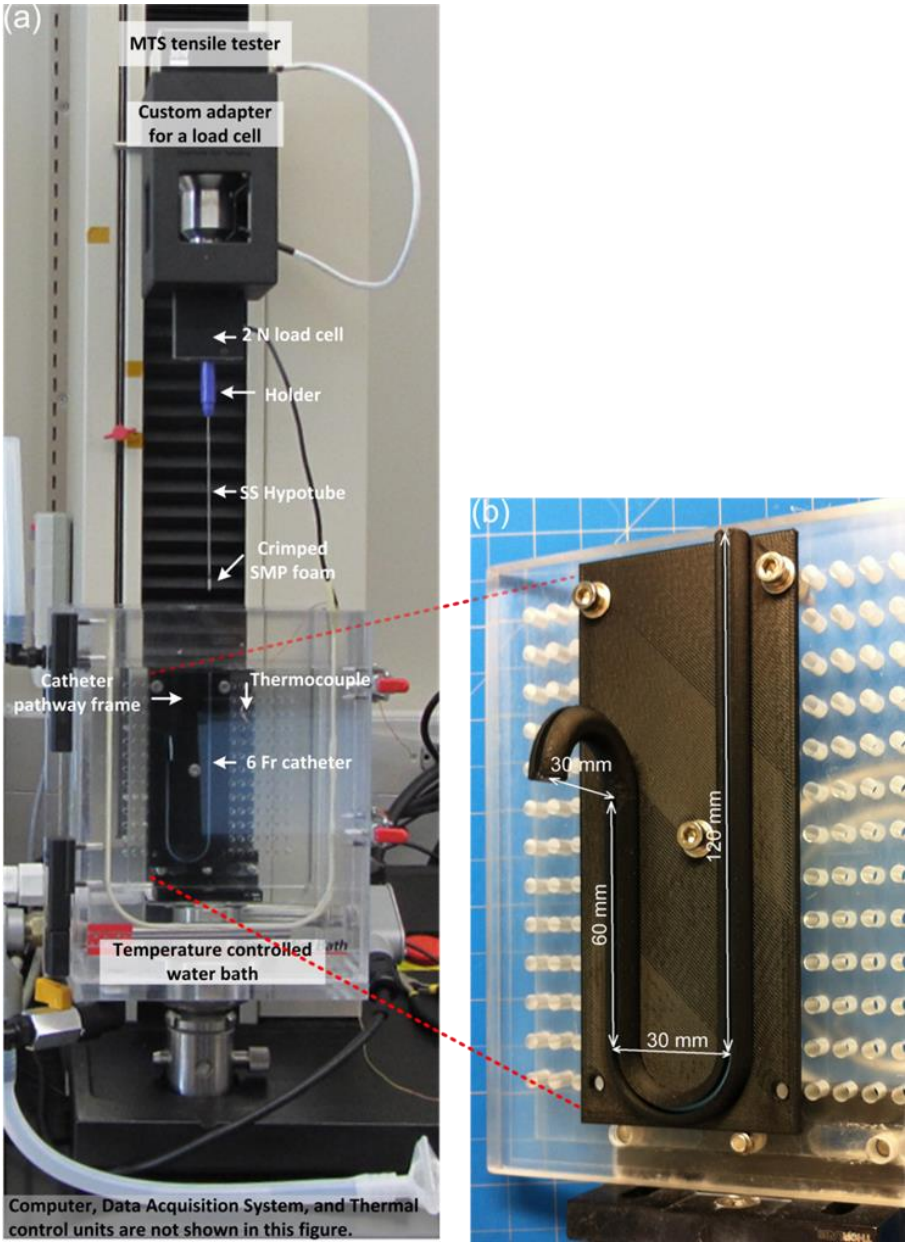

Figure 18 A photograph of (a) the experimental system, which consists of: an electromechanical tensile tester, a temperature-controlled water bath, the custom holder to attach the SMP sample on the load cell, and (b) a standardized 3D pathway including a 6 Fr catheter.

3.3.3.2 SMP foam preparation for test

Two types of delivery devices were prepared for straight and curved pathways. Figure 19 top showed the process of the straight pathway preparation. 0.4 mm diameter of stainless steel (SS) wire (McMaster-Carr Supply, Co.) was threaded through a hypodermic tube, which had 1.1 mm outer diameter and 0.6 mm inner diameter. The length of the device was 162.8 ± 2.2 mm. Both ends were soldered together. One end of the SS wire was sharpened and SMP foam was threaded over the device and compressed. Figure 19 bottom presents the process of the curved pathway preparation. 0.13 mm diameter of nichrome wire wound over 0.31 mm diameter of nitinol wire to ~8 mm length. Overall length of the device was 428.8 ± 12.4 mm. SMP foam was threaded over the device and compressed.

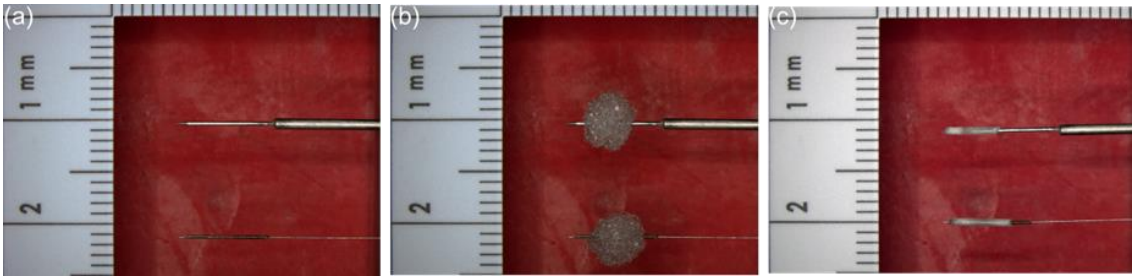

Figure 19 Photograph of the process for the SMP sample preparation. (a) Top: Spear like stainless steel (SS) wire at the distal end and overall length was reinforced with SS tube, bottom: Nichrome wire was wounded over a nitinol wire at distal end and no reinforcement of the overall length. (b) The SMP foams were threaded over the corresponding delivery devices, and (c) The foams were radially compressed.

3.3.3.3 Straight pathway

Five 8 mm SMP foams of H60, 40TM, 60TM, 80TM, and 100 TM compositions were prepared. The compressed foam sample with the delivery device for straight pathway was clamped in the holder of Fig. 18. The compressed foam was placed in the pathway and held in place 3 minutes at 37°C water bath. The sample pushed down at 100 mm per minute over a length of 100 mm in the 120 mm straight pathway. After releasing the grip of the holder, the holder re-clamped the device for pulling up. The sample moved up at the same rate, back to the starting point. The raw data, frictional loads and displacements, were collected at 2000 points per a second. The data is presented with one data point per 5 mm and the averaged frictional loads were graphed along with every one centimeter increment, up to 10 cm.

3.3.3.4 Curved pathway

4 mm, 6 mm, and 8 mm foams of each SMP compositions, which were H60, 40TM, 60TM, 80TM and 100TM, were prepared. Six samples of each set of diameters were prepared. The sample loading tool, which helped to push the compressed SMP foam through the curved pathway, was assembled with the wound stainless steel coil (0.71 mm OD, 0.47 mm ID, Heraeus Medical Components, LLC) and luer-lock hub (2.7 Fr 41523, Qosina). The nitinol wire was placed into the sample loading tool and the assembled system was placed into the standardized pathway. Once the sample was loaded, the loading tool was removed. After 3 minutes submerged at 37°C, the sample was moved along with the pathway at 100 mm/min. The data was collected at 2000

points per second and moving average, 10 points per second, was used to smooth out the data.

3.4 Results

3.4.1 SMP foam compression

Figure 20 presents measurements of original and compressed diameters of SMP foams in each composition, which are H60, 40TM, 60TM, 80TM, and 100TM. In overall, 4 mm, 6 mm, and 8 mm samples show 10 ± 10%, 9 ± 13%, and 20 ± 10% losses in diameters after post processing the foams, respectively. The compressed diameter over delivery devices are 0.58 ± 0.04 mm in 4 mm samples, 0.76 ± 0.06 mm in 6 mm samples, and 0.91 ± 0.08 mm in 8 mm samples.

3.4.2 Foam self-actuation test

3.4.2.1 Normalized minimum diameter

Figure 21 show normalized minimum diameters of the compressed samples along with the time of submersion. Hydrophilic foam, H60, shows almost full recovery within 3 minutes in 3 different sizes of samples. Depending on hydrophobicity of each composition, premature expansions are observed with increasing submerged period. In addition, decreasing sample sizes of foams are related to more premature expansion. 100TM SMP foams of 8 mm, 6mm, and 4mm, in Fig. 21 (a), (b), and (c), present approximately20% expansion of original diameters in 16 minutes, 8 minutes, and 4

minutes, respectively. Once compressed foam is expanded over approximately 20% of the original diameter, large standard deviations of measurements were shown in Fig. 21 (d). These large variations in the diameters can be considered as undeliverable status of the compressed foams. 80TM SMP foams of 8 mm, 6 mm, and 4 mm diameters present approximately 20% expansion of compressed status in 16 minutes, 3 minutes, and within 1 minute, respectively. 8 mm SMP foams of 60TM and 40TM show 20% expansion in 7 minutes, and 3 minutes, respectively. Other sizes in the compositions present 20% expansion in 1 minute.

3.4.2.2 Average normalized length of minimum diameter

Figure 22 presents changes of length in minimum diameter of the samples during submerging at 37°C. Reasonable correlations between hydrophobicity and size of the samples and premature expansion are presented in Fig. 22 (a), (b), and (c). Once compressed foams start expanding, Fig. 22 (d) presents large standard deviation of the measurements.

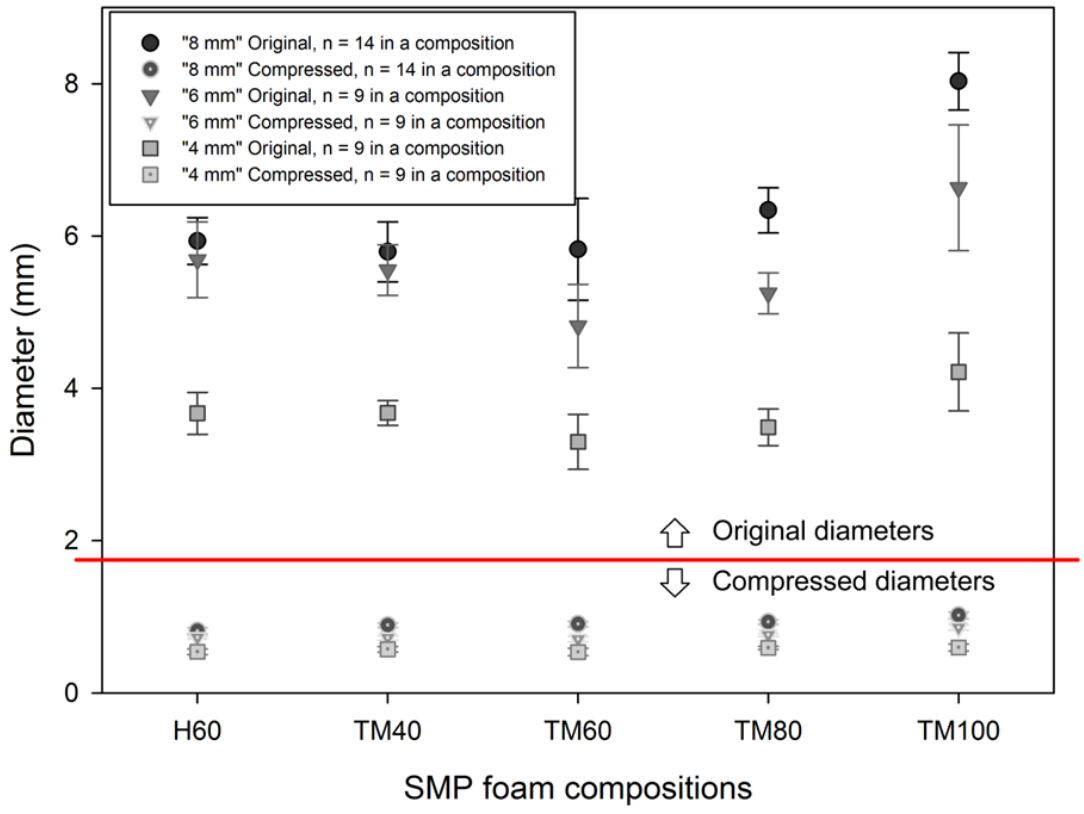

Figure 20 Diameters versus SMP foam compositions in the original and the compressed shapes.

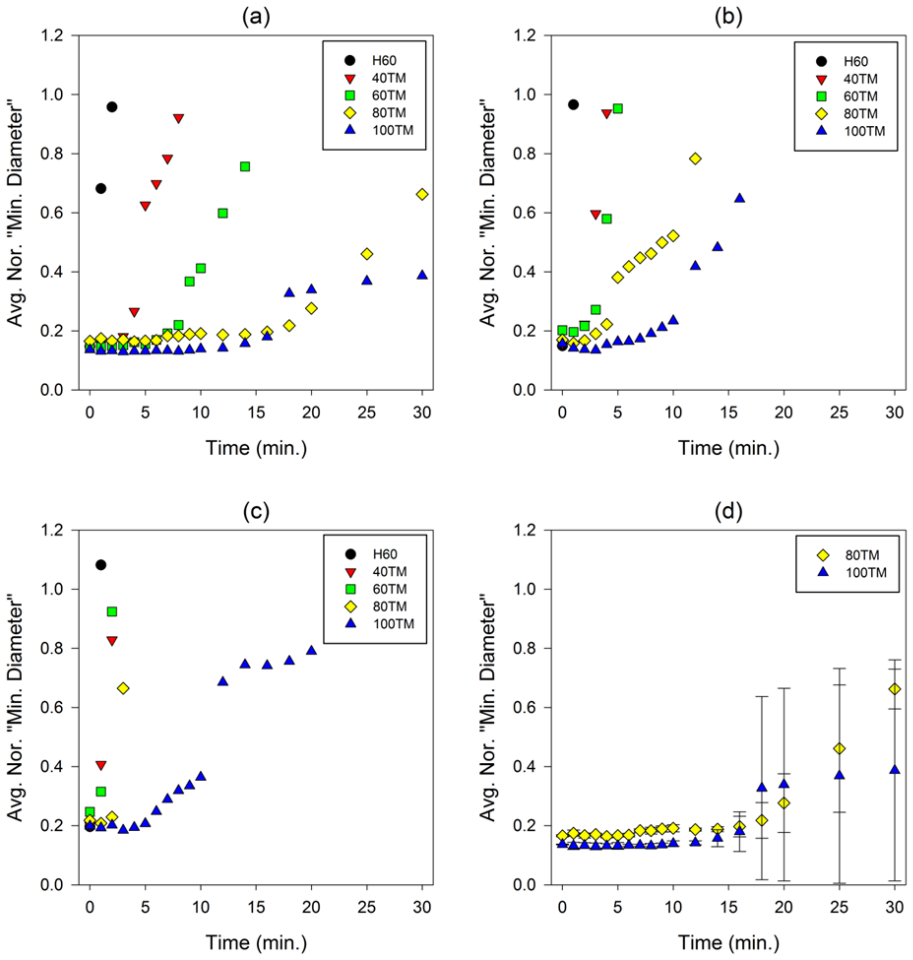

Figure 21 Average normalized minimum diameter of the compressed foams versus submerged time are presented for each set of foam size. (a) 8 mm samples, (b) 6 mm samples, (c) 4 mm samples, and (d) 8 mm samples of 80TM and 100TM compositions with standard deviation. Other panels omit standard deviations for clarity.

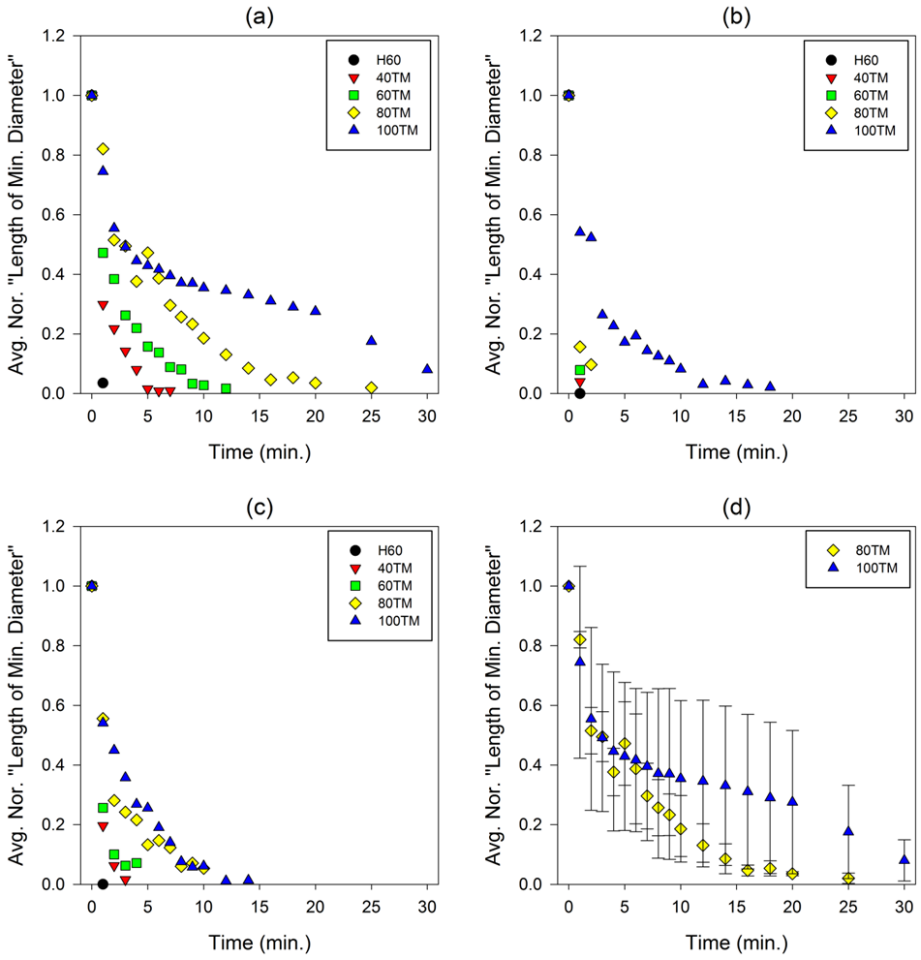

Figure 22 Average normalized Lengths of minimum diameter versus the submerged time are presented for each set of foam size. (a) 8 mm samples, (b) 6 mm samples, (c) 4 mm samples, and (d) 8 mm samples of 80TM and 100TM compositions with standard deviation. Other panels omit standard deviations for clarity.

3.4.3 Frictional load test

3.4.3.1 Straight pathway

Figure 23 shows averaged frictional loads of pushing and pulling motion in a straight pathway, up to 10 cm. Figure 23 (a) show the load of pushing motion about each SMP composition. At beginning of the movements, frictional loads of H60, 40TM, 60TM, 80TM and 100TM are 0.135 ± 0.022 N, 0.095 ± 0.074 N, 0.090 ± 0.008 N, 0.010 ± 0.002 N, and 0.013 ± 0.005 N, respectively. At 10 cm of the displacement, frictional loads of H60, 40TM, 60TM, 80TM, and 100TM are 0.224 ± 0.026 N, 0.168 ± 0.023 N, 0.177 ± 0.024 N, 0.145 ± 0.020 N, and 0.145 ± 0.026 N, respectively. Figure 23 (b) shows the load of pulling motion about each SMP composition. At the beginning of the movements, friction loads of H60, 40TM, 60TM, 80TM, and 100TM are 0.374 ± 0.046 N, 0.327 ± 0.066 N, 0.4325 ± 0.056 N, 0.354 ± 0.060 N, and 0.305 ± 0.035 N, respectively. At the 10 cm of the displacement, the frictional loads of H60, 40TM, 60TM, 80TM, and 100TM are 0.2452 ± 0.037 N, 0.139 ± 0.084 N, 0.134 ± 0.025 N, 0.096 ± 0.057 N, and 0.099 ± 0.016 N, respectively. In addition, reasonable reverse correlation between hydrophobicity of the foams and fictional loads are presented in Fig. 23 (a) and (b).

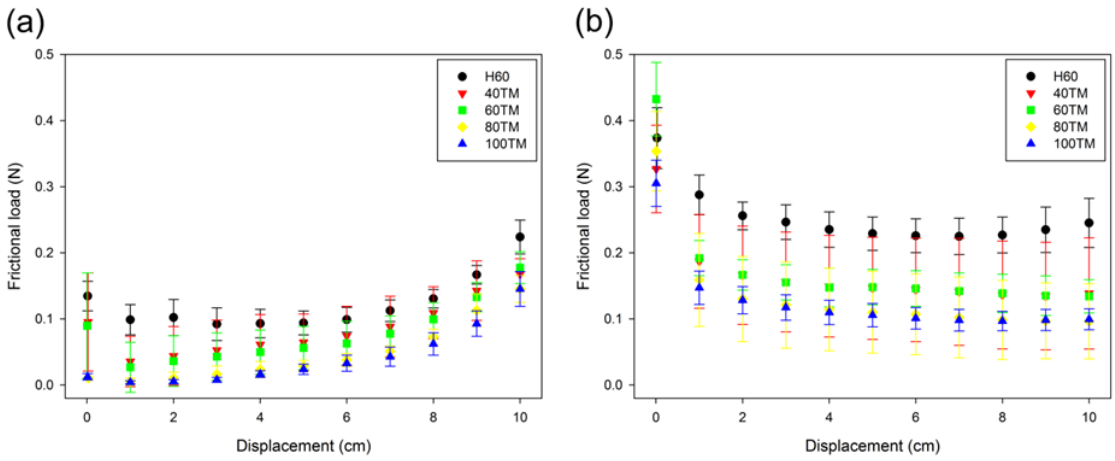

Figure 23 Frictional load versus displacement in the straight pathway. Each foam composition has 5 samples in 8mm samples. (a) frictional load in push and (b) frictional load in pull.

3.4.3.2 Curved pathway

Figure 24 presents the results of the frictional loads in the standardized 3D curved pathway. Panel (a), (b), and (c) present the frictional loads of 4, 6, and 8 mm diameters of the foam compositions, respectively. Around the second curve of the curved pathway, 6 and 8 mm diameters of samples show more fictional loads than other locations in the pathway. In addition, maximum loads in 4, 6, and 8 mm diameters of the samples are 0.12 ± 0.19 N at 10.55 ± 0.27 cm in 100TM composition, 0.55 ± 0.39 N at 9.76 ± 0.29 cm in 40TM composition, and 0.72 ± 0.44 N at 10.11 ± 0.25 cm in H60 composition, respectively. Figure 25 shows averaged maximum loads of the samples in the diameters and the foam compositions. From the results of Fig. 24 and 25, linear relationships between maximum loads and hydrophobicity of the foams with varied sample sizes are not shown in the curved pathway.

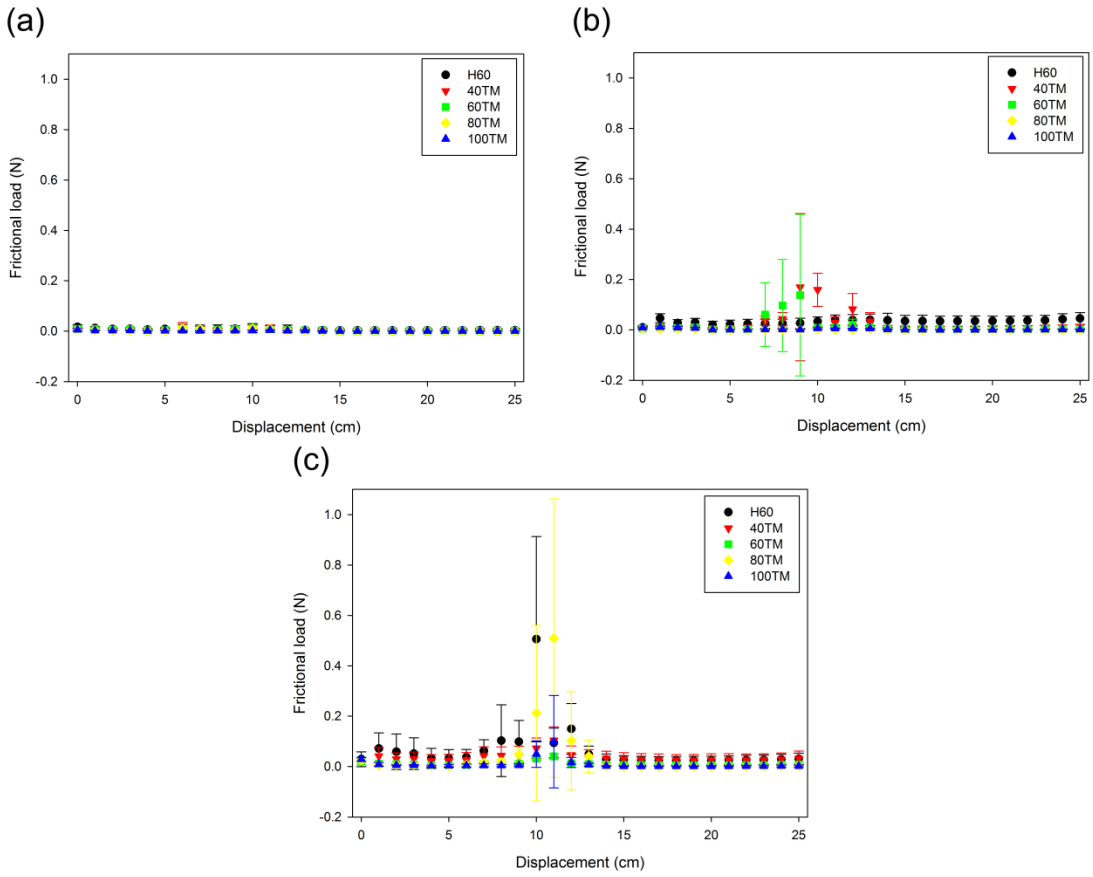

Figure 24 Frictional load versus displacement in the standardized 3D pathway. Each foam composition has 6 samples in a diameter. (a) 4 mm samples, (b) 6 mm samples, and (c) 8 mm samples.

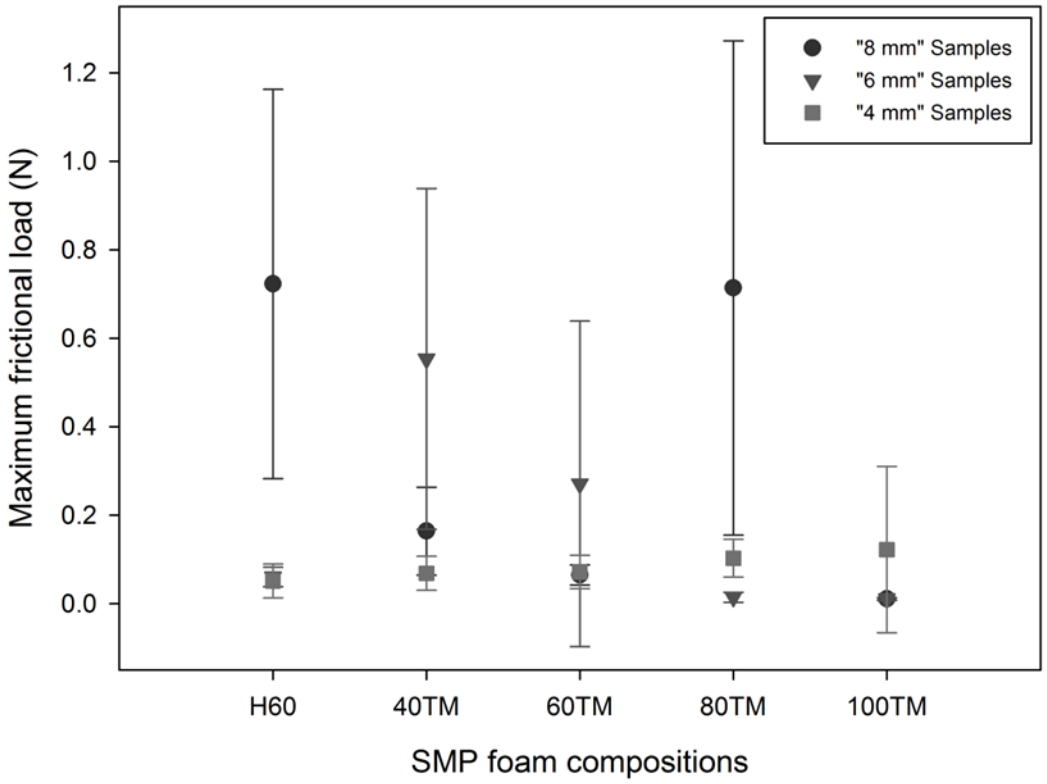

Figure 25 Averaged maximum frictional load versus SMP foam compositions. Each foam composition has 3 types of samples in 4 mm, 6 mm, and 8 mm diameters. And each type has 6 samples. Data points of "6 mm" Samples in H60, "4 mm" Samples in 60TM, and "6 mm" Samples in 100TM were not shown by overlapping other data points which are "4 mm" samples in H60, "8 mm" samples in 60TM, and "8 mm" samples in 100TM, respectively.

3.5 Discussion

In Fig. 20, the diameters of samples of 100 TM composition were more closely achieved to the target of 4 mm, 6mm, and 8 mm than diameters of other samples of H60, 40TM, 60TM, and 80TM compositions. After post processing samples of 100TM SMPs, the measured diameters were approximately 50% larger than initial diameters. This deformation might be caused by residual stresses in foaming process. The deformed foams were cut into the target diameters of spheroid shape using scissors and scalpels. Therefore, the samples of 100TM SMPs showed less volume change from the post processing. Samples of the other compositions were used as they were after post processing. These variations of diameters have to be considered to design diameters for SMP foams. For example, pre-shaped foams may need a margin to have a target diameter. Preparation of 8 mm samples might require an initial cut of 10 mm samples and then verification process would be necessary to compare the target diameter with an actual diameter or select samples within a range.

As per the ASTM standard D-3574-08, Figure 26 presented core densities of SMP foams in bulk and post-processed conditions. 40TM and 60TM foams showed 3x the bulk density. H60 and 80TM foams showed 0.5x the bulk density. 100TM foam showed least change of density between bulk and post-processed conditions. These changes are associated with a decrease in pore cell sizes of foams. A decreased pore cell can negatively affect maximum compression ratio of the SMP foam and blood percolation when the foam is implanted.

From previous reports (Singhal et al. 2012), SMP foams in this study showed heterogeneity in structure such as difference in pore cell sizes and anisotropy in radial and longitudinal axes of the bulk foam. When SMP samples were prepared in this study, locations of the samples in the bulk foam were randomized. For example, the samples could be at a center of or outmost from radial axis and bottom or top of the longitudinal axis. . And the axes of spheroid SMP from the bulk foam were also randomized, when the spheroid sample was mounted on the delivery device. Therefore, variation of the measured diameters of the SMPs with respect to the anisotropy could be an important design factor for a device.

The plasticization of the SMPs in aqueous solution, which is T_g depression, induces premature expansion of the compressed foam. Panel c.2 and d.2 of Fig. 17 represent initial expansion of the compressed foams like a dumbbell shape in no constrained condition. Delayed premature expansion of more hydrophobic SMP foams were observed in Fig. 21 and 22. Once SMP foams start to expand over 20% of the original diameter from the diameter of the compressed foams, considerable standard deviations were observed in the SMP compositions. In addition, lengths of the minimum diameters present wide standard deviations over the time. Even though deviations of the measurements resulted from heterogeneity of the foam characteristics, 20% recovery of the compressed foam may be potential indicator when the device needed to be retracted to a catheter without fractures of a SMP foam.

Density of the compressed foam, which was prepared for the catheter delivery, might be considered as the major factor of leading premature expansion, when

contacting with water. The density of the compressed foam could not be uniform by its heterogeneous structure. Less densely compressed area of the foam allowed to contact water first and the plasticization would be started earlier than tightly compressed area. Most of result in this study showed that start of actuation was happened at the both ends of the compressed foam. This result was coincident with visual examination of the foam, which was a contrast of the color along the length of the foam, right after the compression. The first column of panels in Fig 17 presented the tightly compressed area were darker than loosely compressed area because of transparency of the compressed foam over the black underlay. The second column of panels in Fig 17 supported that brighter area of the foam started actuation earlier than darker area of the foam.

Inconsistent densities in compressed foams were related with premature actuation of its less dense area first. Achieving uniform density of the compressed foam would be a good practice of design control to expect representable working time for transcatheter delivery in clinical application. In the straight pathway, less frictional loads were observed with more hydrophobic SMP foams. In the pushing movement, slightly higher frictional loads were observed due to static friction. In addition, dynamic frictional loads were increased along with advanced movement. This increment may result from compacted foam sections due to the premature expansion of the compressed foam inside of the catheter. The compacted foam was against the wider surface area of the pusher in top panel of Fig 19 (a) and the frictional load kept increasing by the end of the movement. Therefore, in the pulling movement, static frictional loads were higher than them in the pushing movement. However, in the pull, dynamic frictional loads showed

trends of plateau in frictional loads, relative to the push, due to free end of the distal side of the foam.

The delivery device in the curved pathway used a fine nichrome wire to minimize the frictional load between the catheter and the delivery device. The nichrome wire is very compliant and cannot push the foam against the friction between the catheter and SMP foam. Therefore, the experiments in the curved pathway were performed only using pulling movements. Static frictional load in the curved pathway showed lower loads than one in the straight pathway by the different setup of experiments between straight and curved pathways. There were no pushing movements in the curved pathway. And almost no compacted foam at the distal end of the curved pathway was expected.

The different frictional responses in two pathways can consider the following reasons: pushing the foam shears it, causing it to deform towards the delivery device, reducing clearance and increasing friction. While pulling, the foam shears away from the delivery device and, thus, has clearance to deform and fill the center of the lumen, thus reducing the friction. Two factors are import role in the frictional load: one is the plasticization of the foam which is relaxation of the polymer chain and premature expansion; the other is the shearing of the compressed foam by delivering the foam along with the catheter. In this case, the surface of the compressed foam was mechanically stressed and vulnerable to absorb an aqueous solution in the compressed foam, causing swelling and expansion. This premature expansion also will lead significant frictional load to deliver the foam into the target location. In addition, if there

is a mechanically defect area of the compressed foam, this will effect on the frictional load and lead wide standard deviation.

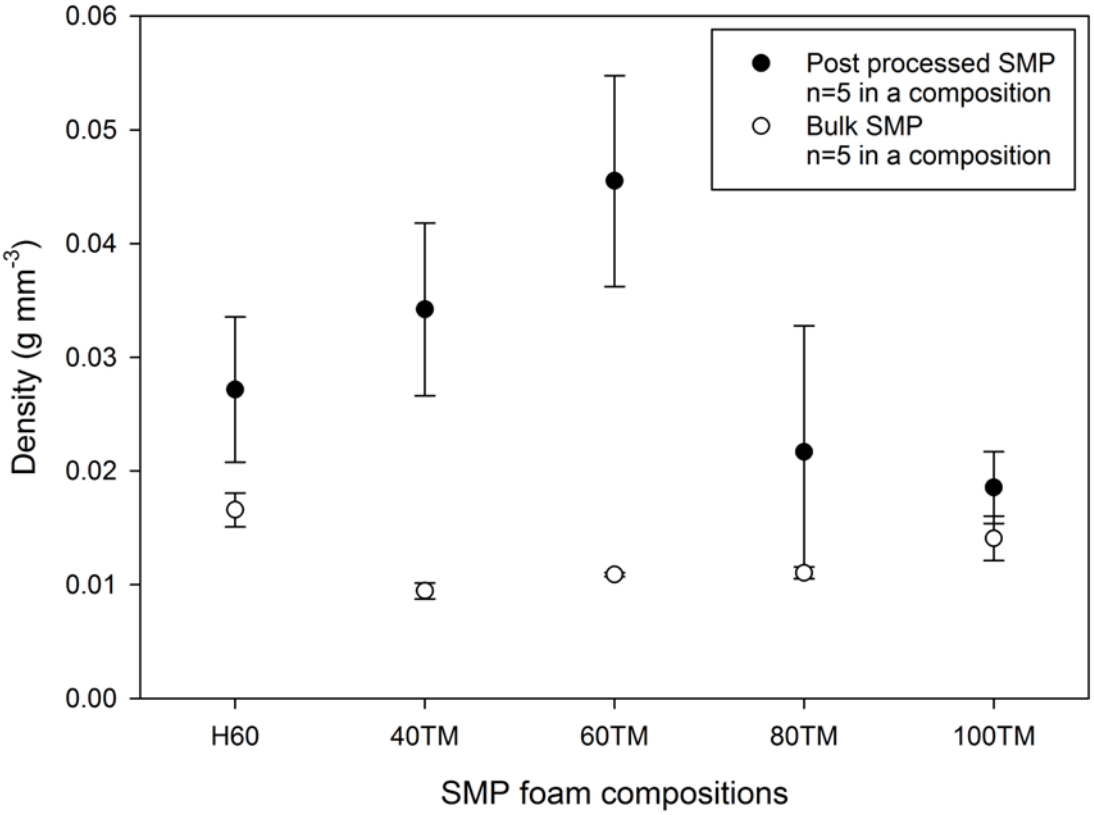

Figure 26 Density versus SMP foam compositions. In each SMP composition, the densities between bulk and post processed SMP foams are presented.

3.6 Conclusion

This study established an experimental setup to measure frictional loads between SMP foam and a catheter in 37°C water . In addition to a straight pathway, a standardized curved pathway, which is a three dimensional tortuous pathway, was proposed for the measurements of frictional loads. After 3 minutes submersion to simulate endovascular delivery, all samples were passed through pathways. As expected, more hydrophobic SMP foams showed less frictional loads in the straight pathway.

A linear relationship of the frictional loads in the curved pathway was not observed among SMP compositions. This result may be the following reasons: 1. Uneven mechanical stimulation through a tortuous pathway with movement of the compressed SMP foam, 2. Heterogeneity in structure of SMP foams, and 3. Variation of plasticization.

Even though passive actuation rate was controlled by changing of hydrophobicity, current working time is no longer than 5 minutes (3 minutes submersion and 2 minutes delivery). For clinical practice, SMP foam may require up to 10-15 minutes working time for transcatheter delivery. The foam samples needs to be tightly controlled for minimal variation in density of the compressed foam due to variation of plasticization in a SMP foam. The density of the compressed foam is also related to structures of the foam such as pore cell sizes in radial and longitudinal axis, when the SMP foam is synthesized. In clinical practice, these controls will allow promising delivery of the device through anatomically various tortuous vessels of patients.

Finally, 80TM or 100TM foam is considered as a potential SMP composition for application of SMP embolic device with minimum requirement of premature actuation and minimal frictional loads during transcatheter delivery.

CHAPTER IV

IN VITRO STUDY OF TRANSCATHETER DELIVERY OF A SHAPE MEMORY POLYMER FOAM EMBOLIC DEVICE FOR TREATING CEREBRAL ANEURYSMS[*]

4.1 Introduction

This study is developing shape memory polymer (SMP) foam devices for embolizing and treating cerebrovascular aneurysms. Cerebral aneurysm rupture occurs in approximately 30,000 people per year in the United States, with devastating consequences (Keedy 2006). Further, three-fourths of patients will either die or become neurologically debilitated (Keedy 2006). The SMP foam device is designed to rapidly and efficiently promote acute blood clotting with one device treating an aneurysm (Ortega 2013). Some key features in the foams that enable the clotting efficacy are biocompatibility (Singhal et al. 2012), open cell architecture with tortuous flow and high surface area to volume ratios (Singhal et al. 2012), and large (50x-100x) volume expansions that permit compact delivery through a catheter with actuation and deployment in the aneurysm.

This study describes additional challenges and engineered solutions for transcatheter delivery of a SMP foam embolic device. The primary challenge addressed here which is the engineering tradeoff between self-deploying foams, which actuate at

[*] Reprinted with permission from "In Vitro Study of Transcatheter Delivery of a Shape Memory Polymer Foam Embolic Device for Treating Cerebral Aneurysms," by Wonjun Hwang; Pooja Singhal; Matthew W. Miller; Duncan J. Maitland, Journal of Medical Devices, Volume 7, 2013, Copyright 2013by ASME

body temperature, versus foams that actuate above body temperature. If body temperature is used to actuate the foams, then they must be physically constrained or sheathed as they are delivered through the catheter. Deployment in the aneurysm then involves unsheathing the foam after it has been placed in the aneurysm. Retractable sheathing systems or other mechanical constraints on the foam become more challenging for devices that are to be delivered through small catheters (3 Fr, ~ 1000 μ ID) and microcatheters (~500 μ ID). Given that the SMP foams can be designed to actuate at temperatures above body temperature (Singhal et al. 2013), we elected to use foams that stay crimped at body temperature and use a resistive heating delivery device to deploy the foams once they are located in the aneurysm.

This study presents a device with second foam shell that inhibits premature device actuation (Singhal et al. 2013). Also, the shell was doped with tungsten to enhance fluoroscopic visualization (Rodriguez et al. 2012) of the device. Further, a resistive heating mechanism was built-in for actuating the device. The development and in vitro validation of this transcatheter delivery and actuation mechanism was an important step towards achieving catheter based delivery of these devices in animal models.

4.2 Methods

Two types of SMP foams were synthesized by a previously reported method: Type A was based on the H60 composition (Singhal et al. 2012); and Type B was based on the 80TM composition (Singhal et al. 2013) with a 4% by volume loading of tungsten particles (Rodriguez et al. 2012). Type A was used for its lower density and higher volume expansion. Type B was used for its higher actuation temperature (71°C) and fluoroscopic visualization. Two types of devices were prepared: Device I comprised a 10 mm diameter sphere of foam A; and Device II was made from a combination of Foams A and B. Specifically for Device II, a 12 mm diameter sphere of foam B was cut and then a cylindrical core (7 mm diameter) was removed from the spherical shell. Then an 8 mm diameter cylinder of foam A was inserted into the void of foam B to make the final hybrid device. Figure 27 (a) & (b) show the two types of devices.

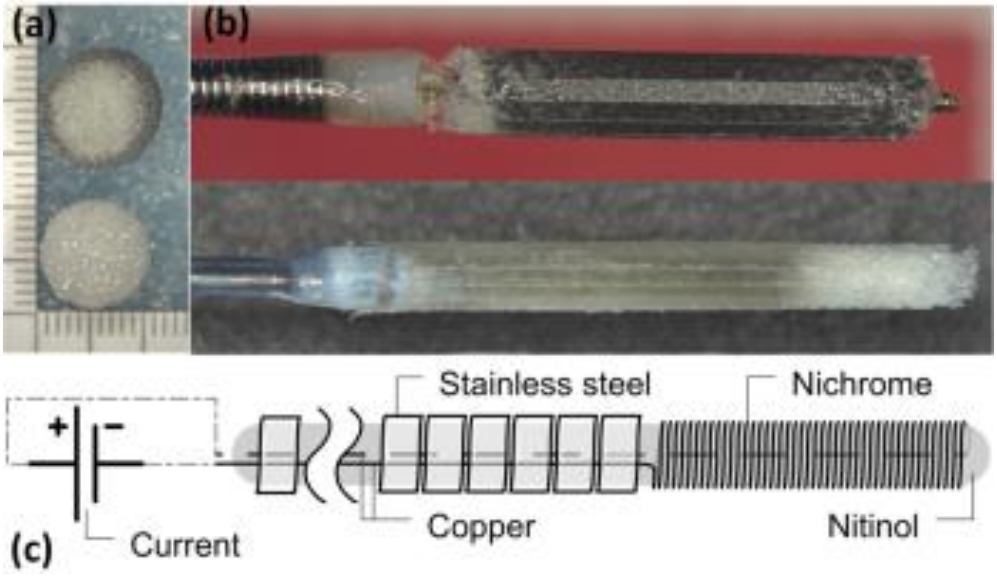

Figure 27 SMP devices: (a) Device I with type A SMP foam (bottom) and Device II with type A and B SMP foams (top), (b) Crimped devices I and II respectively from bottom to top, (c) Schematic diagram of a delivery device.

The foam delivery device was developed and consisted of a resistively heated wire bundle of nitinol, stainless steel, nichrome, and copper. This delivery device (Fig. 27 (c)) utilized an external energy source to actuate the crimped SMP foam within the aneurysm model. The foam devices were crimped to their temporary shape on the resistive–heating delivery device using a stent crimper (SC150-42, Machine Solution Inc.), creating the SMP embolic devices. They were then sterilized using ethylene oxide sterilization.

Two types of polydimethylsiloxane (PDMS) aneurysm phantoms were fabricated from CT based porcine side wall and simplified aneurysm models. For the porcine based side wall aneurysm model, CT images were segmented into a 3D model in the standard tessellation language (STL). A simplified aneurysm was modeled with Solidworks® and also saved as an STL. These files were then printed using a fused deposition modeling (FDM) system (Fortus360mc, STRATASYS®), in Fig. 28 (a). The printed models were embedded in PDMS and then dissolved using lost-wax casting (Fig. 28 (b).

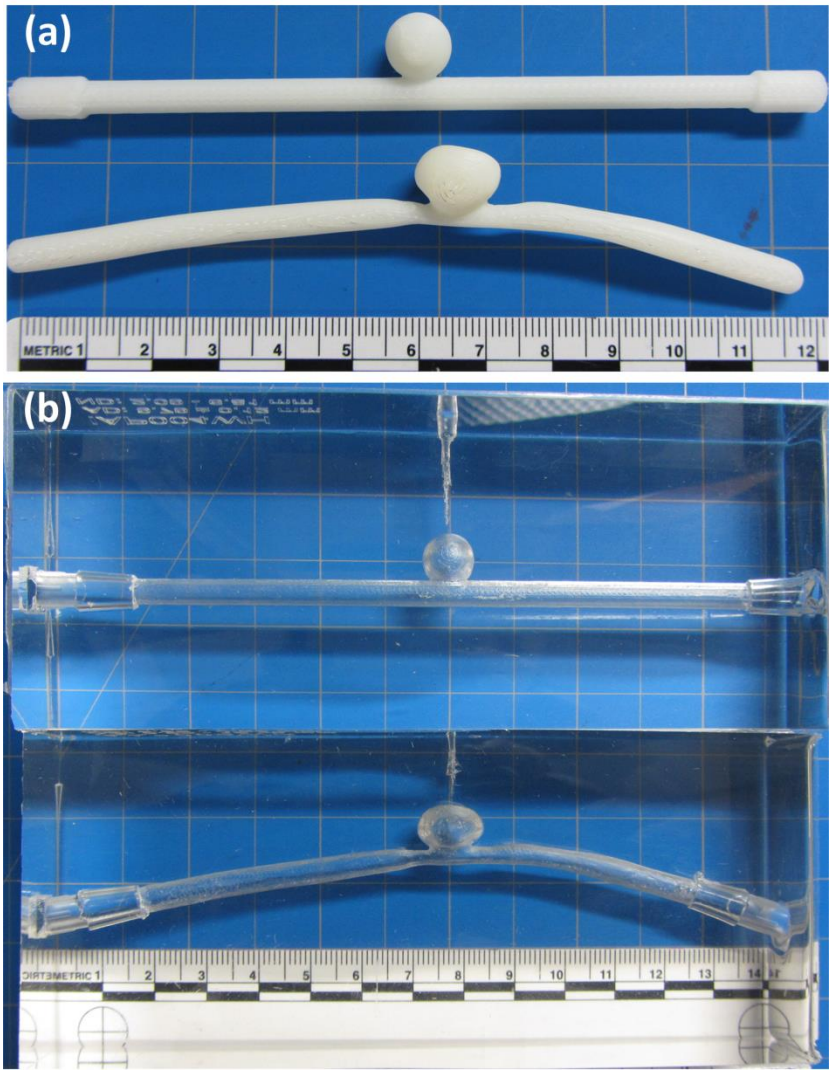

Figure 28 Fabrication of mock aneurysm models. (a) FDM models of an ideal and a porcine side wall aneurysms, (b) PDMS aneurysmal phantoms.

The aneurysm phantoms were connected to the same flow system. In Fig. 29, the flow system was composed of a heated water bath (89032-216, VWR), a peristaltic pump (72-315-000, Thermo Scientific,), a pulse dampener (WU-07596-20, Cole-Parmer), a Touhy Borst valve (80348, Qosina), and a needle thermocouple (HYP1, Omega) with a thermometer (HH23, Omega) at the apex of each aneurysm phantom. The heated water bath was set to maintain a temperature of ~37°C at the aneurysm site. The peristaltic pump and the pulse dampener simulated a steady state flow of ~1.1 L/min in the parent vessel of the aneurysm phantom, which corresponds to average flow rate in the common carotid artery within porcine animal model. A 6 Fr catheter (556-26000, Codman Neurovascular) was taken through the flow system from Touhy Borst valve to the aneurysm model. Device I was delivered in the simplified aneurysm model, while Device II was delivered in the porcine aneurysm model.

After positioning the catheter within the aneurysm dome, Device I and Device II were delivered and actuated with 0.3 amps within 30 seconds and 2 minutes, respectively. The deployment procedures were performed under the C-arm X-ray (Allura Xper FD Rotational Scan , Phillips) in a catheterization laboratory at the Texas Institute for Preclinical Studies.

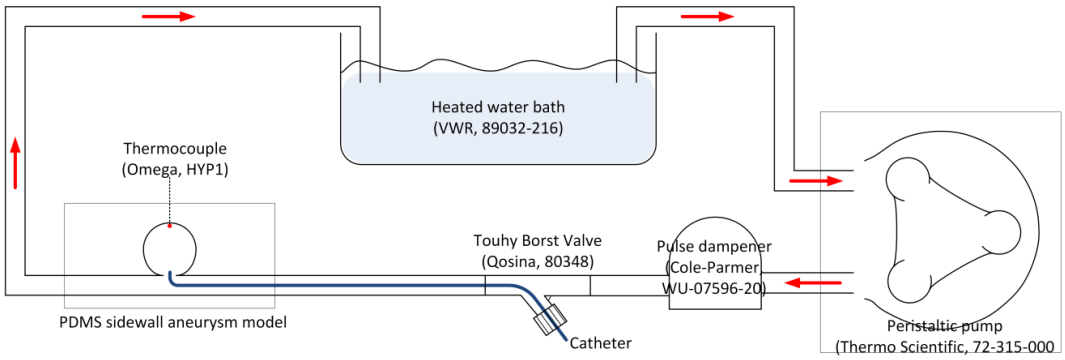

Figure 29 Schematic diagram of in vitro experimental system.

4.3 Results

Figure 30 represents the results of delivery of Device I in the simplified model with the flow system. The dimensions of the diameter of the aneurysm, neck and height was 10 mm, 1.28 mm and 4.73 mm respectively. Figure 30 (a) represents the process of the aneurysm cavity filled at the distal end of the catheter after actuation. The fluoroscopic image (Fig. 30 (b)), represents delivery of the device within the aneurysm void.

Figure 31 shows deployment procedures of Device II in the porcine based phantom. The parent vessel diameter ranged between 8.62-12.73 mm and the neck diameter ranged between 3.06-7.97 mm. A 6 Fr catheter was placed into the aneurysm (Fig. 31 (a)). Figure 31 (b) shows that the SMP foam had been deployed into the aneurysm and the delivery device was placed beyond the distal end of the catheter.

Figures 31 (c)-(f) show the delivery and deployment: (c) The arrow indicates that the crimped SMP foam was delivered via catheter. (d) The crimped SMP foam had been delivered and positioned into the aneurysm. (e) The delivery device actuated the crimped foam via Joule heating, and 50% expansion of primary shape (12 mm D) was seen within 1 minute. (f) The SMP foam was fully expanded within 2 minutes from the initial actuation. The thermocouple, located at the apex of the aneurysm, reported a temperature of 38°C during delivery and deployment.

4.4 Discussion

Complete occlusion of the aneurysm model was achieved in the Device I delivery test. However, type A foam self-deployed at body temperature within 2 minutes which was not expected due to a transition temperature of approximately 61°C. If this result was seen in vivo, this would result in premature recovery of the compressed SMP foam device and hinder its transcatheter delivery. In addition, we could not monitor the real time progress of Device I actuation due to lack of the contrast agent (tungsten) in this device (Fig. 30 (b)).

In an attempt to improve upon the previous design, tungsten was added for radio-opacity and increased working time via the change in chemistry to the type B foam. Demonstration of this device in the porcine side wall aneurysm model showed that device II was also successfully deployed and occluded the aneurysm.

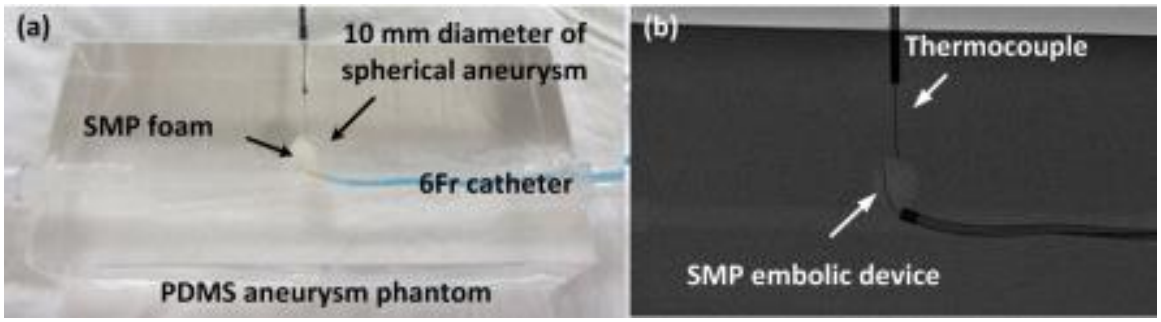

Figure 30 *In vitro* setup of a simplified PDMS aneurysm model after actuation of the type A SMP foam in the aneurysm model as captured via (a) an optical camera (b) fluoroscope.

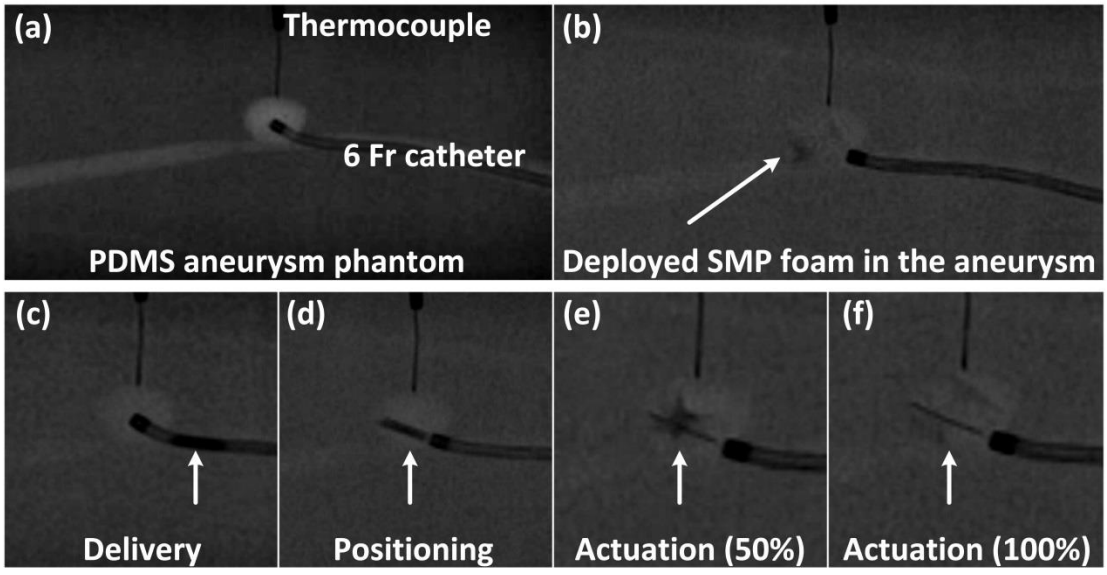

Figure 31 Fluoroscopic images: Delivery and deployment of Device II.

With this change in the addition of foam B, the deployment procedure could be observed under fluoroscopy due to the presence of tungsten. When the foam was crimped, the entire device was visible under fluoroscopy. During the actuation, the outer shell of the device, comprising tungsten doped foam B, could be detected. Full actuation was associated with the change in contrast from dark to light as the foam expanded via resistive heating.

The porcine aneurysm phantom was considered as a wide neck aneurysm, based on its dome to neck ratio and aspect ratio (Brinjikji et al. 2009), which may account for the migration of foam when the flow rate was over 1.1 L/min. Clinically, this is an adverse result. One solution to this adverse result may be the use of an oversized implant. For example, the diameter of the SMP foam used here was the same as that of the aneurysm model. If we were to fill the aneurysm with an oversized SMP foam (Hwang et al. 2012), the stability of the implant may be increased, and an additional device stabilization technique may not be necessary.

4.5 Conclusion

Successful delivery and deployment of the prototypes in an aqueous environment proved deliverability of SMP embolic devices via catheter. This study reported full shape recovery by thermal actuation and fluoroscopic visualization was achieved by tungsten embedded SMP foam.

CHAPTER V

IN VIVO STUDY OF TRANSCATHETER DELIVERY OF A SHAPE MEMORY POLYMER FOAM EMBOLIC DEVICE FOR TREATING CEREBRAL ANEURYSMS

5.1 Introduction

Validation of a medical device is necessary to prove efficacy and safety before a clinical trial. Early state of a device development also requires similar evaluation process. The previous *in vitro* study (Hwang 2013) establishes the experimental setup to evaluate the SMP foam embolic prototype. In transcatheter delivery, the study reports pushability, visibility of the device under X-rays, actuation of the compressed SMP foam on demand, and occlusion of saccular aneurysms. In addition, the experimental setup allows for physicians to be trained before a preclinical study.

This study describes the design and the fabrication of the prototype, animal models for pilot preclinical studies, verification of treating saccular aneurysms, follow-up studies before histological evaluation, and considerations of the device development for a next stage. In addition, this study reports head to head comparisons between the SMP embolic device and a platinum coil in clinic, which is considered as a gold standard in the endovascular treatment of intracranial aneurysms.

SMP foam presents a depression of the glass transition temperature (T_g) in aqueous environment by plasticization (Yang et al. 2004, Yu et al. 2011). This effect leads uncontrolled actuation of the SMP foam, significantly affects pushability of the

device under a tortuous catheter pathway, and eventually fails a delivery of the SMP embolic device. By modifying chemical compositions of the SMP foams (Singhal et al. 2013), the actuation rate of compressed SMP foams is controlled. Ideal requirement of the SMP foam for the deliverability is the actuation of the compressed foam on demand. In addition, the speed of the actuation is also a considerable design factor. The proposed mechanism for the detachment of the SMP from the delivery device is a friction between them.

Radiopacity of the SMP foam is also necessary for physicians to deploy SMP embolic device under X-ray, which is general endovascular process. Rodriguez et al. (Rodriguez et al. 2012) reports opacification of SMP and proposes tungsten as radiopaque medium. Therefore, this study and the previous report (Hwang 2013) presents a hybrid SMP foam using two different types of SMP foams. Outer shell of the hybrid SMP foam is a hydrophobic SMP (80TM (Singhal et al. 2013)) with 4% volume added tungsten, which is able to delay a depression of T_g and visible under X-ray, and inner core is a hydrophilic SMP (H60 (Singhal et al. 2012)), which allows for fast actuation. The assembled device (Hwang 2013) of the hybrids SMP foam and the delivery device is sterilized by ethylene oxide (EtO).

After promising report of in vitro experiments and bench-top testing, this study takes into account the complexity of the *in vivo* environment. These efforts are necessary to find adverse events of therapeutic innovations, to minimize the risks for patients and to limit large-scale clinical investigations to the most promising devices (Bouzeghrane et al. 2010). In aneurysm therapy, various animal models has been developed to test

innovations (Bouzeghrane et al. 2010). An animal model is not specified for a standard preclinical study. *In vivo* aneurysm models use dogs, swine, rodents, and primates, which are well developed from previous researches (German and Black 1954, Guglielmi et al. 1994, Bavinzski et al. 1998, Bavinzski et al. 1999).

Bouzeghrane et al (Bouzeghrane et al. 2010) reports ideal characteristics of a good aneurysm model: "Minimal surgical, and endovascular morbidity; similarity to human aneurysm shear stresses, hemodynamic forces, physical dimensions, perianeurysmal environment, and tissue responses; and stability without spontaneous thrombosis when untreated (Massoud et al. 1994)". There are no available models to satisfy all required characteristics and various animal models aim various purposes (Bouzeghrane et al. 2010).

With the advent of GDC as a clinical therapy in early 1990s, the porcine aneurysm models are developed to test their innovation (GDCs) for treating intracranial aneurysms (Guglielmi et al. 1994). This study presents porcine bifurcated and lateral wall aneurysm models to test the SMP embolic device. Porcine model has similarities of physiology and coagulation systems between human and swine (Kantor et al. 1999). And vessels in interested area have good enough size for our application, which is aneurysm construction and a test for scale-up SMP device.

Construction of porcine aneurysms, endovascular accesses, transcatheter delivery, and occlusions of the aneurysms are performed at the catheterization laboratory of Texas A&M institute for preclinical studies (TIPS). During the studies, research and development team is on site for technical supports, collection of data and feedbacks from

physicians. In addition to occlude an aneurysm with a SMP foam, GDCs are also implanted in an aneurysm for evaluating the innovation of SMP foam embolic device. GDC is a market frontier and considered as a gold standard in intracranial aneurysm therapy. Finally, this study reports angiographies of follow-up study at 0, 90, and 180 days. These results will be used for histological studies later.

5.2 Methods

5.2.1 Device preparation

5.2.1.1 Device fabrication

The SMP foam embolic device consisted of two major components which were the SMP foam and a delivery device with a local heating element.

5.2.1.1.1 Hybrid SMP foam

The hybrid SMP foam was combined with two types of SMP foam. 80TM SMP foam was used for outer shell which was a sphere with a cylindrical void. H60 SMP foam was used for inner core to fill the void volume in the outer shell. Figure 32 presented the process of the hybrid SMP foam fabrication.

The 80TM block out of bulk foam was mounted on rapid prototyping mill (MDX-540SA , Roland DGA Corporation), in Fig. 32 (a), and cut as the design, inner diameters are 3.0, 5.0, 7.5 mm and outer diameters are 6.6, 8.8, and 11.0 mm, respectively. The sets of outer shell (Fig. 32 (b)) were trimmed with scalpel and scissors. 4.0, 6.0, and 8.0 mm biopsy bunches (Sklar Tru-punchTM, Sklar Instruments), respectively, were used for H60 cylindrical cores over 10 mm in height. Under hot air station (210A, Beahm Designs, Inc.) at 120°C, the cores were gently compressed by hand down to approximately 80% of the diameter. The core was inserted into the void space of the outer shell. And the hot air station at 120°C allowed expansion of the H60 foam in the TM80foam. The cylindrical core of H60 which was not covered by the outer shell was trimmed with scissors. Then, the assembled hybrid foam (Fig. 32 (c)) was treated for post-process as the described protocol in Appendix B: the foam was radially compressed and expanded at 97°C using the crimper (SC150-42, Machine Solutions, Inc.). The foam was submerged 0.1 N HCl solution for etching and was cleaned in a solution comprised 80% of RO water and 20% (by weight or volume) of Contrad 70 Cleaner

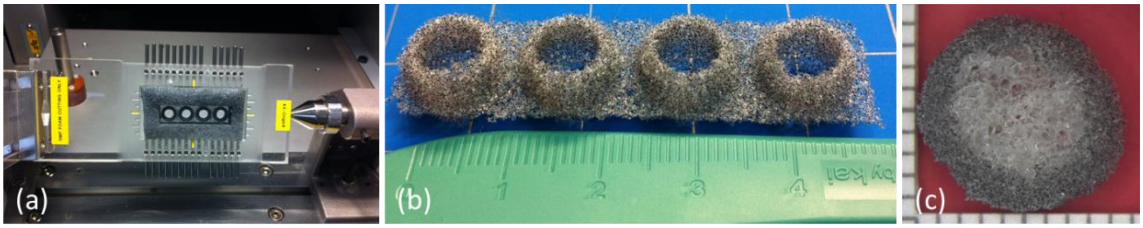

Figure 32 The fabrication of the hybrid SMP foam. (a) a block of 80TM SMP foam with a 4% by volume loading of tungsten particles was mounted to micro CNC milling machine, (b) 4 shells were cut out of the block (c) The assembled hybrid SMP foam with the H60 (a white core to fill the void volume of the shell) and the 80TM with 5% by volume loading of tungsten particles (the outer shell of the assembled foam).

5.2.1.1.2 Delivery device with a heating element

The delivery device was developed to deliver the compressed SMP foam through a tortuous pathway of a catheter and actuate the foam at an aneurysm using electro-resistive (Joule) heating. Figure 33 described the design and the fabrication process of the delivery device.

The 0.127 ± 0.008 mm diameter of nitinol wire (SE508, Nitinol Devices & Components, Inc.), which was the elastic core wire, was cut with 1300 ± 50 mm long. Resistive heating (Nikrothal 80, Kanthal) wire of 0.079 mm diameter was cut with 25-30 cm long and folded in half. The core wire and the folded point of the nichrome wire were gripped by a vise (Norvise, Norlander Company). And the nichrome wires were wounded over the elastic core wire. 4.5, 6.5, and 8.5 mm long of heating elements were prepared for this animal studies, in Fig. 33 (a). The lengths of the heater were dependent on the prepared SMP foam sizes (target diameters of 6, 8, and 10 mm diameter, respectively).

Figure 33 (b) presented a trapezoidal cylinder, which was cut by using the micro CNC milling, was inserted to the preparation of Fig. 33 (a). Table 4 shows the dimensions of the trapezoidal cylinder. In Fig. 33 (c), ultra violet (UV) curable epoxy (203A-CTH-F, Dymax Corp.) was smeared over the heating coil and in void area of the trapezoidal cylinder, and cured with UV light system (Ominicure 1000 system, Lumen Dynamics Group Inc.). Variation of sizes for the trapezoidal cylinder was designed to consider the final diameters of the compressed SMP foams.

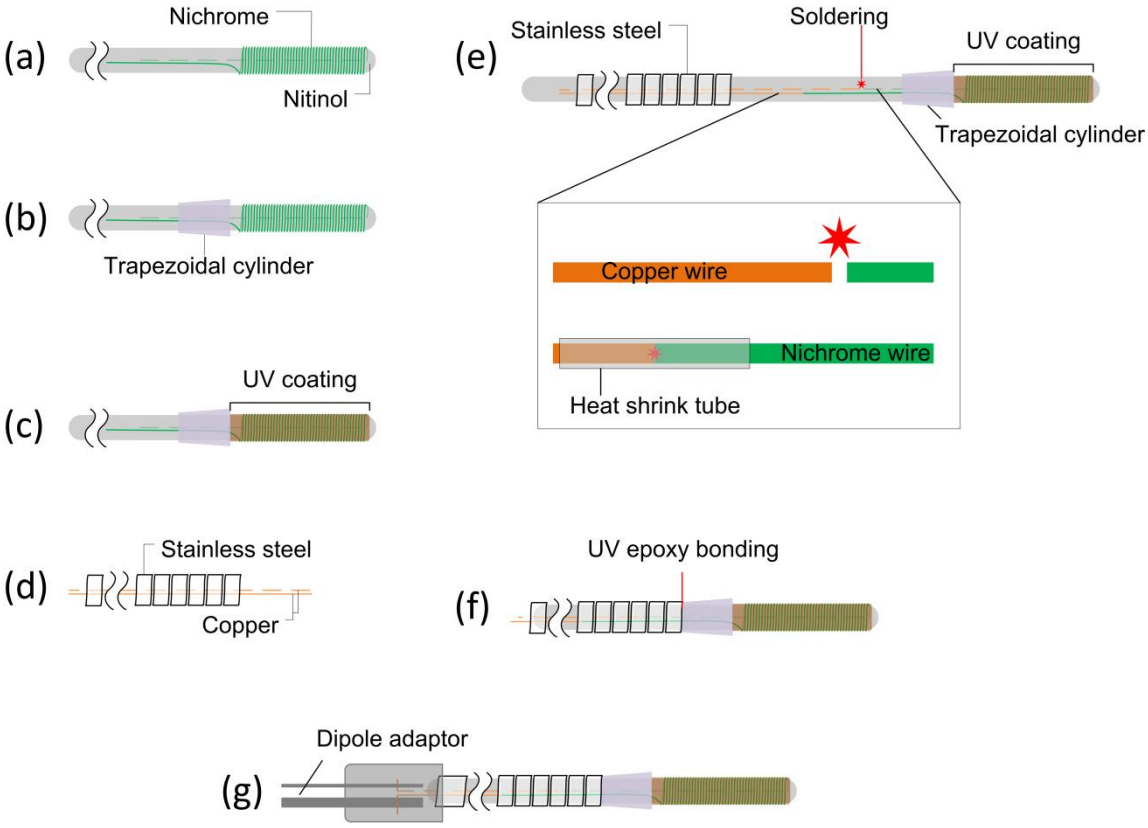

Figure 33 Fabrication process of the delivery device. The diagram is not to scale. The process of delivery device fabrication. (a) The wound nichrome wire creates a coil structure at the distal end of the device. (b) The trapezoidal cylinder is placed at the proximal end of the nichrome coils. (c) UV curable epoxy adheres the nichrome coil to the nitinol wire. (d) The wound SS wires coil shafts increase the flexibility necessary to navigate the tortuous vasculature. The copper wires pass through the inner lumen of the wound SS. (e) Each copper and nichrome wires are welded using a laser. One of line assemblies is sheeted or insulated for preventing an electric short. (f) The SS coils and the trapezoidal cylinder are connected by the laser welding or UV epoxy bonding. (g) The dipole adaptor is attached to the two copper wires. A power supply will be used to pass an electric current through the system.

Table 4 Dimensions of trapezoidal cylinders

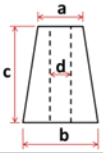	Trapezoidal cylinder (mm)		
	Small	Medium	Large
a	0.45	0.55	0.62
b	0.75	0.95	1.30
c	2.00	2.00	2.00
d	0.40	0.41	0.55

Stainless steel (SS) coils (Heraeus Medical Components, LLC) consisted of three parts over the length. Figure 34 presented schematic diagram of the coil. Proximal part was hypotube, middle part was ribbon wire coil, and distal part was round wire coil. Table 5 presented dimensions and material of the three types of SS coils. The proximal part of the hypotube was cut for adjusting the length of the final device. In Fig. 33 (d), two copper wires (BELDEN, Inc.) were inserted in to the SS coil. The copper wires were used conduit for current delivery over the delivery system. Lower resistance of the copper than one of nichrome wire allowed to minimize unnecessary heating. The coatings of the copper and nichrome wires were removed by a torch (ST2200T, Worthington Cylinder Corporation). The oxidized areas were cleaned by 200 and 300 grit sandpapers (McMaster-Carr Supply, Co.) and alcohol. Flux (7695A1, McMaster-

Carr Supply, Co.) was applied to the area of the soldering. The copper and the nichrome wires were soldered together in Fig. 33 (e).

Two soldering points were cleaned for removing residue of the flux and dried. Then heat shrink tubes (Advanced Polymers, Inc.) insulated over the soldering points to prevent leak of current when the device is on. After soldering, the SS coil was threaded over the bundle of copper and nichrome wires and covered to the trapezoidal cylinder. UV curable epoxy (203A-CTH-F, Dymax Corp.) was smeared between the SS coil and the trapezoidal cylinder and cured by the UV light system (Ominicure 1000 system, Lumen Dynamics Group Inc.). Figure 33 indicated the area of the UV bonding.

Finally, the copper wires at the proximal end were connected to dipole of a terminal (SMPW-CC-K-M, Omega Engineering, Inc.). The resistance of the heater was measured and the areas of UV coatings were examined under a microscope system (MX16, Leica Microsystems, Inc.). Approximately 150 cm long dispensing tubing (T1150, Qosina Corp.) was roll in approximately 25 cm diameter and used for storing the finished delivery device before SMP foam mounting.

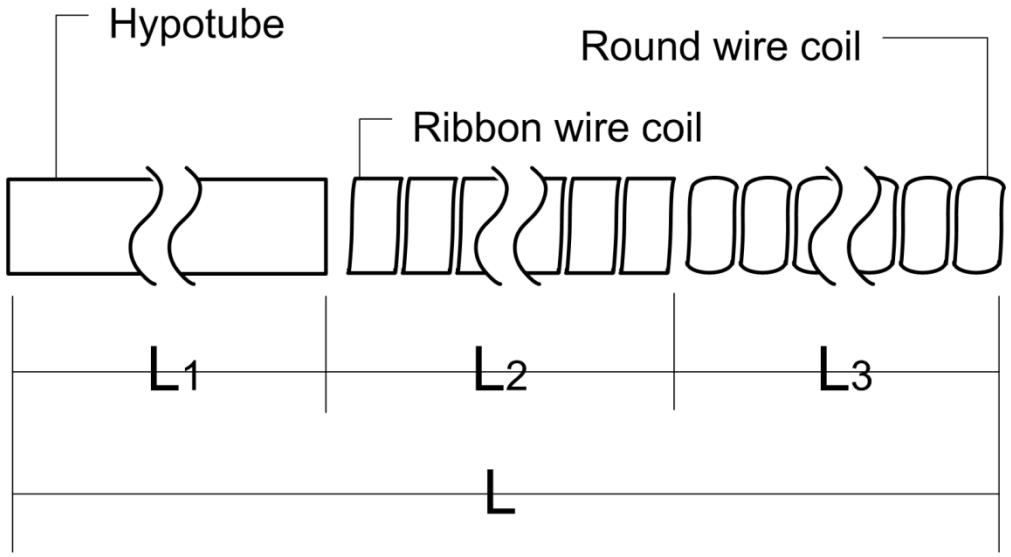

Figure 34 Schematic diagram of the stainless steel coils. The diagram is not to scale.

Table 5 Specification of stainless steel coils.

	Total length	Hypotube (SS304)			Ribbon wire coil (304V SS)					Round wire coil (304V SS)			
		L1	OD	ID	L2	OD	ID	Thickness	Width	L3	OD	ID	Diameter
Unit	(cm)	(cm)	(mm)	(mm)	(cm)	(mm)	(mm)	(mm)	(mm)	(cm)	(mm)	(mm)	(mm)
Small	180 ± 6	110	0.711	0.508	50 ± 2	0.771 ± 0.025	0.472 min	0.102	0.254	20 ± 2	0.771 ± 0.025	0.478 min	0.102
Medium	180 ± 6	110	0.902	0.660	50 ± 2	0.902 ± 0.025	0.597 min	0.127	0.305	20 ± 2	0.902 ± 0.025	0.612 min	0.127
Large	180 ± 6	110	1.080	0.838	50 ± 2	1.080 ± 0.025	0.622 min	0.203	0.305	20 ± 2	1.080 ± 0.025	0.632 min	0.203

5.2.1.1.3 SMP foam embolic device

In Fig. 35, the hybrid SMP foam was thread over the resistive heating coil of the delivery device at the distal end. The assembled distal end was placed in the crimper (SC150-42, Machine Solutions, Inc.) for 5 minutes at 97°C and radially compressed for 5 minutes at the same temperature. Then, the crimper was cool down to 22 ± 2°C during compressing up to 2 hours.

The resistance of the device was measured and compared with the prior measurement. If the difference was within ± 1 Ω, the SMP foam embolic device was placed in the dispensing tubing and stored in a 3.7 L plastic bag (Ziploc, S.C. Johnson & Son, Inc.) with dry agents (3492T34, McMaster-Carr Supply, Co.) before a sterilization process.

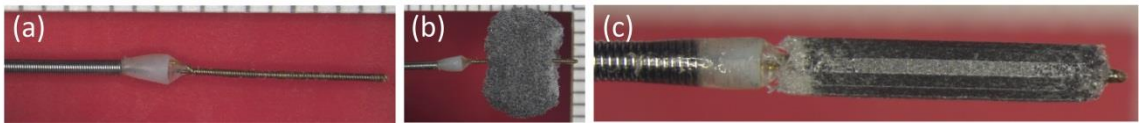

Figure 35 Fabrication process of SMP embolic Device. (a) Delivery device which had a resistive coil at the distal end. (b) The SMP foam was threaded over the device. (c) The foam was radially compressed using clinical stent compression device.

5.2.1.2 Sterilization

The prototype devices were sterilized by ethylene oxide (EtO). The individual sterilization bag had a SMP embolic device in the dispense tubing, two desiccant bags (3492T34, McMaster-Carr Supply, Co.), and a label for tracking the device. An EtO sterilization system (Anprolene AN74i, Andersen Product, Inc.) was used and the sterilization process was followed by the process of Table 6. The sterilized devices were stored at 20-22°C room.

Table 6 Sterilization process.

Order	Sterilization process
1	Inspect each Prototype and separate to be packaged individually
2	Put each prototype into a gas sterilization bag, add the sterile indicator.
3	Seal bag and inspect for thorough sealing around edges.
4	Using permanent marker, mark each individual package with: date, item name, and initials.
5	Put all the individually packaged prototypes into the ETO load bag and add the following: Biological Indicator, gas sterilization ampoule, dehumidifier chip.
6	Load bag into the ETO machine and operate machine according to manufacturer's instructions.
7	After the cycle is complete (26 hours total) remove the load bag from machine, and set the contents on open table to air out. At this time the items are not ready for use.
8	Remove the Biological Indicator and "crush" the liquid end of indicator. Using a permanent marker, initial and date the BI, along with the time, and then place it into the incubator. Allow 48 hours for the BI to be in the incubator before reading the pass/fail. If the indicator reads pass, the items are ready for use in the sterile field. If the indicator reads fail, the items must not be released until the machine has been checked and the entire process has been repeated.

5.2.2 Aneurysm model construction

Saccular aneurysms were created in 3-4 month old Yorkshire swine (31.1 ± 2.8 kg). Anesthesia was induced by intramuscular injection of ketamine, xylazine, and acepromazine (20 mg/kg, 2 mg/kg, and 0.2 mg/kg, respectively) with intubation and use of isoflurane for maintenance of anesthesia. Using sterile technique a 10 cm incision was made in the midline of the neck. After reflecting the sternocleidomastoid muscle medially, a 4 cm long segment of a vein was isolated and excised after a ligature was placed at each end of the segment.

5.2.2.1 Bifurcated aneurysm model

Figure 36 showed the process of the construction for a bifurcated aneurysm. In Fig. 36 (b) and (c), left CCA was shunted using a 5 mm diameter expanded polytetrafluorethlylene (ePTFE) graft (GORE-TEX® Vascular Grafts, W. L. Gore & Associates, Inc.). In Fig. 36 (d), a 4 cm long segment of the internal jugular vein was isolated and excised after a ligature was placed at each end of the segment. This segment of the vein was cleaned of adventitia. The segment of left CCA and the ePTFE graft were anastomosed in Fig. 36 (e). Then, right CCA was bifurcated using the assembled segment in Fig. 36 (e) and (f). Vascular clamps were placed at each end of the area of interest on the bifurcated artery to provide temporary vessel occlusion, in Fig. 36 (g). A 3-4 mm arteriotomy was made, and end-to-side anastomosis of the venous pouch to the apex of the bifurcated artery was performed using 7-0 prolene sutures. In Fig. 36 (h) and

(i), an aneurysm measuring 7-8 mm in diameter was created. After confirming hemostasis, the subcutaneous tissues and skin were sutured closed.

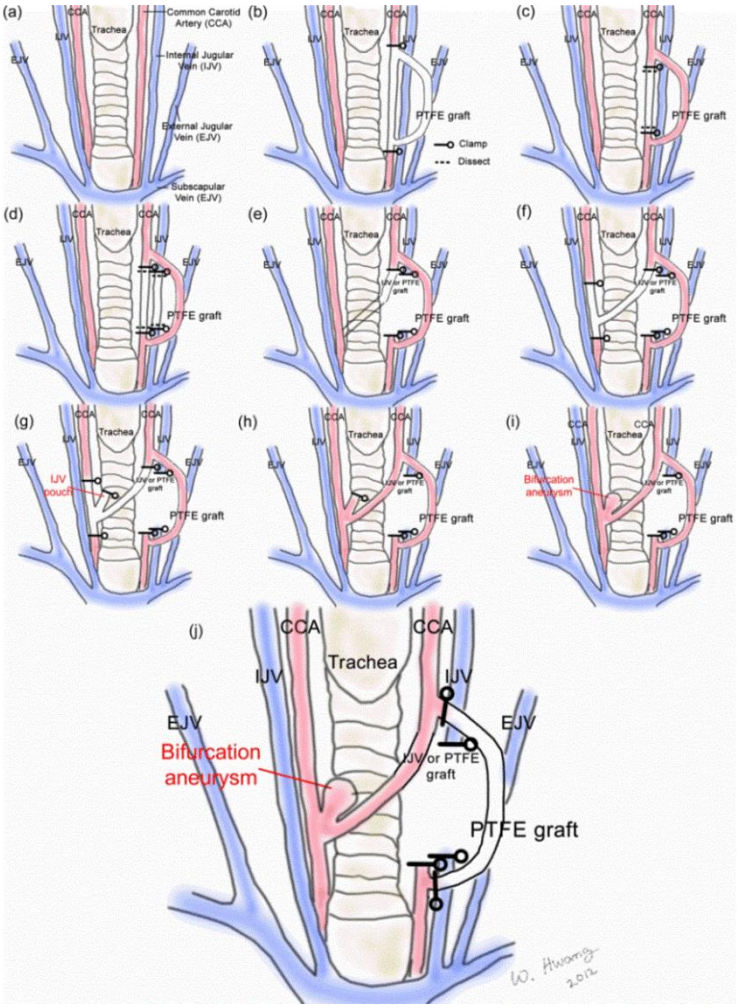

Figure 36 Process of the construction for a bifurcated aneurysm. (a)-(j) showed the process of the bifurcated aneurysm development, (a) Anatomy of a neck of swine, (b) Process of bypassing common carotid artery using ePTFE graft, (c) Bypassed common carotid artery using ePTFE graft, (d) Extraction of internal jugular vein for a pouch, (e) Construction of bifurcated parent vessel, (f) Anastomosis of the bifurcated CCA, (g) Anastomosis of vein pouch at the bifurcated vessel, (h) Ligature of the vein pouch, (i) Bulged vein pouch, and (j) Evaluated hemostasis and terminated the bypass of (c).

5.2.2.2 Sidewall aneurysm model

Figure 37 presented the process of the construction of saccular sidewall aneurysms at CCAs. In Fig. 37 (b), a 4 cm long segment of the external jugular vein was isolated and excised after a ligature was placed at each end of the segment. This segment of the vein will then be divided transversely, yielding two 2 cm open ended pouches. The segment was cleaned of adventitia in Fig. 37 (c). And the carotid arteries will then be exposed. In Fig. 37 (d), vascular clamps will be placed at each end of the area of interest on the artery to provide temporary vessel occlusion. A 3-4 mm arteriotomy was made in Fig. 37 (e), and end-to-side anastomosis of the venous pouch to the carotid artery was performed using 7-0 prolene sutures in Fig. 37 (f). In this fashion, an aneurysm measuring 7-8 mm in diameter was created on each carotid artery (e.g., two aneurysms per animal). After confirming hemostasis, the subcutaneous tissues and skin were sutured closed.

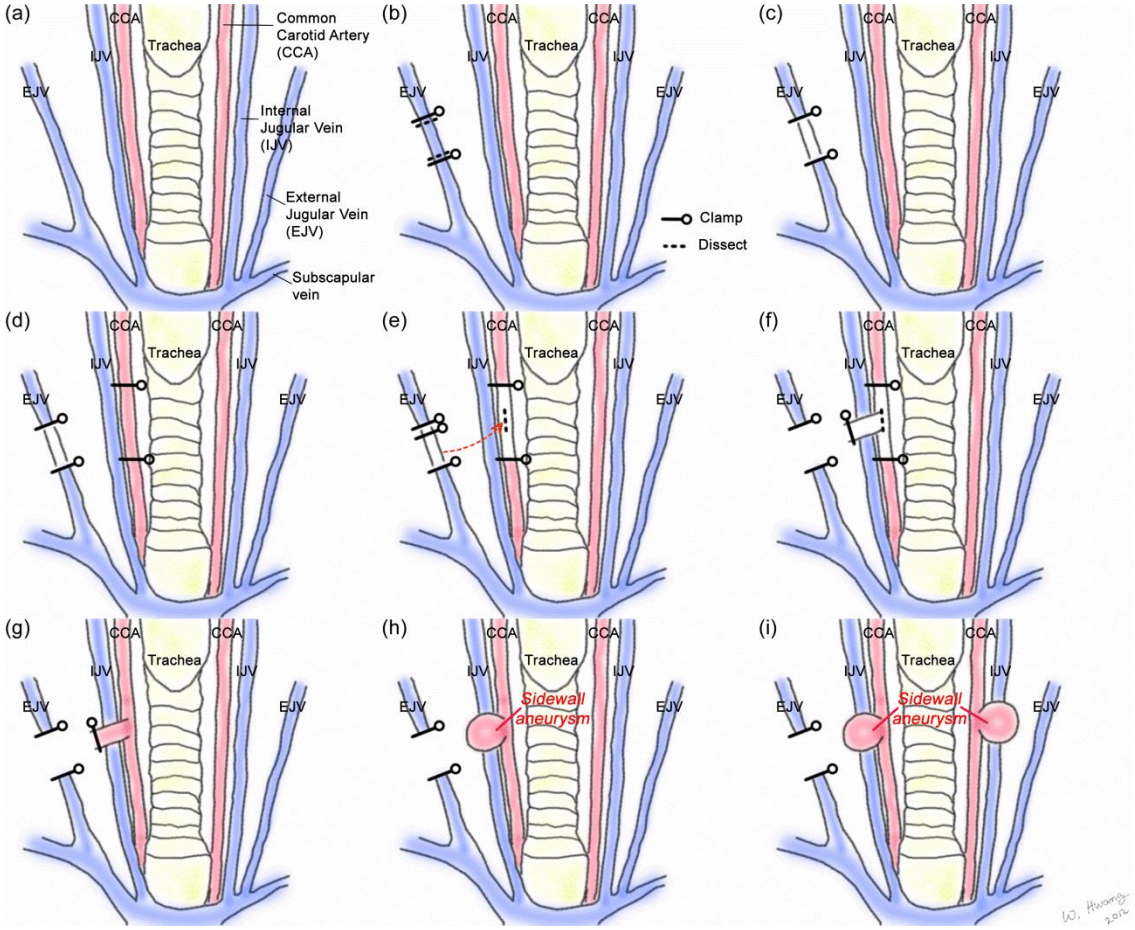

Figure 37 Process of the construction for side wall aneurysms. (a)-(i) showed the process of side wall aneurysm development. (a) Anatomy of a neck of swine, (b) Isolation and excision of external jugular vein, (c) Removing of adventitia, (d) Temporary clamp of CCA, (e) Arteriotomy on CCA, (f) Anastomosis of vein pouch at CCA, (g) ligature of the vein pouch, (h) Evaluation of hemostasis, and (i) Repeat of construction at the other CCA.

5.2.3 Device implant

Delivery and implant of the prototypes were performed under general endovascular method. An introducer sheath (Pinnacle® 6 Fr, Terumo) was inserted on the femoral artery of a swine under ultrasound guidance. A 0.035 inches guidewire (Glidewire®, Terumo) and a 5-6 Fr guiding catheter (Envoy® or Neuropath®, Codman & Shurtleff, Inc.) were passed through the introducer sheath with angiography.

Once the catheter was located in the aneurysm, the SMP foam device was passed through the pathway of the catheter to the aneurysm site. The distal end of the device, which was the compressed SMP foam, was located out of the catheter and positioned in the aneurysm.

Proximal end of the device was connected to the power supply (U3606A, Agilent Technologies, Inc.). A constant 0.3 ampere was applied to the system for actuating the compressed SMP foam. During the actuation of the foam, the aneurysm was continuously monitored under X-ray (Allura Xper FD Rotational Scan, Phillips). After a SMP foam occluded an aneurysm and the delivery device was then retracted into the catheter. The SMP foam was finally deployed. By injecting a contrast medium (Oxilan® 300, Guerbet), hemostasis was confirmed.

5.3 Results

5.3.1 Fabricated devices

Total 45 devices were fabricated and grouped in 3 different sizes of SMP foams. Small, Medium, and Large SMP foams were designed for 6 mm, 8 mm, and 10 mm diameters of aneurysms, respectively. Table 7 presented the details of the prototypes. Small, medium, and large groups of devices were compatible with a 4 Fr catheter with 0.97 mm ID, a 5 Fr catheter with 1.45 mm ID, and a 6 Fr catheter with 1.78 mm ID, respectively.

Table 7 Specifications of SMP embolic devices.

Group of Device	# of devices	SMP				Resistance of actuation device (Ω)
		Primary (expanded) shape in mm		Secondary (crimped) shape in mm		
		Diameter	Length	Diameter	Length	
1 (Small)	14	5.8 ± 0.4	5.3 ± 0.4	0.9 ± 0.0	6.5 ± 0.3	13.2 ± 0.6
2 (Medium)	15	7.7 ± 0.6	6.9 ± 0.4	1.2 ± 0.0	8.3 ± 0.4	15.3 ± 1.1
3 (Large)	16	10.2 ± 0.5	8.1 ± 1.3	1.5 ± 0.0	9.9 ± 1.2	22.0 ± 1.0

5.3.2 Bifurcated aneurysms and sidewall aneurysms

4 bifurcated aneurysms were constructed and 3 of them were implanted with the SMP embolic devices. Each aneurysm was measured from angiography and the diameters of aneurysms were used to select a proper size of SMP embolic device. Table 8 presented the dimensions of the bifurcated aneurysms and number of SMP foam in each aneurysm. Formation of clots in aneurysms of animal #4 and SMP implant was not tried.

The pigs with bifurcated aneurysms were not survived from aneurysm construction and implant of SMP foam. Necropsies were performed and no migration of SMP foams was confirmed.

Table 9 showed constructions of 17 sidewall aneurysms. An aneurysm was measured from angiography and the diameter of the aneurysm was used to select a proper size of SMP foam embolic device. Sidewall aneurysm study had two types of implants. One was SMP foam only implant and the other was a head to head implant, which was a SMP foam versus GDCs at each aneurysm.

For evaluating the implants, treated aneurysms were followed up 90 and 180 days. 3 out of 9 animals were sacrificed with complications.

Table 8 Specifications of bifurcated aneurysm models.

Animal #	Aneurysm dimensions in mm			# of SMP device per aneurysm	Duration of implant in days
	Diameter (a) 	Height (b) 	Neck (c) 		
1	3.92	5.45	n/a	1	3
2	7.00	8.00	n/a	1	0
3	8.02	8.12	3.47	1	0
4	n/a	7.00 – 8.00	n/a	n/a	n/a

Table 9 Specifications of sidewall aneurysm models.

Animal #	Location of common carortid artery	Aneurysm dimensions (mm)			# of implant device per aneurysm		Duration of implant (days)
		Diameter (a) 	Height (b) 	Neck (c) 	SMP	GDC	
1	Left	6.0	6.1	3.0	1	-	0
	Right	4.3	2.3	3.0	1	-	
2	Left	10.0	9.25	4.58	1	-	181
	Right	n/a	n/a	n/a	-	-	
3	Left	3.30	6.63	2.55	1	-	9
	Right	6.23	6.95	3.47	1	-	
4	Left	5.84	7.20	3.38	1	-	180
	Right	n/a	n/a	3.92	1	-	
5	Left	5.44	5.58	2.66	-	3	180
	Right	n/a	4.31	5.38	2	-	
6	Left	6.29	n/a	2.89	-	5	0
	Right	6.53	5.42	3.57	1	-	
7	Left	6.60	2.39	2.95	-	4	179
	Right	7.50	6.30	2.88	1	-	
8	Left	8.18	5.99	4.31	-	6	90
	Right	8.07	4.59	3.40	1	-	
9	Left	8.02	6.35	4.83	1	-	90
	Right	8.11	7.18	4.01	-	8	

5.3.3 Device implants and follows up

Figure 38 presented the SMP foam treatment of a bifurcated aneurysm in swine. In Fig. 38 (a) showed the constructed aneurysm by injection of a contrast medium. The deployed SMP foam was visible in x-ray (Fig. 38 (b)). The outer shell of the hybrid SMP Foam was composed of 4% volume Tungsten which was radiopaque material. The aneurysm was filled with a SMP foam and a contrast agent was injected to confirm hemostasis of interesting area (Fig. 38 (c)).

Figure 39 showed the process of SMP device delivery and deployment in a sidewall aneurysm under angiography. The compressed SMP foam and the delivery device were visible at x-ray. The actuation of the foam was also able to be observed by contrast change of the foam. A SMP foam was occluded the aneurysm in Fig. 39 (f).

Figure 40 showed gross images after a SMP and GDCs implant at aneurysms. Before closing skin and tissue of neck area, Fig. 40 were taken. Through semiopaque vein pouch, outer shell of the SMP foam was shown around darker area of Fig. 40 (a) and Fig. 40 (b) showed the treated aneurysm with multiple GDCs.

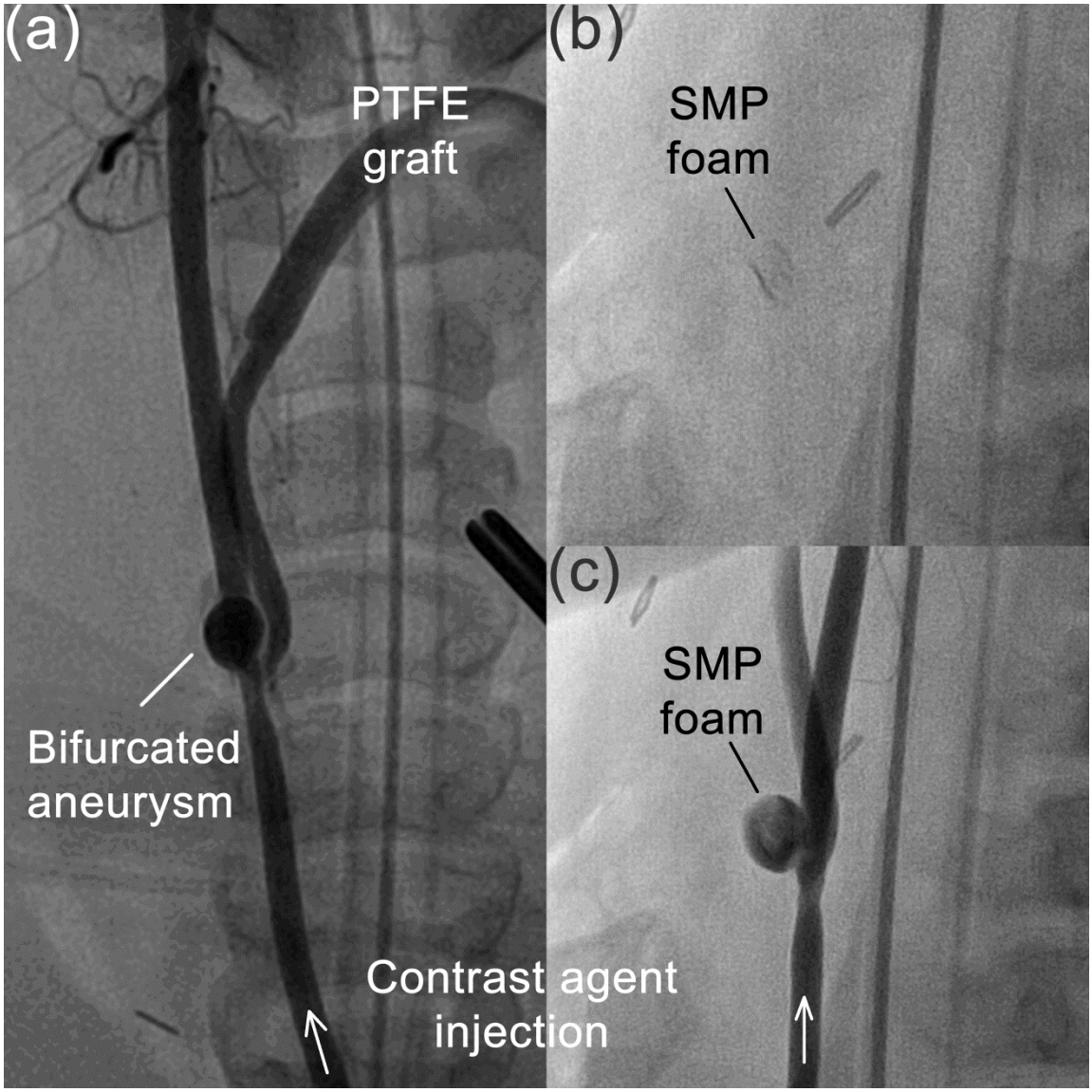

Figure 38 Treatment of a bifurcated aneurysm with SMP foam embolic device. (a) showed fluoroscopy of the bifurcated aneurysm in swine, (b) Implanted SMP foam at the aneurysm was shown. The darker outlier of the SMP foam was radiopaque part of the SMP foam embolic device, and (c) Hemostasis of the treated aneurysm was shown during injection of a contrast agent.

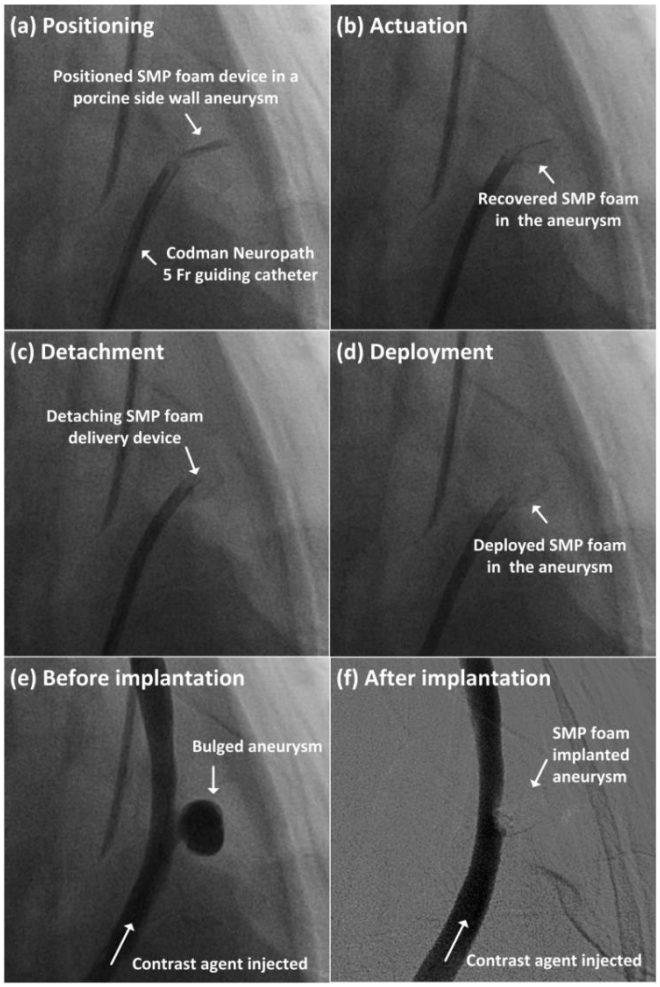

Figure 39 Fluoroscopy of SMP foam delivery and deployment in an animal study. (a) – (d) showed the process of delivery and deployment in a porcine sidewall aneurysm. (a) Codman Neuropath 5 Fr guiding catheter was placed into the aneurysm. The SMP foam device has been delivered and positioned in the aneurysm, along with the pathway of the catheter. (b) The heating element at the distal end of the delivery device actuated the crimped foam using Joule heating. (c) The crimped SMP foam attached on the delivery device by a friction. After a recovery of SMP foam, the decreased friction allowed the SMP foam to be detached from the delivery device. (d) The SMP foam was successfully expanded in the aneurysm. (e) The aneurysm was surgically developed at the left common carotid artery of a swine. Contrast agent was injected through the catheter. Diameters of aneurysm and aneurysm neck were analyzed to select an appropriated size of SMP foam device. (f) Fluoroscopy showed the aneurysm was successfully occluded with the SMP foam.

Both treated aneurysms were properly occluded with embolic materials and no rupture was observed. Sutures at the apex of each aneurysm were used for ligature to construct 7-8 mm height of aneurysms.

For 90 days, two swine were survived and sacrificed to evaluate SMP devices and compare with GDCs. Figure 5. 10 showed angiography of aneurysm construction (x.0), implants (x,1), and 90 days follow up (c) before sacrificing. Even though Fig. 41 (a.1) showed not fully occluded cavity, angiography after 90 days, in Fig. 41 (c), showed no aneurysm. Clean and smooth surface at the location of the implant was observed and the implanted SMP was not shown.

Four swine were survived and sacrificed 180 days later to evaluate SMP devices and compare with GDCs. Figure 42 showed angiography of the treated aneurysms with SMP and GDCs, panel (a) was immediately after implant and panel (b) was after 180 days implant.

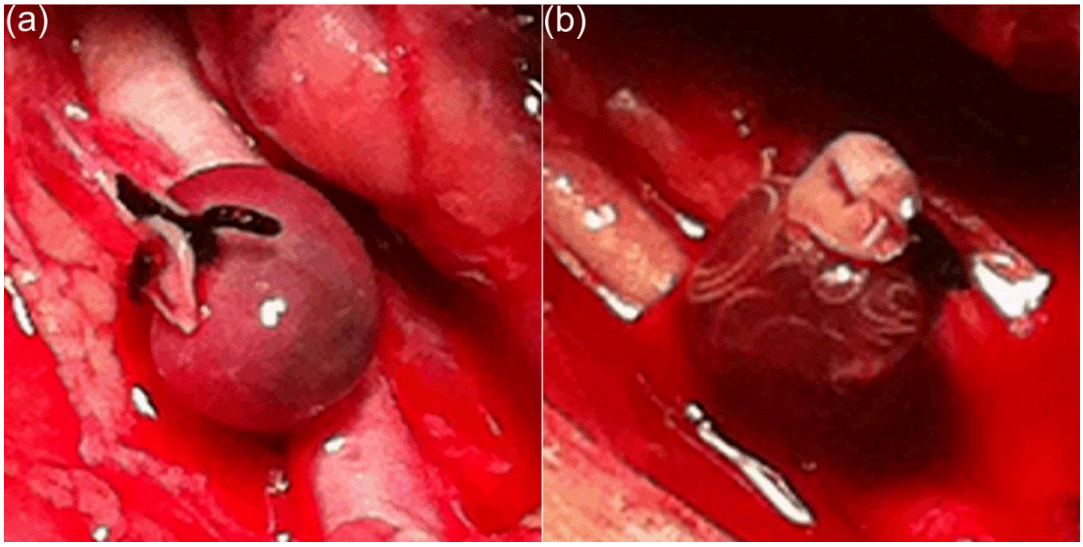

Figure 40 Gross images of treated sidewall aneurysms: (a) SMP foam implanted aneurysm and (b) GDCs implanted aneurysm.

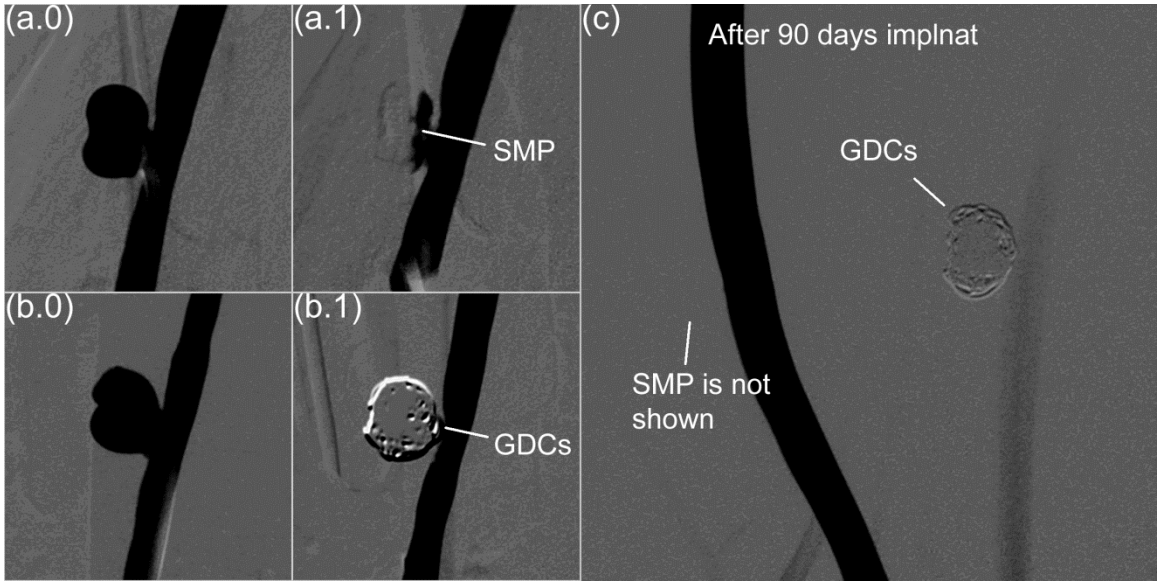

Figure 41 90 day follow up of SMP foam treated and GDCs treated side wall aneurysms at porcine common carotid arteries. (a.0) and (b.0) showed fluoroscopic imaging of carotid artery with vein pouch aneurysms model, (a.1) and (b.1) showed the treated aneurysms immediately after, and (c) Angiogram of CCA, which had aneurysms.

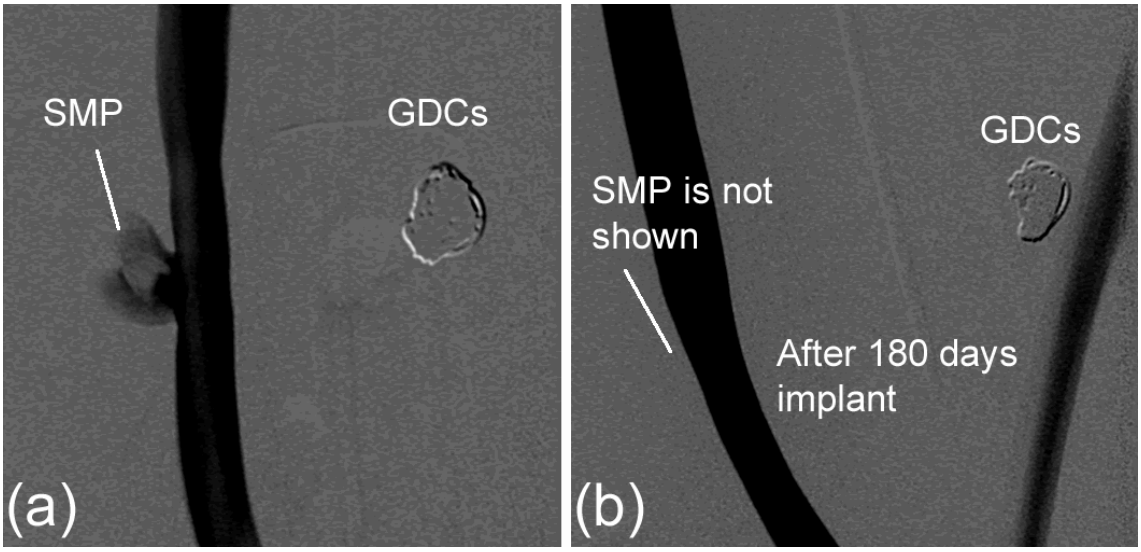

Figure 42 180 day follow up of SMP foam treated and GDCs treated side wall aneurysms at porcine common carotid arteries. (a) showed SMP and GDCs treated aneurysms at day 0, (b) showed the treated area after 180 days.

5.4 Discussion

45 SMP embolic devices in three different groups were fabricated for various sizes of the constructed aneurysms. 3-4 months old Yorkshire swine with 31.1 ± 2.8 kg was used for the studies. Diameters of each vein pouch from jugular veins were varied from a subject to a subject.

Even though 4 bifurcated aneurysms were constructed and treated with SMP foams, the three subjects were not wake up from anesthesia. Major possible cause was severe blood losses during construction of the aneurysm. Only one animal with the bifurcated aneurysm survived for 3 days.

Three out of nine swine with sidewall aneurysms were not survived for intended period. Two of them did not wake up from anesthesia. One had collapsed trachea and was not wake up from anesthesia. Another one was not wake up from anesthesia. One was diagnosed with pneumonia and euthanized. No direct relationships to the sacrifice were reported with respect to SMP foam implant.

The deliveries of the devise were effortlessly and very smoothly performed in catheters. Only one of the deliveries had a resistance of push-ability because the compressed SMP foam was contacted with saline and blood for more than 10 minutes before the delivery to an aneurysm. However, the device was delivered and deployed.

The process of actuation of the compressed SMP foam was visible under x-ray but the contrast of the foam was not clear. The heater at distal tip of the device initiated the actuation but full actuation of the foam also was induced by depression of glass transitional temperature. Parent artery was not occluded for the resistive heating

actuation and the energy delivered to the device was not efficient to overcome the dissipation. From fluoroscopic video analysis with high resolution monitor, the compressed outer shell was confirmed not fully to be expanded during the resistive heating.

Figure 43 showed that a possible problem of this prototype. SMP foams were degraded over the resistive heater. The composite of SMP foam, clots, and the surface of the resistive heater actually required a non-negligible pulling force (eg. tugging) for detachment of the SMP foam from the delivery device.

Therefore, convective energy may not be ideal source to actuate the foam fully in physiological system. However, in some case of the aneurysm with a very narrow neck, the placed catheter was ideally block the neck from the parent artery and the SMP foam was fully recovered to the primary shape (eg. expanded foam). The detachment was performed without noticeable tugging effort. A flow diverter or stopper during the actuation was recommended to the design of the delivery device.

The 16 SMP foam devices out of 16 attempts were successfully performed to occlude the aneurysms. 26 GDCs were required to fill the 5 aneurysms. Angiographies of 90 and 180 days did not show any SMP foams around treated aneurysms. This may be interpreted as the compressed outer shell SMP was fully expanded. And the contained tungsten in the unit volume of SMP was not noticeable under x-ray. Otherwise, Tungsten particles might be washed away or degraded.

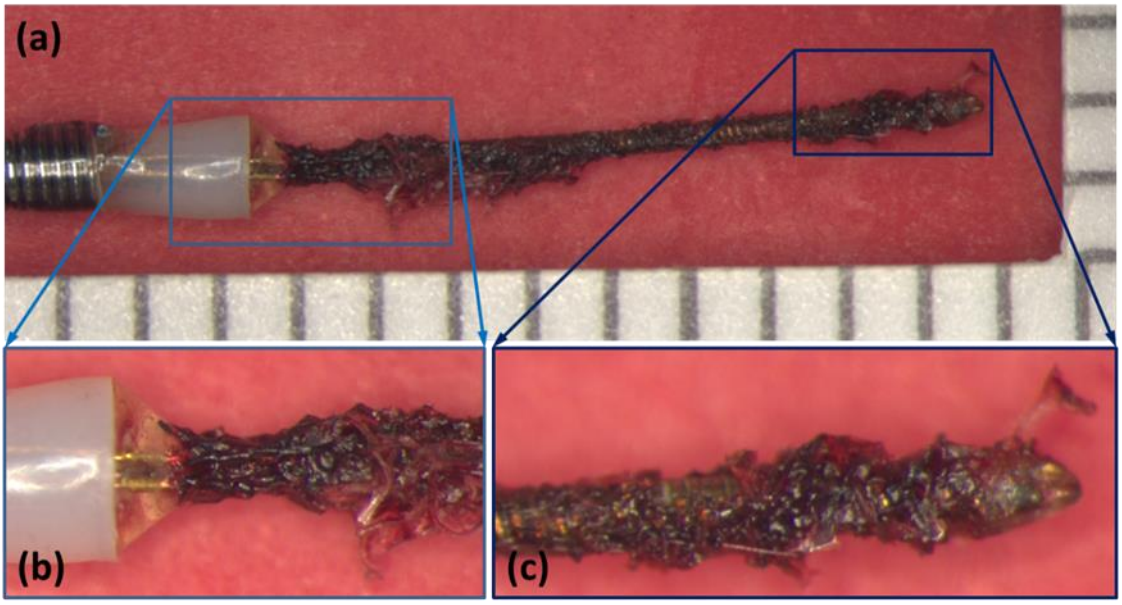

Figure 43 Image of the delivery device after treating the aneurysm. (a) Distal tip of the delivery device with the heating element. (b) and (c) are magnified images over the heating element.

5.5 Conclusion

This study confirmed the proof concept of SMP embolic device to treat saccular aneurysms. The delivery device was designed and fabricated for transcatheter delivery of a SMP foam. The SMP foam was re-designed using assembly of two different types of foams to satisfy minimum requirements of radiopacity and working time. Porcine saccular aneurysm models were established to test the prototypes. 90 and 190 days follow up studies also showed a potential of a device to treat saccular aneurysms.

Comparing number of device between SMPs and GDCs to treat aneurysm, SMP foam is a promising device to minimize the amount of time to treat aneurysm. However, current prototype was developed under three times scaled up pathway. Therefore, efforts to be compatible to microcatheter which are currently used in clinic are necessary. And will be an engineering challenge.

CHAPTER VI

CONCLUSION, LIMITATIONS, AND FUTURE WORK

6.1 Conclusion

This study aims a pilot study to prove the concept of the SMP embolic device to treat an intracranial aneurysm. As generally understanding, medical device development requires multiple iterations of research and development for a new or modified device. This study covers optimization efforts for early stage of SMP embolic prototype from a concept to an animal study.

Experimental setups were designed and manufactured, and the systems characterized the interests of this study, which are the stresses exerted by SMP foam expansion in an aneurysm, frictional loads between SMP foams and catheter, *in vitro* test for verification of transcatheter delivery and training of a physician, and validation of animal studies.

The use of oversized SMP foam as embolic devices can promote a more complete filling of an aneurysm while generating stresses that are well below the threshold that may cause the aneurysm wall to break. Thus, these foams may present reduced risk of rupture resulting from the embolic implant compared to microcoils.

Measurements of frictional loads between SMP foams and catheter are critical information for push-ability of device through a tortuous pathway of a catheter. The experimental system is fabricated to measure the frictions in the 37°C water bath with

idealized 3-dimensional pathway, which is developed to test the SMPs in a controlled condition. Material team in our research group synthesized various hydrophobicity of the SMP foams. 80TM composition of SMPs allowed 3 minutes working time, which is able to move SMP foam in a catheter.

In vitro experimental system showed that successful delivery and deployment of the prototypes in an aqueous environment proved deliverability of SMP embolic devices via catheter. This study reported full shape recovery by thermal actuation and fluoroscopic visualization was achieved by tungsten embedded SMP foam.

PDMS aneurysm models were fabricated to simulate the porcine aneurysm model. The model was extracted from 3D CT images and printed in 3D printer. The benchtop experimental system offered realistic environment for physician to test and evaluate the SMP devices. The feedback from physician through the mock system would allow for engineers to optimize the device for animal studies.

Animal studies confirmed the proof of concept about SMP embolic device to treat saccular aneurysms. The delivery device and SMP foams were visible under x-rays. All SMP foams, which were implanted to aneurysm, were successfully occluded aneurysms. No migration of SMP foams were observed for the entire studies.

From follow up studies of 90 and 180 days, there were no sign of blood flow in the aneurysms. Comparing with standard coils in clinic showed successful occlusion of aneurysms. The coiling methods needed multiple devices for occluding am aneurysm but A SMP foam device was used for treating an aneurysm.

6.2 Limitations and future work

Limitation of this study is approximately three times larger dimensions of the pathway. In human intracranial access, micro catheter less than 3 Fr are used but this study uses 5 and 6 Fr catheters. Therefore, the diameter of the SMP embolic device should be less than 450μm. This requires the followings: 1. Optimize the SMP foam geometry that can be compressed and maneuvered through a microcatheter; 2. Miniaturize the resistive heating delivery device to deliver the SMP foam through a microcatheter.

The current working time of the device is around 3 minutes to deliver the SMP foam. Ideal working time is infinite before full actuation of the device on demand. Practical working, however, have to be minimum 10 minutes. This working is based on hydrogel coil device in current clinic for aneurysm therapy. Thus, one of following challenges has to be addressed: a modification of chemical composition in the SMP foam, a mechanical sheath for constraining the premature actuation of the SMP foam, or a hydrophobic barrier of the compressed foam.

Even though the SMP foam is actuated and occludes the aneurysms, resistive heater presents a degradation of the SMP foam over the heater. This adverse effect disturbs smooth release of the SMP foam in an aneurysm. Desired temperature for the actuation is around 50°C without thermal damages of surrounding cells. The resistive heater is instantly able to increase temperature up to 200°C at the surface of the heater but blood circulations into aneurysm dissipate the energy.

Over-heating allows for the outer and mid volume of the foam to be reached to the target temperature but there are two challenges. First is the degradation of the SMP foam and the foam is stuck to the heater. Second is possibility of air embolization. Air embolization was not observed through this study. This is a severe problem to happen ischemic stroke. Following ideas may be a solution: 1. Prevent a blood flow during the actuation by a design of blood flow stopper at parent artery, 2. Change a heating mechanism from convection to conduction (ex. Radio frequency or laser heater).

Radiopacity of the proposed design satisfies the minimum requirement for this study. The aneurysm model is constructed at common carotid arteries. The surrounding area is only covered by soft tissue. Therefore, when the SMP embolic device is passed through human skull, the level of radiopacity may not be good enough to be visible under x-ray. And more radiopaque material embedded SMP foam is required to satisfy the followings: 1. Compressed and expanded SMP foam have to be visible under x-ray, 2. Compression ratio of the SMP foam allows to delivery device through a microcatheter.

In addition to aneurysm therapy with the SMP embolic device, other medical applications can be considered if the pathway to access an interesting area allows 4 Fr or higher Fr catheters. Especially, the application to vascular occlusion in perivascular therapy will be a good candidate. The raised challenges in this chapter will be significantly relieved. The SMP medical therapy is expected to be introduced in clinic, shortly.

REFERENCES

Abruzzo, T., G. G. Shengelaia, R. C. Dawson, 3rd, D. S. Owens, C. M. Cawley, et al. (1998). "Histologic and Morphologic Comparison of Experimental Aneurysms with Human Intracranial Aneurysms." AJNR Am J Neuroradiol **19**(7): 1309-1314.

Acevedo-Bolton, G., L.-D. Jou, B. P. Dispensa, M. T. Lawton, R. T. Higashida, et al. (2006). "Estimating the Hemodynamic Impact of Interventional Treatments of Aneurysms: Numerical Simulation with Experimental Validation: Technical Case Report." Neurosurgery **59**(2): E429-E430.

Ahuja, A. A., R. W. Hergenrother, C. M. Strother, A. A. Rappe, S. L. Cooper, et al. (1993). "Platinum Coil Coatings to Increase Thrombogenicity - a Preliminary-Study in Rabbits." American Journal of Neuroradiology **14**(4): 794-798.

Akkas, N. (1990). "Aneurysms as a Biomechanical Instability Problem." Biomechanical transport processes: 303-311.

Alderliesten, T., M. K. Konings and W. J. Niessen (2007). "Modeling Friction, Intrinsic Curvature, and Rotation of Guide Wires for Simulation of Minimally Invasive Vascular Interventions." IEEE Trans Biomed Eng **54**(1): 29-38.

Appelboom, G., K. Kadri, F. Hassan and X. Leclerc (2010). "Infectious Aneurysm of the Cavernous Carotid Artery in a Child Treated with a New-Generation of Flow-Diverting Stent Graft: Case Report." Neurosurgery **66**(3): E623-624; discussion E624.

Austin, G. M., W. Schievink and R. Williams (1989). "Controlled Pressure-Volume Factors in the Enlargement of Intracranial Aneurysms." Neurosurgery **24**(5): 722-730.

Bavinzski, G., A. al-Schameri, M. Killer, I. Schwendenwein, A. Gruber, et al. (1998). "Experimental Bifurcation Aneurysm: A Model for in Vivo Evaluation of Endovascular Techniques." Minim Invasive Neurosurg **41**(3): 129-132.

Bavinzski, G., B. Richling, B. R. Binder, A. Gruber, V. Talazoglu, et al. (1999). "Histopathological Findings in Experimental Aneurysms Embolized with Conventional and Thrombogenic/Antithrombolytic Guglielmi Coils." Minim Invasive Neurosurg **42**(4): 167-174.

Bederson, J. B., I. A. Awad, D. O. Wiebers, D. Piepgras, E. C. Haley, Jr., et al. (2000). "Recommendations for the Management of Patients with Unruptured Intracranial Aneurysms: A Statement for Healthcare Professionals from the Stroke Council of the American Heart Association." Stroke **31**(11): 2742-2750.

Bendszus, M., A. J. Bartsch and L. Solymosi (2007). "Endovascular Occlusion of Aneurysms Using a New Bioactive Coil: A Matched Pair Analysis with Bare Platinum Coils." Stroke **38**(10): 2855-2857.

Bertmer, M., A. Buda, I. Blomenkamp-Hofges, S. Kelch and A. Lendlein (2005). "Biodegradable Shape-Memory Polymer Networks: Characterization with Solid-State Nmr." Macromolecules **38**(9): 3793-3799.

Biondi, A., V. Janardhan, J. M. Katz, K. Salvaggio, H. A. Riina, et al. (2007). "Neuroform Stent-Assisted Coil Embolization of Wide-Neck Intracranial Aneurysms: Strategies in Stent Deployment and Midterm Follow-Up." Neurosurgery **61**(3): 460-468; discussion 468-469.

Bouzeghrane, F., O. Naggara, D. F. Kallmes, A. Berenstein, J. Raymond, et al. (2010). "In Vivo Experimental Intracranial Aneurysm Models: A Systematic Review." AJNR Am J Neuroradiol **31**(3): 418-423.

Brilstra, E. H., G. J. Rinkel, Y. van der Graaf, W. J. van Rooij and A. Algra (1999). "Treatment of Intracranial Aneurysms by Embolization with Coils: A Systematic Review." Stroke **30**(2): 470-476.

Brinjikji, W., H. J. Cloft and D. F. Kallmes (2009). "Difficult Aneurysms for Endovascular Treatment: Overwide or Undertall?" AJNR Am J Neuroradiol **30**(8): 1513-1517.

Brisman, J. L., Y. Niimi, J. K. Song and A. Berenstein (2005). "Aneurysmal Rupture During Coiling: Low Incidence and Good Outcomes at a Single Large Volume Center." Neurosurgery **57**(6): 1103-1109; discussion 1103-1109.

Brisman, J. L., J. K. Song and D. W. Newell (2006). "Cerebral Aneurysms." N Engl J Med **355**(9): 928-939.

Cekirge, H. S., I. Saatci, M. H. Ozturk, B. Cil, A. Arat, et al. (2006). "Late Angiographic and Clinical Follow-up Results of 100 Consecutive Aneurysms Treated with Onyx Reconstruction: Largest Single-Center Experience." Neuroradiology **48**(2): 113-126.

Choudhari, K. A., P. A. Flynn and S. C. McKinstry (2007). "Spontaneous Extrusion of Guglielmi Detachable Coils from Anterior Communicating Artery Aneurysm." Neurology India **55**(2): 148-150.

Cloft, H. J. and D. F. Kallmes (2002). "Cerebral Aneurysm Perforations Complicating Therapy with Guglielmi Detachable Coils: A Meta-Analysis." AJNR Am J Neuroradiol **23**(10): 1706-1709.

Criscione, J. C. (2003). "Rivlin's Representation Formula Is Ill-Conceived for the Determination of Response Functions Via Biaxial Testing." Journal of Elasticity **70**(1-3): 129-147.

Dandy, W. E. (1938). "Intracranial Aneurysm of the Internal Carotid Artery: Cured by Operation." Ann Surg **107**(5): 654-659.

David, G. and J. D. Humphrey (2003). "Further Evidence for the Dynamic Stability of Intracranial Saccular Aneurysms." Journal of Biomechanics **36**(8): 1143-1150.

Ferguson, G. G. (1972). "Physical Factors in the Initiation, Growth, and Rupture of Human Intracranial Saccular Aneurysms." Journal of Neurosurgery **37**(6): 666-677.

Finlay, H. M., P. Whittaker and P. B. Canham (1998). "Collagen Organization in the Branching Region of Human Brain Arteries." Stroke **29**(8): 1595-1601.

Fiorella, D., F. C. Albuquerque, H. Woo, P. A. Rasmussen, T. J. Masaryk, et al. (2006). "Neuroform in-Stent Stenosis: Incidence, Natural History, and Treatment Strategies." Neurosurgery **59**(1): 34-42; discussion 34-42.

Fiorella, D., M. E. Kelly, F. C. Albuquerque and P. K. Nelson (2009). "Curative Reconstruction of a Giant Midbasilar Trunk Aneurysm with the Pipeline Embolization Device." Neurosurgery **64**(2): 212-217; discussion 217.

Fiorella, D., H. H. Woo, F. C. Albuquerque and P. K. Nelson (2008). "Definitive Reconstruction of Circumferential, Fusiform Intracranial Aneurysms with the Pipeline Embolization Device." Neurosurgery **62**(5): 1115-1120; discussion 1120-1111.

Gaba, R. C., S. A. Ansari, S. S. Roy, F. A. Marden, M. A. Viana, et al. (2006). "Embolization of Intracranial Aneurysms with Hydrogel-Coated Coils Versus Inert Platinum Coils: Effects on Packing Density, Coil Length and Quantity, Procedure Performance, Cost, Length of Hospital Stay, and Durability of Therapy." Stroke **37**(6): 1443-1450.

George J. Hademenos, T. F. M. (1998). The Physics of Cerebrovascular Diseases: Biophysical Mechanisms of Development, Diagnosis and Therapy. New York, Springer-Verlag. 311.

German, W. J. and S. P. Black (1954). "Experimental Production of Carotid Aneurysms." N Engl J Med **250**(3): 104-106.

Geyik, S., O. Ertugrul, K. Yavuz, P. Geyik, I. Saatci, et al. (2010). "Comparison of Bioactive Coils and Bare Platinum Coils for Treatment of Intracranial Aneurysms: A Matched-Pair Analysis." Journal of Neurosurgery **112**(4): 709-713.

Guglielmi, G., C. Ji, T. F. Massoud, A. Kurata, S. P. Lownie, et al. (1994). "Experimental Saccular Aneurysms. Ii. A New Model in Swine." Neuroradiology **36**(7): 547-550.

Guglielmi, G., F. Vinuela, J. Dion and G. Duckwiler (1991a). "Electrothrombosis of Saccular Aneurysms Via Endovascular Approach. Part 2: Preliminary Clinical Experience." Journal of Neurosurgery **75**(1): 8-14.

Guglielmi, G., F. Vinuela, I. Sepetka and V. Macellari (1991b). "Electrothrombosis of Saccular Aneurysms Via Endovascular Approach. Part 1: Electrochemical Basis, Technique, and Experimental Results." Journal of Neurosurgery **75**(1): 1-7.

Gunnarsson, T., F. C. Tong, P. Klurfan, C. M. Cawley and J. E. Dion (2009). "Angiographic and Clinical Outcomes in 200 Consecutive Patients with Cerebral Aneurysm Treated with Hydrogel-Coated Coils." AJNR Am J Neuroradiol **30**(9): 1657-1664.

Harrod, C. G., B. R. Bendok and H. H. Batjer (2005). "Prediction of Cerebral Vasospasm in Patients Presenting with Aneurysmal Subarachnoid Hemorrhage: A Review." Neurosurgery **56**(4): 633-652.

Hassan, T., E. V. Timofeev, T. Saito, H. Shimizu, M. Ezura, et al. (2005). "A Proposed Parent Vessel Geometry-Based Categorization of Saccular Intracranial Aneurysms: Computational Flow Dynamics Analysis of the Risk Factors for Lesion Rupture." Journal of Neurosurgery **103**(4): 662-680.

Heistand, M. R., R. M. Pedrigi, S. L. Delange, J. Dziezyc and J. D. Humphrey (2005). "Multiaxial Mechanical Behavior of the Porcine Anterior Lens Capsule." Biomech Model Mechanobiol **4**(2-3): 168-177.

Henkes, H., S. Fischer, W. Weber, E. Miloslavski, S. Felber, et al. (2004). "Endovascular Coil Occlusion of 1811 Intracranial Aneurysms: Early Angiographic and Clinical Results." Neurosurgery **54**(2): 268-280; discussion 280-265.

Hirsch, J. A., B. R. Bendok, R. D. Paulsen, C. Cognard, J. Campos, et al. (2007). "Midterm Clinical Experience with a Complex-Shaped Detachable Platinum Coil System for the Treatment of Cerebral Aneurysms: Trufill Dcs Orbit Detachable Coil System Registry Interim Results." J Vasc Interv Radiol **18**(12): 1487-1494.

Horowitz, M., D. Samson and P. Purdy (1997). "Does Electrothrombosis Occur Immediately after Embolization of an Aneurysm with Guglielmi Detachable Coils?" AJNR Am J Neuroradiol **18**(3): 510-513.

Humphrey, J. D. (2002). Cardiovascular Solid Mechanics: Cells, Tissues, and Organs. New York, Springer-Verlag.

Humphrey, J. D. and S. Na (2002). "Elastodynamics and Arterial Wall Stress." Annals of Biomedical Engineering **30**(4): 509-523.

Humphrey, J. D. and C. A. Taylor (2008). "Intracranial and Abdominal Aortic Aneurysms: Similarities, Differences, and Need for a New Class of Computational Models." Annual Review of Biomedical Engineering **10**: 221-246.

Hung, E. J. and M. R. Botwin (1975). "Mechanics of Rupture of Cerebral Saccular Aneurysms." Journal of Biomechanics **8**(6): 385-392.

Hwang, W., Pooja Singhal, Matt W. Miller, and Duncan J. Maitland (2013). "In Vitro Study of Transcatheter Delivery of a Shape Memory Polymer Foam Embolic Device for Treating Cerebral Aneurysms." Journal of Medical Devices: (Accepted, February 5th, 2013).

Hwang, W., P. Singhal, M. W. Miller and D. J. Maitland (2013). "In Vitro Study of Transcatheter Delivery of a Shape Memory Polymer Foam Embolic Device for Treating Cerebral Aneurysms." Journal of Medical Devices **7**(2): 020932-020932.

Hwang, W., B. L. Volk, F. Akberali, P. Singhal, J. C. Criscione, et al. (2012). "Estimation of Aneurysm Wall Stresses Created by Treatment with a Shape Memory Polymer Foam Device." Biomech Model Mechanobiol **11**(5): 715-729.

Investigators, T. I. S. o. U. I. A. (1998). "Unruptured Intracranial Aneurysms — Risk of Rupture and Risks of Surgical Intervention." The New England Journal of Medicine **339**(24): 1725 - 1733.

Ionita, C. N., A. M. Paciorek, A. Dohatcu, K. R. Hoffmann, D. R. Bednarek, et al. (2009). "The Asymmetric Vascular Stent: Efficacy in a Rabbit Aneurysm Model." Stroke **40**(3): 959-965.

Ionita, C. N., A. M. Paciorek, K. R. Hoffmann, D. R. Bednarek, J. Yamamoto, et al. (2008). "Asymmetric Vascular Stent: Feasibility Study of a New Low-Porosity Patch-Containing Stent." Stroke **39**(7): 2105-2113.

Kallmes, D. F., M. K. Borland, H. J. Cloft, T. A. Altes, J. E. Dion, et al. (1998a). "In Vitro Proliferation and Adhesion of Basic Fibroblast Growth Factor-Producing Fibroblasts on Platinum Coils." Radiology **206**(1): 237-243.

Kallmes, D. F., Y. H. Ding, D. Dai, R. Kadirvel, D. A. Lewis, et al. (2007). "A New Endoluminal, Flow-Disrupting Device for Treatment of Saccular Aneurysms." Stroke **38**(8): 2346-2352.

Kallmes, D. F. and N. H. Fujiwara (2002). "New Expandable Hydrogel-Platinum Coil Hybrid Device for Aneurysm Embolization." American Journal of Neuroradiology **23**(9): 1580-1588.

Kallmes, D. F., D. Williams, H. J. Cloft, M. B. S. Lopes, G. R. Hankins, et al. (1998b). "Platinum Coil-Mediated Implantation of Growth Factor-Secreting Endovascular Tissue Grafts: An in Vivo Study." Radiology **207**(2): 519-523.

Kantor, B., K. Ashai, D. R. Holmes, Jr. and R. S. Schwartz (1999). "The Experimental Animal Models for Assessing Treatment of Restenosis." Cardiovasc Radiat Med **1**(1): 48-54.

Keedy, A. (2006). "An Overview of Intracranial Aneurysms." Mcgill J Med **9**(2): 141-146.

Kilic, T., M. Sohrabifar, O. Kurtkaya, O. Yildirim, I. Elmaci, et al. (2005). "Expression of Structural Proteins and Angiogenic Factors in Normal Arterial and Unruptured and Ruptured Aneurysm Walls." Neurosurgery **57**(5): 997-1006.

Konings, M. K., E. B. van de Kraats, T. Alderliesten and W. J. Niessen (2003). "Analytical Guide Wire Motion Algorithm for Simulation of Endovascular Interventions." Medical & Biological Engineering & Computing **41**(6): 689-700.

Kwan, E. S. K., C. B. Heilman, W. A. Shucart and R. P. Klucznik (1991). "Enlargement of Basilar Artery Aneurysms Following Balloon Occlusion - Water-Hammer Effect - Report of 2 Cases." Journal of Neurosurgery **75**(6): 963-968.

Kyriacou, S. K. and J. D. Humphrey (1996). "Influence of Size, Shape and Properties on the Mechanics of Axisymmetric Saccular Aneurysms." Journal of Biomechanics **29**(8): 1015-1022.

Lai, W. M., Rubin David, Krempl Erhard (1993). Introduction to Continuum Mechanics. Woburn, Butterworth-Heinemann.

Lendlein, A. and R. Langer (2002). "Biodegradable, Elastic Shape-Memory Polymers for Potential Biomedical Applications." Science **296**(5573): 1673-1676.

Leonardi, M., M. Dall'olio, C. Princiotta and L. Simonetti (2008). "Treatment of Carotid Siphon Aneurysms with a Microcell Stent. A Case Report." Interv Neuroradiol **14**(4): 429-434.

Liang, G., X. Gao, Z. Li, X. Wei and H. Xue (2010). "Neuroform Stent-Assisted Coiling of Intracranial Aneurysms: A 5 Year Single-Center Experience and Follow-Up." Neurol Res **32**(7): 721-727.

Liu, Y., Gall, K., Dunn, M.L., McCluskey, P., Shandas, R. (2003). "Shape Memory Polymers for Medical Applications." Advanced Materials and Processes **161**(12): 31.

Lubicz, B., A. Bandeira, M. Bruneau, A. Dewindt, D. Baleriaux, et al. (2009). "Stenting Is Improving and Stabilizing Anatomical Results of Coiled Intracranial Aneurysms." Neuroradiology **51**(6): 419-425.

Lylyk, P., C. Miranda, R. Ceratto, A. Ferrario, E. Scrivano, et al. (2009). "Curative Endovascular Reconstruction of Cerebral Aneurysms with the Pipeline Embolization Device: The Buenos Aires Experience." Neurosurgery **64**(4): 632-642; discussion 642-633; quiz N636.

MacDonald, D. J., H. M. Finlay and P. B. Canham (2000). "Directional Wall Strength in Saccular Brain Aneurysms from Polarized Light Microscopy." Annals of Biomedical Engineering **28**(5): 533-542.

Maitland, D. J., W. Small IV, P. Singhal, W. Hwang, J. N. Rodriguez, et al. (2009). "Design and Realization of Biomedical Devices Based on Shape Memory Polymers." Material Research Society Symposium **1190**(NN06): 1-13.

Maitland, D. J., W. t. Small, J. M. Ortega, P. R. Buckley, J. Rodriguez, et al. (2007). "Prototype Laser-Activated Shape Memory Polymer Foam Device for Embolic Treatment of Aneurysms." J Biomed Opt **12**(3): 030504.

Massoud, T. F., C. Ji, G. Guglielmi, F. Vinuela and J. Robert (1994). "Experimental Models of Bifurcation and Terminal Aneurysms: Construction Techniques in Swine." AJNR Am J Neuroradiol **15**(5): 938-944.

Melkerson, M. N. (2009). 510(K) Approval of Medshape Solutions Smp Shoulder Anchor.

Metcalfe, A., A. C. Desfaits, I. Salazkin, L. Yahia, W. M. Sokolowski, et al. (2003). "Cold Hibernated Elastic Memory Foams for Endovascular Interventions." Biomaterials **24**(3): 491-497.

Mitchell, P., A. Gholkar, R. R. Vindlacheruvu and A. D. Mendelow (2004). "Unruptured Intracranial Aneurysms: Benign Curiosity or Ticking Bomb?" Lancet Neurol **3**(2): 85-92.

Molyneux, A. J., S. Cekirge, I. Saatci and G. Gal (2004). "Cerebral Aneurysm Multicenter European Onyx (Cameo) Trial: Results of a Prospective Observational Study in 20 European Centers." AJNR Am J Neuroradiol **25**(1): 39-51.

Murayama, Y., Y. L. Nien, G. Duckwiler, Y. P. Gobin, R. Jahan, et al. (2003). "Guglielmi Detachable Coil Embolization of Cerebral Aneurysms: 11 Years' Experience." Journal of Neurosurgery **98**(5): 959-966.

Murayama, Y., F. Vinuela, G. R. Duckwiler, Y. P. Gobin and G. Guglielmi (1999a). "Embolization of Incidental Cerebral Aneurysms by Using the Guglielmi Detachable Coil System." Journal of Neurosurgery **90**(2): 207-214.

Murayama, Y., F. Vinuela, Y. Suzuki, Y. Akiba, A. Ulihoa, et al. (1999b). "Development of the Biologically Active Guglielmi Detachable Coil for the Treatment of Cerebral Aneurysms. Part Ii: An Experimental Study in a Swine Aneurysm Model." AJNR Am J Neuroradiol **20**(10): 1992-1999.

Murayama, Y., F. Vinuela and S. Tateshima (2002). "Matrix: New Bio-Absorbable Polymeric Coils for the Treatment of Intracranial Aneurysms." Developments in Neuroscience, Proceedings **1247**: 119-126.

Nelken, N., M. T. Caps and P. A. Schneider (2005). "Establishing Sheath Access for Carotid Interventions: Tips and Pitfalls." Perspect Vasc Surg Endovasc Ther **17**(2): 97-109.

Neves-Junior, W. F. P., M. Ferreira, M. C. O. Alves, C. F. O. Graeff, M. Mulato, et al. (2006). "Influence of Fabrication Process on the Final Properties of Natural-Rubber Latex Tubes for Vascular Prosthesis." Brazilian Journal of Physics **36**(2B): 586-591.

Ogata, N., K. Goto and K. Uda (1997). "An Evaluation of the Physical Properties of Current Microcatheters and Guidewires. The Development of the "Catheter-Glide Approach" in Response to Weaknesses of Current Materials." Interv Neuroradiol **3**(1): 65-80.

Ortega, J., D. Maitland, T. Wilson, W. Tsai, O. Savas, et al. (2007). "Vascular Dynamics of a Shape Memory Polymer Foam Aneurysm Treatment Technique." Annals of Biomedical Engineering **35**(11): 1870-1884.

Ortega, J. M., J. Hartman, J. N. Rodriguez and D. J. Maitland (2013). "Virtual Treatment of Basilar Aneurysms Using Shape Memory Polymer Foam." Annals of Biomedical Engineering.

Patriciu, A., D. Mazilu, D. Petrisor, H. S. Bagga, L. Kavoussi, et al. (2005). "A Computer Assisted Method for Guide-Wire and Catheter Evaluation." 2005 27th Annual International Conference of the IEEE Engineering in Medicine and Biology Society, Vols 1-7: 436-439

7776.

Piske, R. L., L. H. Kanashiro, E. Paschoal, C. Agner, S. S. Lima, et al. (2009). "Evaluation of Onyx Hd-500 Embolic System in the Treatment of 84 Wide-Neck Intracranial Aneurysms." Neurosurgery **64**(5): E865-875; discussion E875.

Rinkel, G. J., M. Djibuti, A. Algra and J. van Gijn (1998). "Prevalence and Risk of Rupture of Intracranial Aneurysms: A Systematic Review." Stroke **29**(1): 251-256.

Rodriguez-Feo, J. A., J. P. Sluijter, D. P. de Kleijn and G. Pasterkamp (2005). "Modulation of Collagen Turnover in Cardiovascular Disease." Curr Pharm Des **11**(19): 2501-2514.

Rodriguez, J. N., F. J. Clubb, T. S. Wilson, M. W. Miller, T. W. Fossum, et al. (2014). "In Vivo Response to an Implanted Shape Memory Polyurethane Foam in a Porcine Aneurysm Model." J Biomed Mater Res A **102**(5): 1231-1242.

Rodriguez, J. N., Y. J. Yu, M. W. Miller, T. S. Wilson, J. Hartman, et al. (2012). "Opacification of Shape Memory Polymer Foam Designed for Treatment of Intracranial Aneurysms." Annals of Biomedical Engineering **40**(4): 883-897.

Schievink, W. I. (1997). "Intracranial Aneurysms." N Engl J Med **336**(1): 28-40.

Schmidt, W., P. Lanzer, P. Behrens, L. D. Topoleski and K. P. Schmitz (2009). "A Comparison of the Mechanical Performance Characteristics of Seven Drug-Eluting Stent Systems." Catheter Cardiovasc Interv **73**(3): 350-360.

Schroder, J. (1993a). "The Mechanical Properties of Guidewires. Part I: Stiffness and Torsional Strength." Cardiovasc Intervent Radiol **16**(1): 43-46.

Schroder, J. (1993b). "The Mechanical Properties of Guidewires. Part Iii: Sliding Friction." Cardiovasc Intervent Radiol **16**(2): 93-97.

Scott, S., G. G. Ferguson and M. R. Roach (1972). "Comparison of the Elastic Properties of Human Intracranial Arteries and Aneurysms." Can J Physiol Pharmacol **50**(4): 328-332.

Serbinenko, F. A. (1971). "Catheterization and Occlusion of Major Cerebral Vessels and Prospects for the Development of Vascular Neurosurgery." Vopr Neirokhir **35**(5): 17-27.

Serbinenko, F. A. (1974). "Balloon Catheterization and Occlusion of Major Cerebral Vessels." J Neurosurg **41**(2): 125-145.

Shah, A. D. and J. D. Humphrey (1999). "Finite Strain Elastodynamics of Intracranial Saccular Aneurysms." Journal of Biomechanics **32**(6): 593-599.

Simkins, T. E., Stehbens, W.E. (1973). "Vibrational Behavior of Arterial Aneurysms." Letters in Applied and Engineering Sciences **1**: 85-100.

Singhal, P., A. Boyle, M. L. Brooks, S. Infanger, S. Letts, et al. (2013). "Controlling the Actuation Rate of Low-Density Shape-Memory Polymer Foams in Water." Macromolecular Chemistry and Physics **214**(11): 1204-1214.

Singhal, P., J. N. Rodriguez, W. Small, S. Eagleston, J. Van de Water, et al. (2012). "Ultra Low Density and Highly Crosslinked Biocompatible Shape Memory Polyurethane Foams." J Polym Sci B Polym Phys **50**(10): 724-737.

Small, W., P. R. Buckley, T. S. Wilson, W. J. Benett, J. Hartman, et al. (2007). "Shape Memory Polymer Stent with Expandable Foam: A New Concept for Endovascular Embolization of Fusiform Aneurysms." IEEE Trans Biomed Eng **54**(6 Pt 2): 1157-1160.

Small, W., P. Singhal, T. S. Wilson and D. J. Maitland (2010). "Biomedical Applications of Thermally Activated Shape Memory Polymers." Journal of Materials Chemistry **20**(17): 3356-3366.

Stehbens, W. E. (1990). "Pathology and Pathogenesis of Intracranial Berry Aneurysms." Neurol Res **12**(1): 29-34.

Steiger, H. J., R. Aaslid, S. Keller and H. J. Reulen (1989). "Strength, Elasticity and Viscoelastic Properties of Cerebral Aneurysms." Heart Vessels **5**(1): 41-46.

Suzuki, J. and H. Ohara (1978). "Clinicopathological Study of Cerebral Aneurysms. Origin, Rupture, Repair, and Growth." Journal of Neurosurgery **48**(4): 505-514.

Szikora, I., Z. Berentei, Z. Kulcsar, M. Marosfoi, Z. S. Vajda, et al. (2010). "Treatment of Intracranial Aneurysms by Functional Reconstruction of the Parent Artery: The Budapest Experience with the Pipeline Embolization Device." AJNR Am J Neuroradiol **31**(6): 1139-1147.

Tamatani, S., T. Ozawa, T. Minakawa, S. Takeuchi, T. Koike, et al. (1997). "Histological Interaction of Cultured Endothelial Cells and Endovascular Embolic Materials Coated with Extracellular Matrix." Journal of Neurosurgery **86**(1): 109-112.

Toth, M., G. L. Nadasy, I. Nyary, T. Kerenyi, M. Orosz, et al. (1998). "Sterically Inhomogenous Viscoelastic Behavior of Human Saccular Cerebral Aneurysms." Journal of Vascular Research **35**(5): 345-355.

Tummala, R. P., R. M. Chu, M. T. Madison, M. Myers, D. Tubman, et al. (2001). "Outcomes after Aneurysm Rupture During Endovascular Coil Embolization." Neurosurgery **49**(5): 1059-1066; discussion 1066-1057.

Ujiie, H., K. Sato, H. Onda, A. Oikawa, M. Kagawa, et al. (1993). "Clinical Analysis of Incidentally Discovered Unruptured Aneurysms." Stroke **24**(12): 1850-1856.

Veznedaroglu, E., C. J. Koebbe, A. Siddiqui and R. H. Rosenwasser (2008). "Initial Experience with Bioactive Cerecyte Detachable Coils: Impact on Reducing Recurrence Rates." Neurosurgery **62**(4): 799-805; discussion 805-796.

Wakhloo, A. K., M. J. Gounis, J. S. Sandhu, N. Akkawi, A. E. Schenck, et al. (2007). "Complex-Shaped Platinum Coils for Brain Aneurysms: Higher Packing Density, Improved Biomechanical Stability, and Midterm Angiographic Outcome." AJNR Am J Neuroradiol **28**(7): 1395-1400.

Wardlaw, J. M. and P. M. White (2000). "The Detection and Management of Unruptured Intracranial Aneurysms." Brain **123**: 205-221.

Wiebers, D., J. P. Whisnant, J. Huston, I. Meissner, R. D. Brown, et al. (2003). "Unruptured Intracranial Aneurysms: Natural History, Clinical Outcome, and Risks of Surgical and Endovascular Treatment." Lancet **362**(9378): 103-110.

Wijdicks, E. F., D. F. Kallmes, E. M. Manno, J. R. Fulgham and D. G. Piepgras (2005). "Subarachnoid Hemorrhage: Neurointensive Care and Aneurysm Repair." Mayo Clin Proc **80**(4): 550-559.

Willinsky, R. A. (1999). "Detachable Coils to Treat Intracranial Aneurysms." CMAJ **161**(9): 1136.

Wilson, T. S., and D. J. Maitland. (2005). Shape Memory Polymer Foams for Endovascular Therapies. U.S. Patent.

Wilson, T. S., J. P. Bearinger, J. L. Herberg, J. E. Marion, W. J. Wright, et al. (2007). "Shape Memory Polymers Based on Uniform Aliphatic Urethane Networks." Journal of Applied Polymer Science **106**(1): 540-551.

Yang, B., W. M. Huang, C. Li, C. M. Lee and L. Li (2004). "On the Effects of Moisture in a Polyurethane Shape Memory Polymer." Smart Materials & Structures **13**(1): 191-195.

Yu, Y. J., K. Hearon, T. S. Wilson and D. J. Maitland (2011). "The Effect of Moisture Absorption on the Physical Properties of Polyurethane Shape Memory Polymer Foams." Smart Materials & Structures **20**(8).

Zhang, B. P., K. Fugleholm, L. B. Day, S. Ye, R. O. Weller, et al. (2003). "Molecular Pathogenesis of Subarachnoid Haemorrhage." International Journal of Biochemistry & Cell Biology **35**(9): 1341-1360.

Zoarski, G. H., J. M. Mathis and J. R. Hebel (1998). "Performance Characteristics of Microcatheter Systems in a Standardized Tortuous Pathway." AJNR Am J Neuroradiol **19**(8): 1571-1576.

APPENDIX A

DERIVATION OF ANALYTICAL SOLUTION IN CYLINDRICAL COORDINATION USING MOONEY-RIVLIN

Position vector field in cylindrical coordinate

$$r = r(R), \quad \theta = \Theta + \gamma Z, \quad z = \Lambda Z$$

Position in reference (unloaded) configuration: (R, Θ, Z)

Position in current (loaded) configuration: (r, θ, z)

In our study, latex aneurysm model is assumed as pure inflation and extension. Therefore, there is no torsion term in circumferential direction.

$$r = r(R), \quad \theta = \Theta, \quad z = \Lambda Z$$

Deformation gradient tensor $\mathbf{F}$

$$\mathbf{F} = \begin{bmatrix} \frac{\partial r}{\partial R} & \frac{1}{R}\frac{\partial r}{\partial \Theta} & \frac{\partial r}{\partial Z} \\ r\frac{\partial \theta}{\partial R} & \frac{r}{R}\frac{\partial \theta}{\partial \Theta} & r\frac{\partial \theta}{\partial Z} \\ \frac{\partial z}{\partial R} & \frac{1}{R}\frac{\partial z}{\partial \Theta} & \frac{\partial z}{\partial Z} \end{bmatrix} = \begin{bmatrix} \frac{\partial r}{\partial R} & 0 & 0 \\ 0 & \frac{r}{R} & 0 \\ 0 & 0 & \Lambda \end{bmatrix}$$

$$\mathbf{F} = \mathbf{F}^{\mathrm{T}}$$

Enforcing incompressibility, $\det\mathbf{F} \equiv 1$

$$\frac{\partial r}{\partial R} \times \frac{r}{R} \times \Lambda = 1 \quad \Rightarrow \quad \frac{\partial r}{\partial R} = \frac{R}{\Lambda r}$$

$$\mathbf{F} = \begin{bmatrix} \frac{R}{\Lambda r} & 0 & 0 \\ 0 & \frac{r}{R} & 0 \\ 0 & 0 & \Lambda \end{bmatrix}$$

We can rewrite the deformation gradient

$\mathbf{C} = \mathbf{F}^{\mathrm{T}}\mathbf{F}, \quad \mathbf{B} = \mathbf{F}\mathbf{F}^{\mathrm{T}}, \quad \mathbf{C} = \mathbf{B}$

$$\mathbf{C}^{-1} = \mathbf{B}^{-1} = \begin{bmatrix} \frac{\Lambda^2 r^2}{R^2} & 0 & 0 \\ 0 & \frac{R^2}{r^2} & 0 \\ 0 & 0 & \frac{1}{\Lambda^2} \end{bmatrix}$$

$$\mathbf{E} = \frac{1}{2}(\mathbf{C} - \mathbf{I})$$

$$E_{rr} = \frac{1}{2}\left(\frac{R^2}{\Lambda^2 r^2} - 1\right), \quad E_{\theta\theta} = \frac{1}{2}\left(\frac{r^2}{R^2} - 1\right), \quad E_{zz} = \frac{1}{2}\left(\Lambda^2 - 1\right)$$

$\mathbf{t} = -p^*\mathbf{I} + 2\frac{\partial W}{\partial I_C}\mathbf{B} - 2\frac{\partial W}{\partial II_C}\mathbf{B}^{-1}$, where p^* is Lagrange multiplier

$W = C_{10}(I_c - 3) + C_{01}(II_C - 3)$

$$\frac{\partial W}{\partial I_C} = C_{10}, \quad \frac{\partial W}{\partial II_C} = C_{01}$$

$\mathbf{t} = -p^*\mathbf{I} + 2C_{10}\mathbf{B} - 2C_{01}\mathbf{B}^{-1}$

$$t_{rr} = -p^{*} + \frac{2C_{10}R^{2}}{\Lambda^{2}r^{2}} - \frac{2C_{01}\Lambda^{2}r^{2}}{R^{2}}$$

$$t_{\theta\theta} = -p^{*} + \frac{2C_{10}r^{2}}{R^{2}} - \frac{2C_{01}R^{2}}{r^{2}}$$

$$t_{zz} = -p^{*} + 2C_{10}\Lambda^{2} - \frac{2C_{01}}{\Lambda^{2}}$$

Lagrange multiplier

Equilibrium equation,

$$t_{rr}(r)-t_{rr}(r_i)=\int_{r_i}^{r}(t_{\theta\theta}-t_{rr})\frac{1}{r}dr$$

$t_{rr}(r_i)=-\mathrm{P_i}$; Luminal pressure (Boundary condition)

$$t_{rr}(r_i)=-P^*+\frac{2C_{10}R^2}{\Lambda^2 r^2}-\frac{2C_{01}\Lambda^2 r^2}{R^2}$$

$$-p^*+\frac{2C_{10}R^2}{\Lambda^2 r^2}-\frac{2C_{01}\Lambda^2 r^2}{R^2}+\mathrm{P_i}=\int_{r_i}^{r}\left(t_{\theta\theta}-t_{rr}\right)\frac{1}{r}dr$$

$$p^*=\left(\frac{2C_{10}R^2}{\Lambda^2 r^2}-\frac{2C_{01}\Lambda^2 r^2}{R^2}\right)+\mathrm{P_i}-\int_{r_i}^{r}\left(t_{\theta\theta}-t_{rr}\right)\frac{1}{r}dr$$

$$t_{\theta\theta}-t_{rr}=-p^*+\left(\frac{2C_{10}r^2}{R^2}-\frac{2C_{01}R^2}{r^2}\right)-\left(-p^*+\frac{2C_{10}R^2}{\Lambda^2 r^2}-\frac{2C_{01}\Lambda^2 r^2}{R^2}\right)$$

$$=\left(\frac{2C_{10}r^2}{R^2}-\frac{2C_{01}R^2}{r^2}\right)-\left(\frac{2C_{10}R^2}{\Lambda^2 r^2}-\frac{2C_{01}\Lambda^2 r^2}{R^2}\right)$$

$$\int_{r_i}^{r}\left(t_{\theta\theta}-t_{rr}\right)\frac{1}{r}dr=\int_{r_i}^{r}\frac{t_{\theta\theta}}{r}dr-\int_{r_i}^{r}\frac{t_{rr}}{r}dr$$

$$=\int_{r_i}^{r}\left(\frac{2C_{10}r^2}{R^2}-\frac{2C_{01}R^2}{r^2}\right)\frac{1}{r}dr-\int_{r_i}^{r}\left(\frac{2C_{10}R^2}{\Lambda^2 r^2}-\frac{2C_{01}\Lambda^2 r^2}{R^2}\right)\frac{1}{r}dr$$

Thus,

$$p^*=\left(\frac{2C_{10}R^2}{\Lambda^2 r^2}-\frac{2C_{01}\Lambda^2 r^2}{R^2}\right)+\mathrm{P_i}-\int_{r_i}^{r}\left(\frac{2C_{10}r^2}{R^2}-\frac{2C_{01}R^2}{r^2}\right)\frac{1}{r}dr-\int_{r_i}^{r}\left(\frac{2C_{10}R^2}{\Lambda^2 r^2}-\frac{2C_{01}\Lambda^2 r^2}{R^2}\right)\frac{1}{r}dr$$

Finally,

Cauchy stress in radial, circumferential, and longitudinal directions and Lagrange multiplier, respectively

$$t_{rr} = -p^* + \frac{2C_{10}R^2}{\Lambda^2 r^2} - \frac{2C_{01}\Lambda^2 r^2}{R^2}$$

$$t_{\theta\theta} = -p^* + \frac{2C_{10}r^2}{R^2} - \frac{2C_{01}R^2}{r^2}$$

$$t_{zz} = -p^* + 2C_{10}\Lambda^2 - \frac{2C_{01}}{\Lambda^2}$$

$$p^* = \left(\frac{2C_{10}R^2}{\Lambda^2 r^2} - \frac{2C_{01}\Lambda^2 r^2}{R^2}\right) + \mathrm{P_i} - \int_{r_i}^{r}\left(\frac{2C_{10}r^2}{R^2} - \frac{2C_{01}R^2}{r^2}\right)\frac{1}{r}dr - \int_{r_i}^{r}\left(\frac{2C_{10}R^2}{\Lambda^2 r^2} - \frac{2C_{01}\Lambda^2 r^2}{R^2}\right)\frac{1}{r}dr$$

APPENDIX B

POST PROCESSING PROTOCOL OF SMP FOAMS

B. 1 Post-Foaming Mechanical Processing

After rough or final dimensional cutting, foams shall be equilibrated to a temperature above Tg, compressed to 10% of their original volume and then allowed to re-expand. This step effectively fractures residual cell membranes to allow for more effective etching and cell membrane removal.

B. 2 Post-Foaming Etching for Cell Opening

Post-foaming etching of the samples is done in order to remove residual mobile species (catalyst, plasticizers, …) as well as open cells by removal of cell membranes. This step requires the foam sample from section 5 to be submerged in 0.1 N HCl solution. The HCl solution and foam should be immersed in a sonicator during the etching. After 2 hours, the foam shall be rinsed 3 times in an excess of DI water

B. 3 Post-Foaming Cleaning

This cleaning step further removes debris and any biological material that the foams may have been exposed to in the lab prior to sterilization.

B. 4 Cleaning

a. Wash the foams in a solution comprised 80% of RO water and 20% (by weight or volume) of Contrad 70 Cleaner. The foams shall be washed successively for two 15 minute periods in an excess of this cleaning solution under sonication, with new solution used in each of the 15 minute treatments. Note that DI water can be substituted for RO.

b. Wash the foams in RO water under gentle stirring to remove the soap. Multiple rinses might be required to completely remove the soap residue.

c. The foams shall be washed successively for two 15 minute periods in RO water under sonication, with DI water used in each of the 15 minute treatments.

d. Dry the foams for 15 minutes under dry air or nitrogen at 50 ˚C.

e. Store these foams in a sealed jar prior to further processing.

APPENDIX C

RESEARCH OF INVENTION: RESISTIVE HEATING DELIVERY DEVICE

C. 1 Introduction

The device, we are proposing, is a shape memory polymer (SMP) embolic device to treat saccular aneurysm. SMPs are a class of polymeric materials that can be formed into a specific primary shape, deformed into a stable secondary shape, and then controllably actuated (e.g., via temperature) to recover the primary shape. The shape memory characteristic of the foams allows them to be crimped to a small size, delivered endovascularly, and then thermally expanded to achieve complete occlusion of the aneurysm. After the occlusion of the aneurysm, blood percolating through the porous structure produces a blood clot and foreign body reaction, which then leads to fibrosis and eventual isolation of the aneurysm from the parent vessel.

The device is an endovascular delivery of SMP embolic implant and the actuation of the crimped SMP foam using electro-resistive (Joule) heating. After embolizing (filling) aneurysm with SMP foam, low friction between the delivery device and SMP foam allows the SMP foam detaching from the delivery device.

C. 2 Design Concept

The device consists of the following components (see Fig. 44):

C. 2. 1Resistive Heating Element (see Fig. 45)

C. 2. 1. 1 Resistive Heating Coils

For local heating, higher resistive wires are used at the distal end. The resistive heating coil, nitinol wire (see section C. 2. 1. 3.1) is used for a core wire. Nichrome (or copper) wire is wound around the core wire. After winding the wire, additional insulation is applied (see section C. 2. 1.5.1 and C. 2. 1.7)

C. 2. 1. 1. 1 Nichrome Wires

Polyimide coated nickel chrome alloy (Nichrome) wire (≤ 0.08 mm diameter & ≤ 150 mm long): Supplier: Kanthal; Item #: Nikrothal 80, PF002091.

C. 2. 1. 1. 2 Copper Wires

Modified polyurethane resin with a polyimide (nylon) coated copper wires (≤ 0.08 mm diameter & ≤ 150 mm long): Supplier: techfixx.com.

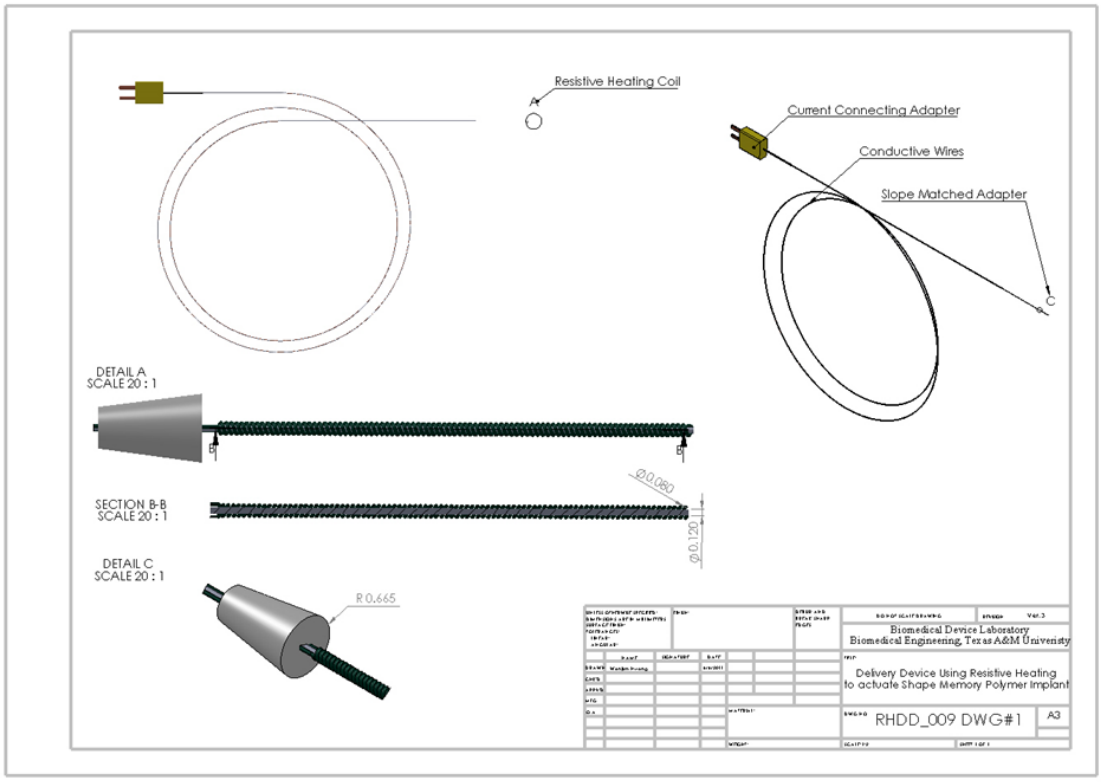

Figure 44 Schematic diagram illustrates the resistive heating device for the shape memory polymer embolic foam to treat a saccular aneurysm: whole device (top left and top right) and distal details (middle and bottom). The diagram is to scale.

C. 2. 1. 2 Conductive Wires from Resistive Heating Coil to the Proximal End

To minimize excessive heating by a resistance, less resistive conductive wires are used. Lead free silver (3%) added solder is used to connect conductive wires and resistive heating coils and the connected locations are insulated using polyester heat shrink tubes (see Section C. 2. 1.5.2)

C. 2. 1. 2. 1 Copper Wires

Polyurethane/Nylon coated copper wires (≤0.28 mm diameter and ≤1220 mm long): Supplier: Allied Electronics; Item#: BELDEN 8055.

C. 2. 1. 3 Core & Support Wires

Super elastic nickel titanium alloy (nitinol) wires are used for a flexible guide wire system. Core wire is used for making and holding resistive coils. Supporting wire is used for forming a straight shape. Like medical guidewires, the device use nitinol wires for elastic recovery and strength to overcome friction when the device are pushed through a catheter.

C. 2. 1. 3. 1 Nitinol Wire (Core)

Nitinol wire (≤ 0.12 mm diameter and ≤1300 mm long): Supplier: Small Parts; Item#: NW-005-72-05.

C. 2. 1. 3. 2 Nitinol Wire (Supporting)

Nitinol wire (0.30 ~ 0.50 mm diameter and ≤1220 mm long): Supplier: Small Parts; Item#: NW—012-72-05.

C. 2. 1. 4 Power Supply Connector

A connector connects the conductive wires to a power supply. The wires draw a current that induces resistive heating at the distal end of the coil.

C. 2. 1. 4. 1 Miniature thermocouple connector is used to connect between power source and conductive wires (Omega SMPW-CC-K-M) (see Fig. 46 (a))

C. 2. 1. 4. 2 If the miniature thermocouple connector is not allowed for clinical trial, a power supply connector will be fabricated; an example (see Fig. 46 (b))

C. 2. 1. 5. Heat Shrink Tube

C. 2. 1. 5. 1 Polytetrafluoroethylene (PTFE) Heat Shrink Tube

Device is wrapped with PTFE heat shrink sheaths for insulating and minimizing friction when the device is navigating through a tortuous pathway (≤ 6 Fr Catheter) of a vascular system.

During heat shrinking, the tube is drawn under hot air and the overall device is tightly wrapped by the tube. PTFE heat shrink tube (≤0.97 mm inner diameter and ≤1220 mm long): Supplier: Zeus; Item#: OPN 91479 and OPN 88037.

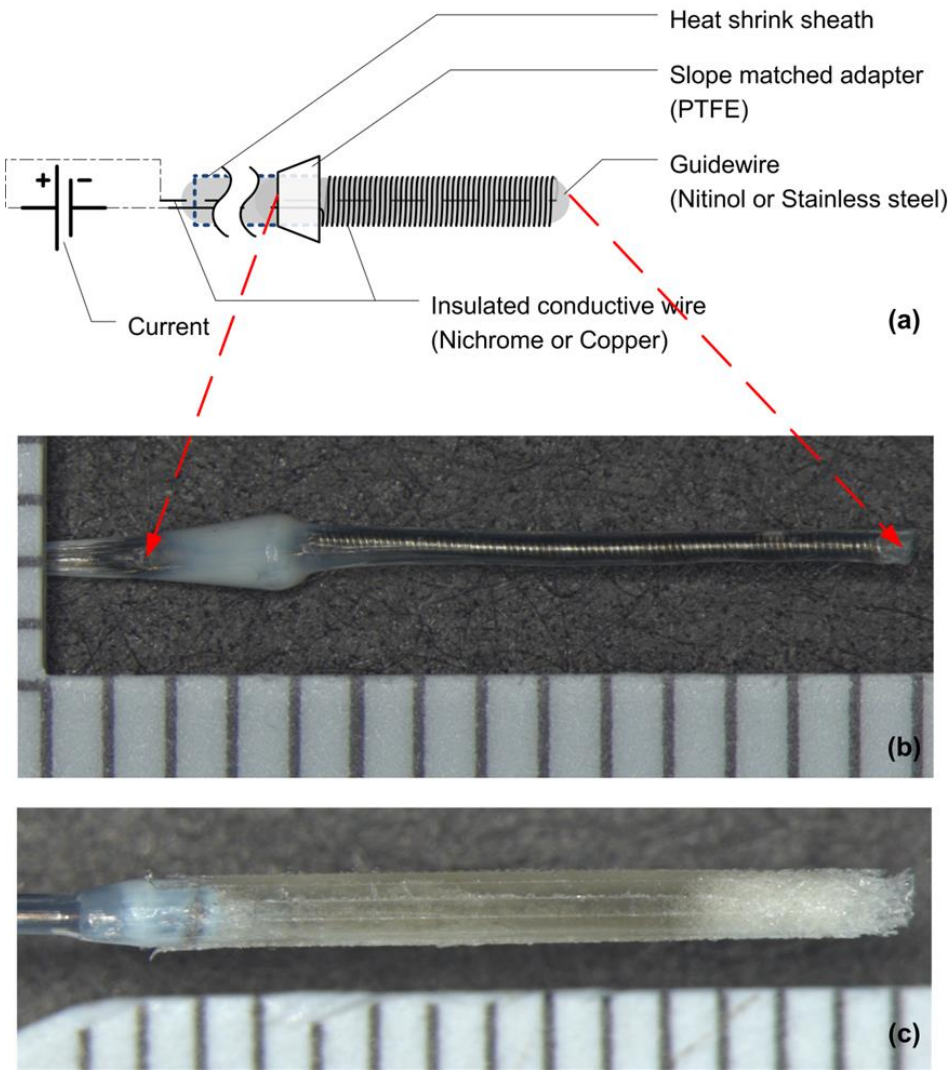

Figure 45 SMP embolic device system: (a) Schematic diagram for a releasing mechanism. The diagram shows the primary components of the heat actuating system: a guidewire, insulated conductive wires (a heating coil and conductive wire), a slope matched adapter, a heat shrink sheath for insulation and a power source. (b) Photograph of a nichrome wire coil at the tip of the device. (c) Photograph of crimped SMP foam on the heating system (i.e. the coiled tip) of (b). 10 mm SMP sphere with 1 mm channel was crimped by a radial compression stent crimper. Total length of the prototype was 120 cm (proximal part was not shown in the photo).

Figure 46 Connectors for delivering the energy, needed to actuate SMP implant, from the power supply are shown in the photograph. (a) Miniature thermocouple connector is used for connecting the device to a power source. (b) Electrical connector of Micrus coil, Micrus Corp.

C. 2. 1. 5. 2 Polyester Heat Shrink Tube

Soldered spot between the resistive heating coil and conductive wires is insulated using polyester tubes. These polyester tubes are thinner than the PTFE tubes. After PTFE tube wrapping, there are no bumps at outmost surface: Supplier: Advanced Polymer; Item#: Various items are used depending on an outer diameter of the connected part.

C. 2. 1. 6 Slope Matched Adapter

The diameter of crimped SMP foam on the resistive heating coil is around 1.30 mm and the diameter of the resistive heating coil is 0.30 ~ 0.50 mm. After the crimped SMP foam is pushed out of the catheter, the difference of diameters prevent from pulling back inside of a catheter. The slope matched adapter allows for smooth moving at the distal end of the catheter (see Fig. 47).

C. 2. 1. 7 Additional Insulation of the Resistive Heating Coil

PTFE insulation of the resistive heating coil may be removed during heating of the coil. Because the PTFE tube is drawn under hot air for tight fitting, high temperature of the device can lead a recovery of an original shape of PTFE tube. In this situation, polyimide coated coil may be removed over 250°C and an electric current leaking is a possible scenario.

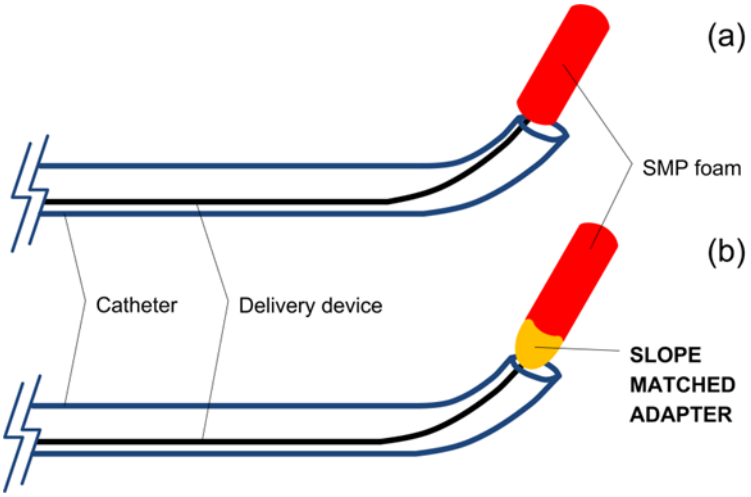

Figure 47 Illustration of a slope matched adapter: (a) After the device is out of the catheter, the difference in diameters between the crimped SMP and the delivery system make the device hard to pull back into a catheter. (b) Slope matched adapter allows a smooth slope between the delivery device and the crimped SMP foam. The adapter helps repositioning the device before actuation.

To get rid of any possibility about an electric current leaking from the device, the resistive heating coil is dip-coated using a biocompatible UV curable epoxy (Epotek OG603). The epoxy coating allows insulation up to 400°C.

C. 2. 2 SMP Foam Machining

SMP foam can be fabricated in various shapes such as a cylinder, a sphere, a star or a patient specific aneurysm by using a micro computer numerical control (CNC) milling machine (see Fig. 48). In addition to various shapes, the foam has a cylindrical channel. The resistive heating coil of the delivery device can be placed inside of the channel. The diameter of the channel is larger than the diameter of the coil and this allows friction free for detaching mechanism (see Fig. 49).

C. 2. 3 Assemble SMP Foam and the Delivery Device

Once a SMP foam and a delivery devices are prepared, they are assembled and the SMP foam is crimped in the SC150 crimper (see Fig. 50).

C. 3 Proof-of-Principle Device

To demonstrate proof-of-principle, a bench top prototype was fabricated. The resistive heating coil actuates a crimped SMP foam (see Fig. 51).

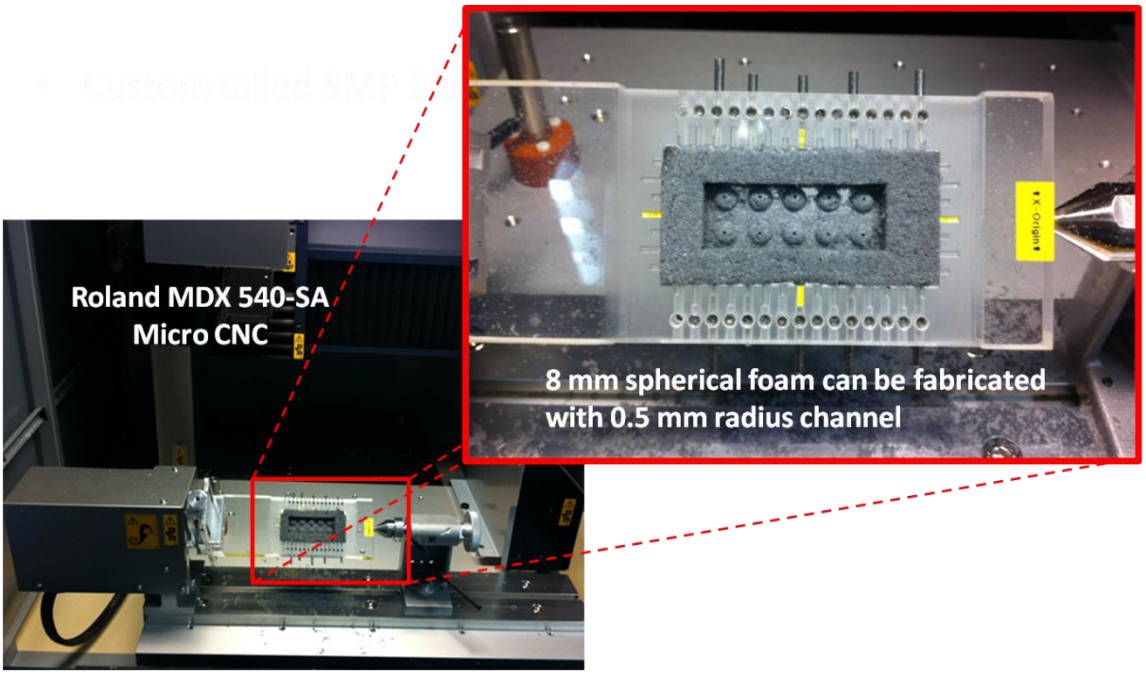

Figure 48 SMP foam can be fabricated into a primary shape using micro CNC milling machine.

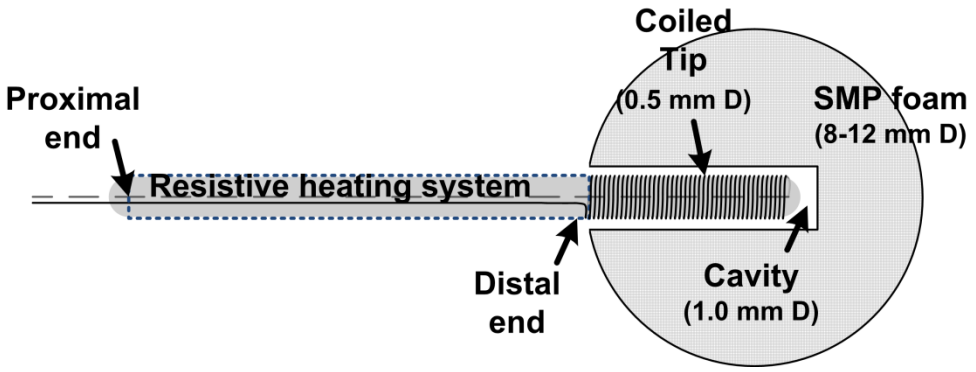

Figure 49 Schematic diagram of the SMP embolic device. The volume of the foam can be reduced by making a inner cavity or modification of the outer surface.

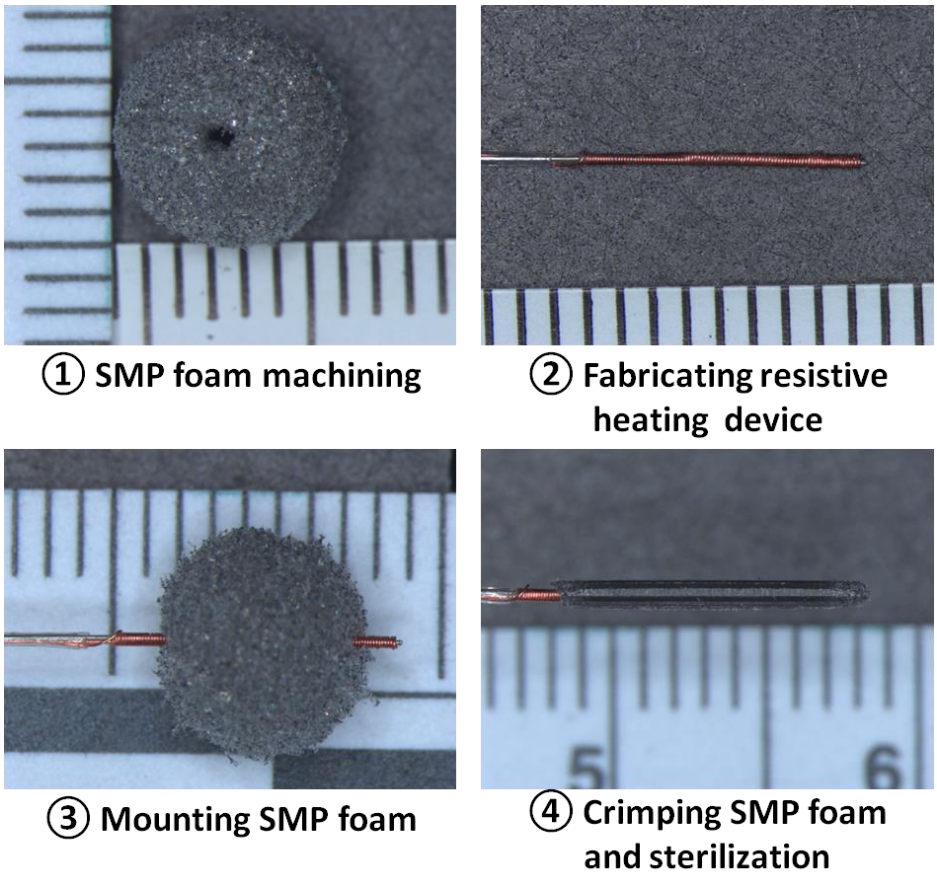

Figure 50 Process of fabrication for a SMP embolic device. 4% Tungsten by volume was added to the SMP foam as a contrast agent for fluoroscopy.

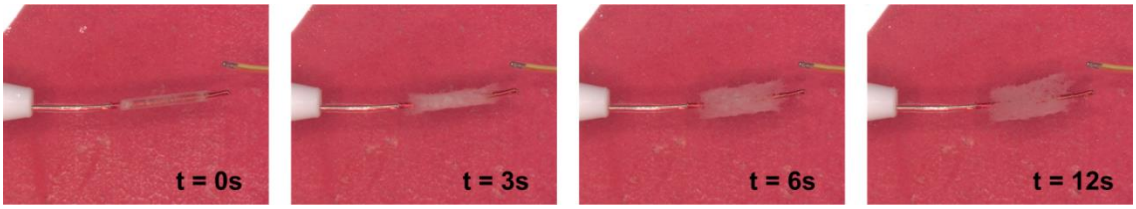

Figure 51 The bench top SMP embolic device was submerged in a 23 ℃ water bath without flow. An 8 mm diameter cylindrical SMP foam with a Tg=60 ℃ was mounted on the resistive heating coil. A 6 volt battery connected the coiled tip of the heating system. Crimped SMP foam recovered its primary shape within 20 seconds.

APPENDIX D

DESIGN HISTORY FILE OF SMP DEVICE

Table 10, 11, and 12 presents specification of SMP embolic devices.

Table 10 Specification of SMP embolic devices - 1

Device #	SMP foam dimensions in mm				Heating element dimensions in mm		SMP foam batch		Crimper #
	Expanded diameter	Expanded Length	Crimped diameter	Crimped length	Resistance (Ω)	Diameter	Length	Outer shell	Core cylinder	
L-L01	10.73±0.29	9.98±0.63	1.54±0.01	11.38±0.29	23.41	0.38±0.01	8.53±0.06	111102QLEFOP506 80% TMHDI otw Gen 1 w/Tungsten	110519LEFOP502 Gen1	1
L-L02	10.56±0.28	10.12±0.17	1.44±0.02	11.79 ±0.15	21.75	0.41±0.03	8.33±0.11	111102QLEFOP506 80% TMHDI otw Gen 1 w/Tungste	110519LEFOP502 Gen1	2
L-L03	10.20±0.13	9.51±0.27	1.45±0.01	10.79±0.32	22.56	0.37±0.02	8.30±0.04	111102QLEFOP506 80% TMHDI otw Gen 1 w/Tungsten	110519LEFOP502 Gen1	1
L-L04	9.87±0.10	7.45±0.10	1.41±0.02	8.90±0.14	22.90	0.37±0.03	8.82±0.26	111121LLEFOP505 80% TMHDI otw Gen 1 w/Tungsten	110519LEFOP503 Gen1	2
L-L05	8.97±0.29	7.09±0.19	1.46±0.01	9.59±0.04	22.39	0.37±0.03	8.77±0.11	111121LLEFOP505 80% TMHDI otw Gen 1 w/Tungsten	110519LEFOP503 Gen1	1
L-L06	9.47±0.29	7.14±0.19	1.45±0.04	8.51±0.58	20.23	0.36±0.02	8.26±0.22	111121LLEFOP505 80% TMHDI otw Gen 1 w/Tungsten	110519LEFOP503 Gen1	2
L-L07	10.45±0.30	6.79±0.44	1.53±0.03	8.66±0.32	20.16	0.35±0.01	8.24±0.23	111121LLEFOP505 80% TMHDI otw Gen 1 w/Tungsten	110519LEFOP503 Gen1	1
L-L08	10.22±0.34	7.11±0.21	1.44±0.01	9.20±0.33	22.21	0.34±0.01	8.68±0.12	111121LLEFOP505 80% TMHDI otw Gen 1 w/Tungsten	110519LEFOP503 Gen1	2
L-M01	10.71±0.15	9.01±0.26	1.50±0.01	11.38±0.29	21.53	0.36±0.02	8.30±0.21	111102QLEFOP506 80% TMHDI otw Gen 1 w/Tungsten	110519LEFOP502 Gen1	2
L-M02	10.77±0.30	10.53±0.45	1.46±0.03	12.18±0.32	21.07	0.35±0.03	8.26±0.24	111102QLEFOP506 80% TMHDI otw Gen 1 w/Tungsten	110519LEFOP502 Gen1	1
L-M03	10.35±0.11	9.08±0.57	1.52±0.02	10.55±0.20	21.75	0.34±0.01	8.01±0.13	111102QLEFOP506 80% TMHDI otw Gen 1 w/Tungsten	110519LEFOP502 Gen1	2
L-M04	10.31±0.26	7.03±0.08	1.43±0.02	8.63±0.14	21.30	0.36±0.00	8.86±0.23	111121LLEFOP505 80% TMHDI otw Gen 1 w/Tungsten	110519LEFOP503 Gen1	1
L-M05	10.41±0.13	6.70±0.13	1.46±0.01	9.06±0.11	22.03	0.34±0.01	8.25±0.02	111121LLEFOP505 80% TMHDI otw Gen 1 w/Tungsten	110519LEFOP503 Gen1	2
L-M06	10.97±0.30	7.06±0.19	1.51±0.01	8.97±0.71	23.82	0.34±0.01	9.31±0.30	111121LLEFOP505 80% TMHDI otw Gen 1 w/Tungsten	110519LEFOP503 Gen1	1
L-M07	10.01±0.26	7.27±0.26	1.40±0.02	9.06±0.22	22.12	0.35±0.03	9.01±0.08	111121LLEFOP505 80% TMHDI otw Gen 1 w/Tungsten	110519LEFOP503 Gen1	2
L-S01	9.57±0.48	8.23±0.45	1.48±0.04	10.08±0.08	22.39	0.37±0.01	9.60±0.20	111102QLEFOP506 80% TMHDI otw Gen 1 w/Tungsten	110519LEFOP502 Gen1	1

Table 11 Specification of SMP embolic devices - 2

Device #	SMP foam dimensions in mm				Heating element dimensions in mm		Resistance (Ω)	SMP foam batch		Crimper #
	Expanded diameter	Expanded Length	Crimped diameter	Crimped length	Diameter	Length		Outer shell	Core cylinder	
M-M08	7.67±0.26	7.13±0.43	1.25±0.03	9.26±0.12	0.33±0.01	7.06±0.14	17.05	111121LLFOPS06 80% TMHDI otw Gen 1 w/Tungsten	110915LLFOPS02 Gen1	1
M-M09	8.64±0.43	6.76±0.10	1.20±0.02	7.74±0.22	0.33±0.02	6.45±0.13	15.22	120510LLFOPS01 80% TMHDI otw Gen 1 w/Tungsten	110915LLFOPS02 Gen1	1
M-M10	8.22±0.38	6.59±0.13	1.19±0.02	7.77±0.06	0.33±0.01	6.34±0.22	15.23	120510LLFOPS01 80% TMHDI otw Gen 1 w/Tungsten	110915LLFOPS02 Gen1	2
M-M11	7.18±0.19	7.19±0.10	1.21±0.02	8.18±0.32	0.32±0.01	6.38±0.03	14.71	111121LLFOPS06 80% TMHDI otw Gen 1 w/Tungsten	110915LLFOPS02 Gen1	1
M-M12	7.96±0.16	6.28±0.23	1.21±0.02	7.75±0.18	0.34±0.01	6.19±0.11	16.04	111121LLFOPS06 80% TMHDI otw Gen 1 w/Tungsten	110915LLFOPS02 Gen1	2
M-M13	7.37±0.26	6.91±0.13	1.16±0.01	8.53±0.12	0.32±0.01	6.33±0.20	16.77	120510LLFOPS01 80% TMHDI otw Gen 1 w/Tungsten	110915LLFOPS02 Gen1	1
M-M14	7.51±0.10	6.60±0.22	1.22±0.02	7.77±0.09	0.32±0.01	6.21±0.02	16.37	120510LLFOPS01 80% TMHDI otw Gen 1 w/Tungsten	110915LLFOPS02 Gen1	2
M-M15	7.85±0.33	6.99±0.23	1.19±0.03	8.51±0.03	0.33±0.02	6.16±0.11	15.73	120510LLFOPS01 80% TMHDI otw Gen 1 w/Tungsten	110915LLFOPS02 Gen1	1
M-M16	7.43±0.14	6.27±0.13	1.20±0.01	7.98±0.01	0.32±0.01	6.44±0.16	16.46	120510LLFOPS01 80% TMHDI otw Gen 1 w/Tungsten	110915LLFOPS02 Gen1	2
M-M17	7.33±0.22	7.12±0.18	1.23±0.01	8.37±0.12	0.32±0.01	5.79±0.03	12.93	111121LLFOPS06 80% TMHDI otw Gen 1 w/Tungsten	110915LLFOPS02 Gen1	1
M-M18	7.12±0.24	7.59±0.11	1.19±0.01	8.59±0.11	0.33±0.01	6.95±0.13	15.33	111121LLFOPS06 80% TMHDI otw Gen 1 w/Tungsten	110915LLFOPS02 Gen1	2
M-M19	8.75±0.20	6.58±0.17	1.25±0.03	8.67±0.20	0.31±0.01	6.55±0.09	14.31	120510LLFOPS01 80% TMHDI otw Gen 1 w/Tungsten	110915LLFOPS02 Gen1	1
M-M20	8.51±0.58	6.94±0.10	1.25±0.03	8.47±0.11	0.31±0.01	6.25±0.10	14.23	120510LLFOPS01 80% TMHDI otw Gen 1 w/Tungsten	110915LLFOPS02 Gen1	2
M-M21	7.61±0.28	6.91±0.19	1.21±0.02	8.71±0.13	0.32±0.01	6.24±0.13	14.29	120510LLFOPS01 80% TMHDI otw Gen 1 w/Tungsten	110915LLFOPS02 Gen1	1
M-M22	7.08±0.20	7.15±0.12	1.12±0.02	8.56±0.05	0.32±0.01	6.41±0.09	14.47	120510LLFOPS01 80% TMHDI otw Gen 1 w/Tungsten	110915LLFOPS02 Gen1	2

Table 12 Specification of SMP embolic devices - 3

Device #	SMP foam dimensions in mm				Heating element dimensions in mm			SMP foam batch		Crimper #
	Expanded diameter	Expanded Length	Crimped diameter	Crimped length	Resistance (Ω)	Diameter	Length	Outer shell	Core cylinder	
S-S02	6.37±0.22	5.40±0.11	0.96±0.02	6.64±0.16	13.80	0.34±0.01	4.12±0.02	120510LLFOPS01 80% TMHDI otw Gen 1 w/Tungsten	110915LLFOPS02 Gen1	1
S-S03	5.75±0.16	5.30±0.11	0.89±0.02	6.60±0.15	13.23	0.32±0.01	4.02±0.11	120510LLFOPS01 80% TMHDI otw Gen 1 w/Tungsten	110915LLFOPS02 Gen1	2
S-S04	5.91±0.24	5.51±0.06	0.93±0.02	6.52±0.20	13.31	0.32±0.00	4.56±0.06	120510LLFOPS01 80% TMHDI otw Gen 1 w/Tungsten	110915LLFOPS02 Gen1	1
S-S05	5.41±0.13	5.15±0.23	0.88±0.03	6.32±0.12	14.01	0.32±0.01	4.43±0.13	120510LLFOPS01 80% TMHDI otw Gen 1 w/Tungsten	110915LLFOPS02 Gen1	2
S-S06	5.64±0.07	5.45±0.26	0.92±0.02	6.53±0.24	12.88	0.33±0.02	4.26±0.08	120510LLFOPS01 80% TMHDI otw Gen 1 w/Tungsten	110915LLFOPS02 Gen1	1
S-S07	5.46±0.13	4.70±0.22	0.93±0.01	5.76±0.11	11.80	0.33±0.01	3.68±0.30	120510LLFOPS01 80% TMHDI otw Gen 1 w/Tungsten	110915LLFOPS02 Gen1	2
S-S08	5.87±0.14	5.66±0.20	0.94±0.02	6.55±0.04	13.50	0.29±0.01	3.82±0.15	120510LLFOPS01 80% TMHDI otw Gen 1 w/Tungsten	110915LLFOPS02 Gen1	1
S-S09	6.66±0.08	5.62±0.08	0.93±0.03	6.87±0.14	12.95	0.29±0.01	4.29±0.15	120510LLFOPS01 80% TMHDI otw Gen 1 w/Tungsten	110915LLFOPS02 Gen1	2
S-S10	5.74±0.12	5.05±0.13	0.96±0.01	6.26±0.06	13.59	0.32±0.02	5.43±0.08	120510LLFOPS01 80% TMHDI otw Gen 1 w/Tungsten	110915LLFOPS02 Gen1	1
S-S11	6.36±0.33	5.40±0.08	0.92±0.02	6.53±0.08	12.93	0.33±0.02	4.75±0.07	120510LLFOPS01 80% TMHDI otw Gen 1 w/Tungsten	110915LLFOPS02 Gen1	2
S-S12	5.67±0.30	5.61±0.30	1.02±0.01	6.53±0.11	12.27	0.32±0.00	4.59±0.17	120510LLFOPS01 80% TMHDI otw Gen 1 w/Tungsten	110915LLFOPS02 Gen1	1
S-S13	6.06±0.09	5.55±0.05	0.93±0.02	6.83±0.26	13.59	0.32±0.02	5.36±0.13	120510LLFOPS01 80% TMHDI otw Gen 1 w/Tungsten	110915LLFOPS02 Gen1	2
S-S14	5.37±0.43	4.46±0.35	0.93±0.01	5.90±0.10	13.66	0.31±0.01	5.65±0.07	120510LLFOPS01 80% TMHDI otw Gen 1 w/Tungsten	110915LLFOPS02 Gen1	1
S-S15	5.57±0.16	5.83±0.24	0.91±0.01	7.00±0.14	13.95	0.31±0.01	5.26±0.09	120510LLFOPS01 80% TMHDI otw Gen 1 w/Tungsten	110915LLFOPS02 Gen1	2

APPENDIX E

HISTORY FILES OF ANIMAL STUDY

Total number of the animal studies was 13 which were 4 bifurcated aneurysms and 9 sidewall aneurysms. The table xx presented index of the animal and types of aneurysm in the animal studies. Log files of the animal studies were generated and documented from Texas A&M Institute for Preclinical Studies.

Table 13 Index of animal studies between log files and this dissertation.

	Bifurcated aneurysm				Sidewall aneurysm								
Dissertation	1	2	3	4	1	2	3	4	5	6	7	8	9
Log files	M126	M127	T201	T202	T203	T204	T211	T212	T207	T208	T225	T226	T228

Bifurcation Aneurysm Data

EXACT COPY

Procedure Date: 5-4-12 **Study Protocol:** IIPS-00612 **AUP:** 2011-254

Animal ID: M126 **Species:** Swine **PI:** Miller

Measurements:

Right Aneurysm: A N/A mm B N/A mm C N/A mm D N/A mm E 3.92 mm F 5.45 mm

No Aneurysm ____

Left Aneurysm: A ____ mm B ____ mm C ____ mm D ____ mm E ____ mm F ____ mm

No Aneurysm X

Devices
① LO5 SMP D: 1.47mm R: 22.39Ω
② LO4 SMP D: 1.43mm R: 22.90

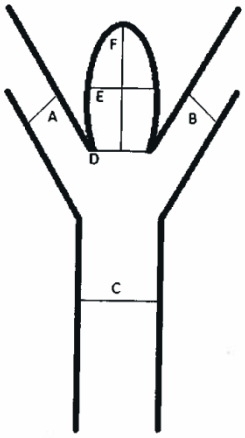

Comments 27.5kg weight, 1605-5F in aneurysm - devices will not fit into 5F 1610. Attempting 6F again: previously would not go into aneurysm 1620-6F in aneurysm 1635- angiogram - aneurysm occluded, distal sidewall aneurysm not treated, Device #1 used for implantation of bifurcation

QD 5-4-12

Recorded by: QD Dt **Date:** 5-4-12

N/A = Not applicable

EXACT COPY

Sidewall Aneurysm Data

Procedure Date: 5-4-12 **Study Protocol:** TIPS- 00612 **AUP:** 2011-254

Animal ID: M126 **Species:** Swine **PI:** Miller

Measurements:

Left QS 5-4-12

~~Right~~ Side Wall Aneurysm: A ____ mm B ____ mm C ____ mm D ____ mm

E ____ mm F ____ mm G ____ mm H ____ mm I ____ mm J ____ mm

No Aneurysm X

Right QS 5-4-12

~~Left~~ Side Wall Aneurysm: A N/A mm B N/A mm C N/A mm D N/A mm

remeasured QS 5-4-12

E N/A mm F N/A mm G N/A mm H N/A mm I 3.9 mm J N/A mm

4.4 remeasured QS 5-4-12

6.57 had trouble with calibration of equipment QS 5-4-12

No Aneurysm ____

AP Projection

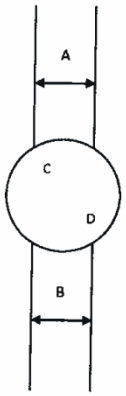

Lateral Projection

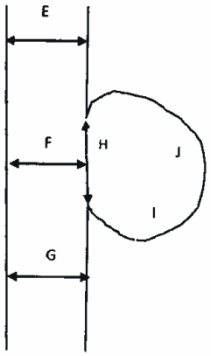

Comments Sidewall aneurysm not treated

QS 5-4-12

Recorded by: [illegible] **Date:** 5-4-12

N/A = Not applicable

EXACT COPY

Support Article Information

Procedure Date: 5-4-12 **Study Protocol:** TIPS-00612 **AUP:** 2011-254

Animal ID: M126 **Species:** Swine **PI:** Miller **Weight:** 27.5 kg

Products used:

Product Type	Brand, Size, etc.
Introducer sheath	6F Terumo Pinnacle Ref RSS601 Lot MD17
Guide catheter	6F Cordis Brite Tip First ↑ Second → Third → 5F Cordis. 670-098-00 6F JCR 4 .070"I.D. LOT 16263774 +H73967009809U +13273162637748J+ Vista Brite Tip
Guide wire	Radiofocus Glidewire Order GS3510 Lot 091204 0.035" x 260cm Angled Stiff
	JD 5-4-12

Comments 4.4 Aortic Punch used

JD 5-4-12

Recorded by: JE JDS **Date:** 5-4-12

EXACT COPY

Bifurcation Aneurysm Data

Procedure Date: 6-22-12 **Study Protocol:** TIPS-00612 **AUP:** 2011-254

Animal ID: M127 **Species:** Swine **PI:** Miller

Weight 34.5 kg

Measurements:

Right Aneurysm: A N/A mm B N/A mm C N/A mm D N/A mm E 7 mm F 8 mm

No Aneurysm ____

Left Aneurysm: A ____ mm B ____ mm C ____ mm D ____ mm E ____ mm F ____ mm

No Aneurysm X

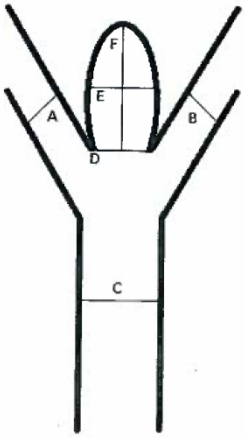

Comments Device M15 D: 1.19mm L: 8.51mm R: 15.73 Ω

11 minutes blood time from start to catheter removal

6-22-12

Recorded by: [illegible] **Date:** 6-22-12

N/A = Not applicable

EXACT COPY

Support Article Information

Procedure Date: 6-22-12 **Study Protocol:** TIPS-00612 **AUP:** 2011-254

Animal ID: M127 **Species:** Swine **PI:** Miller **Weight:** 34.5 Kg

Products used:

Product Type	Brand, Size, etc.
Introducer sheath	Pinnacle GF Ref RSSG01 Lot LK19 10cm
Guide catheter	Cordis 556-260-00 6F STR .066"I.D. LOT 16582282 +H7396562600090 +16059155822820W Cordis Neuropath SF MPD
Guide wire	0.035" x 260cm Exchange Length Angled Radiofocus Glidewire Ref GS3510 Lot 091204

6-22-12

Comments

6-22-12

Recorded by: [illegible] **Date:** 6-22-12

EXACT COPY

Bifurcation Aneurysm Data

Procedure Date: 7-25-12 **Study Protocol:** TIPS-00612 **AUP:** 2011-254

Animal ID: T201 **Species:** Swine **PI:** Miller

Measurements:

Right Aneurysm: A 4.33 mm B 4.20 mm C 3.37 mm D 3.47 mm E 8.02 mm JD 7-25-12 F 8.12 mm JD 7-25-12 used measurement from 3D image

No Aneurysm ____

Left Aneurysm: A ____ mm B ____ mm C ____ mm D ____ mm E ____ mm F ____ mm

No Aneurysm X

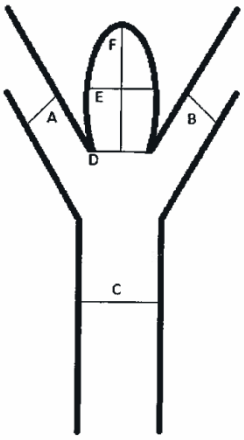

Comments Weight 35.5 kg 8.64 Diameter x 6.8 Length foam

D# M09 (device ID code)

1 minute – blood → aneurysm no resistance in catheter

12:55 entire blood → catheter removal

JD 7-25-12

Recorded by: JD **Date:** 7-25-12

N/A = Not applicable

EXACT COPY

Support Article Information

Procedure Date: 7-25-12 **Study Protocol:** TIPS-00612 **AUP:** 2011-254

Animal ID: T201 **Species:** Swine **PI:** Miller **Weight:** 35.5 kg

Products used:

Product Type	Brand, Size, etc.
Introducer sheath	6F Terumo Pinnacle 10cm Ref RSS601 Lot NC02
Guide catheter	5F 90cm repackaged
Guide wire	RadiofocusGlidewire Ref GS3510 Lot 091204 Catheter Exchange Long Taper Angled Stiff Shaft
	JD 7-25-12

Comments

JD 7-25-12

Recorded by: JD **Date:** 7-25-12

EXACT COPY

Bifurcation Aneurysm Data

Procedure Date: 8-21-12 **Study Protocol:** TIPS-00612 **AUP:** 2011-254

Animal ID: T202 **Species:** Swine **PI:** Matthew Miller

Measurements:

Right Aneurysm: A N/A mm B N/A mm C N/A mm D N/A mm E N/A mm F 7-8 mm
measured with a ruler on the outside JD 8-21-12

No Aneurysm ____

Left Aneurysm: A N/A mm B N/A mm C N/A mm D N/A mm E N/A mm F N/A mm

No Aneurysm X

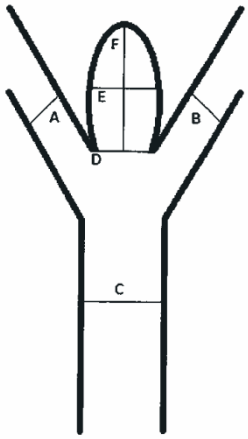

Comments Vessels distal to aneurysm and then the aneurysm itself filled with clots. Animal euthanized.

JD 8-21-12

Recorded by: JD **Date:** 8-21-12

N/A = Not applicable

EXACT COPY

Support Article Information

Procedure Date: 8-21-12 **Study Protocol:** TIPS-00612 **AUP:** 2011-254

Animal ID: T202 **Species:** Swine **PI:** Matthew Miller **Weight:** 75 lbs (74.9 lbs actually) JD 8-21-12

Products used:

Product Type	Brand, Size, etc.
Introducer sheath	Terumo Pinnacle R/O II HighFlo 6 Fr Ref RSB604H Lot NF11 Terumo Pinnacle Ref RSS601 Lot LK19 6F – Placed in right femoral
Guide catheter	5 Fr ~~Cto~~ Curved 100cm Cordis (spelling JD 8-21-12)
Guide wire (Spelling JD 8-21-12)	~~Radiof~~ Radifocus Glidewire Catheter Exchange Long Taper Angled Stiff Shaft Order GS3510 0.035" x 260cm Lot 091204
	JD 8-31-12

Comments

JD 8-31-12

Recorded by: JD **Date:** 8-21-12

EXACT COPY

Sidewall Aneurysm Data

Procedure Date: 9-3-12 **Study Protocol:** TIPS-00612 **AUP:** 2011-254

Animal ID: T203 **Species:** Swine **PI:** Miller

Measurements:

Right Side Wall Aneurysm: A N/A mm B N/A mm C N/A mm D N/A mm

E 2.91 mm on 2D F 2.97 mm on 2D G 3.57 mm on 2D H 3 mm measured directly 2.08 mm on 2D I 4.27 mm measured on 3D 2.92 on 2D J 2.29 mm on 2D

No Aneurysm ____

Left Side Wall Aneurysm: A 3.00 mm on 2D B 3.59 mm on 2D C 3.85 mm D 4.18 mm

E 2.84 mm on 2D F 2.73 mm on 2D G 3.42 mm on 2D H 3 mm measured directly 3.34 on 2D I 6.0 mm measured on 3D ~~6.08~~ on 2D 4.32 QD 9-3-12 J 6.08 mm on 2D

No Aneurysm ____

AP Projection

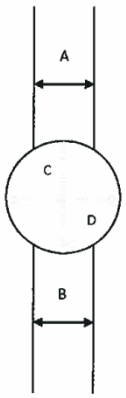

Lateral Projection

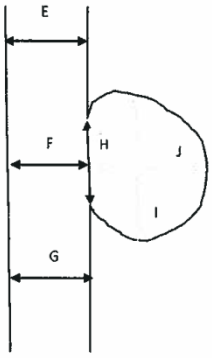

Comments Device Left Side = 509 Blood to blood time = 16min 17sec, Power 4 times slides easily - no resistance whatsoever, after power stopped - some expansion (first power), recommend to not attach black cable at beginning as lose fine control during placement

Device Right Side = 505 Blood to blood time = 10min 34sec, Power 2 times no resistance, after first power activated a lot more than left side, uniform expansion

Recorded by: JL DT **Date:** 9-3-12

N/A = Not applicable

EXACT COPY

Support Article Information

Procedure Date: 9-3-12 **Study Protocol:** IIPS-00612 **AUP:** 2011-254

Animal ID: T203 **Species:** Swine **PI:** Miller **Weight:** 27.0 Kg

Products used:

Product Type	Brand, Size, etc.
Introducer sheath	Terumo Pinnacle 6 Fr. Ref RSS601 Lot NM12 - femoral artery Terumo Pinnacle 6 Fr. Ref RSS601 Lot NC02 - femoral vein
Guide catheter	5 Fr Curved 100cm NeuroPath - Left Side 5 F Curved 90 cm Cordis - Right Side (NeuroPath would not go into aneurysm)
Guide wire	Radifocus Glidewire Long Taper Stiff Shaft Ref GS3510 Lot 091204

Comments

wrong date

Recorded by: [signature] Date: 9-3-12

EXACT COPY

Support Article Information

Procedure Date: 10-18-12 **Study Protocol:** TIPS-00612 **AUP:** 2011-254

Animal ID: T204 **Species:** Swine **PI:** Miller **Weight:** 31 Kg

Products used:

Product Type	Brand, Size, etc.
Introducer sheath	6F Terumo Pinnacle Ref RSSG01 Lot NM12 in ~~right~~ left femoral artery wrong side written QS 10-18-12
Guide catheter	5F Curved 100cm Neuropath
Guide wire	Cook 0.35" x 180 cm MG-35-180-GRAD (01)00827002095083(17)130800(10)2158422
	QS 10-18-12

Comments

QS 10-18-12

Recorded by: QS Date: 10-18-12

EXACT COPY

Sidewall Aneurysm Data

Procedure Date: 10-18-12 **Study Protocol:** TIPS-00612 **AUP:** 2011-254

Animal ID: T204 **Species:** Swine **PI:** Miller

Measurements:

Right Side Wall Aneurysm: A ____ mm B ____ mm C ____ mm D ____ mm

E ____ mm F ____ mm G ____ mm H ____ mm I ____ mm J ____ mm

No Aneurysm X

Left Side Wall Aneurysm: A N/A mm B N/A mm C ~~10.06~~ 10.09* mm D ~~10.09~~ 10.48* mm * remeasured at different angle JD 10-18-12

E 4.82 mm F N/A mm G 4.15 mm H 4.58 mm I 10.0 mm J 9.25 mm

No Aneurysm ____ Measurements from 3D reconstruction

AP Projection

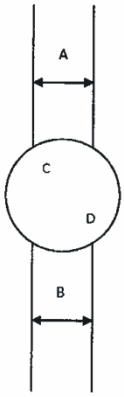

Lateral Projection

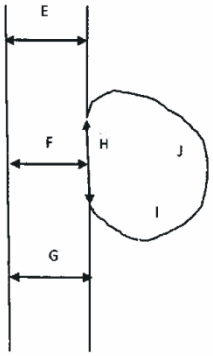

Comments M10 - 8.22 x 6.59 sizes, moves effortlessly through catheter @ 1117 at 1:0 minutes - in aneurysm, at 2:0 minutes - applying power, at 3,4 applying power, at 9:4 minutes power applied, total time blood to removal of pusher wire = ~~10:30~~ 11:15 approximately minutes. JD 10-18-12 removing wire from pusher - did not want to come easily - possibly still attached approximate blood → removal time due to miscommunication of timer stopping (misunderstanding)

Recorded by: JD **Date:** 10-18-12

N/A = Not applicable

Sidewall Aneurysm Data

Procedure Date: 10-30-12 **Study Protocol:** TIPS-00612 **AUP:** 2011-254

Animal ID: T211 **Species:** Swine **PI:** Miller

Measurements:

wrong side QD 10-30-12 ~~Left~~ ~~Right~~ Side Wall Aneurysm: A N/A mm B N/A mm C N/A mm D N/A mm

E N/A mm F N/A mm G N/A mm H 2.55 mm I 3.30 mm J 6.63 mm Measured from 2D subtracted image

No Aneurysm ____

wrong side QD 10-30-12 ~~Left~~ Right Side Wall Aneurysm: A N/A mm B N/A mm C N/A mm D N/A mm

E N/A mm F N/A mm G N/A mm H 4.24 mm I 6.23 mm J 6.95 mm Measured from 2D subtracted image

3.47mm remeasured from another image

No Aneurysm ____

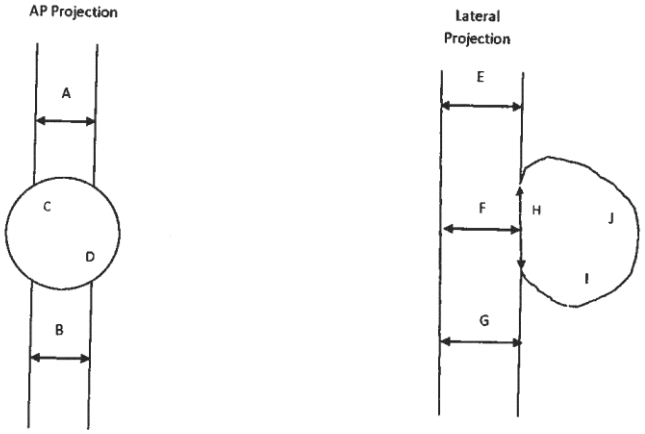

wrong side QD 10-30-12 **Comments** ~~right~~ left aneurysm developed leak on angiogram from guide wire - sutured

wrong side QD 10-30-12 ~~Right~~ Left side device S07 - "slides effortlessly" - total time 7 minutes 31 seconds

wrong side QD 10-30-12 ~~Left~~ Right side device M13 - little bit of friction/resistance at the end of deployment - total time 10 minutes 24 seconds

Left side friction 0/10 and right side friction 4/10 (may have been due to exposure to air time - unsheathed then waited to reposition catheter)

Recorded by: JLS **Date:** 10-30-12

N/A = Not applicable

Support Article Information

Procedure Date: 10-30-12 **Study Protocol:** TIPS-00612 **AUP:** 2011-254

Animal ID: T211 **Species:** Swine **PI:** Miller **Weight:** 69.3 lbs

Products used:

Product Type	Brand, Size, etc.
Introducer sheath	6Fr Terumo Pinnacle Ref RSS601 Lot NM12
Guide catheter	SF Neuropath
Guide wire	Radiofocus Glidewire Catheter Exchange Long Taper Angled Stiff Shaft Order Number GS3510 0.035" x 260cm Lot 120518
	QZ 10-30-12

Comments

QZ 10-30-12

Recorded by: JL DT **Date:** 10-30-12

Sidewall Aneurysm Data

Procedure Date: 10-31-12 **Study Protocol:** TIPS-00612 **AUP:** 2011-254

Animal ID: T212 **Species:** Swine **PI:** Miller

Measurements:

Right Side Wall Aneurysm: A N/A mm B N/A mm C 6.22 mm D 7.01 mm measured from 3D image
E N/A mm F N/A mm G N/A mm H 3.92 mm I N/A mm J N/A mm

No Aneurysm ____

Left Side Wall Aneurysm: A N/A mm B N/A mm C N/A mm D N/A mm measured from 3D image
E N/A mm F N/A mm G N/A mm H 3.38 mm I 5.84 mm J 7.20 mm

No Aneurysm ____

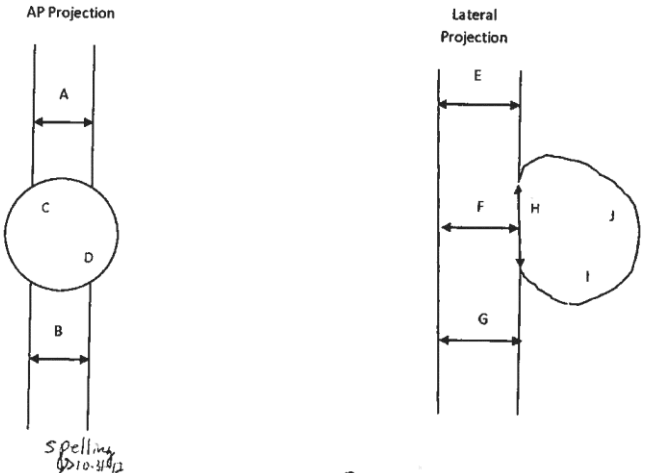

spelling 10-31-12

Comments Left ~~device~~ device = 504 Right device = M11
Right side - little resistance - maybe kink in catheter - contrast injection at 17:00 minutes
Total time = 18 minutes 20 seconds, Left side - little kink in device wire - very
easy to deploy - contrast injection at 13:07 minutes, during removal of wire - foam
really compressed against catheter tip, total time 19 minutes 53 seconds - injected
contrast while removing catheter to ensure foam was not caught

Recorded by: JL DT **Date:** 10.31.12

N/A = Not applicable

Support Article Information

Procedure Date: 10-31-12 **Study Protocol:** TIPS-00C12 **AUP:** 2011-254

Animal ID: T212 **Species:** Swine **PI:** Miller **Weight:** 27.5 kg

Products used:

Product Type	Brand, Size, etc.
Introducer sheath	6 Fr Terumo Pinnacle Ref RSSC01 Lot NC02 6 Fr Terumo Pinnacle Ref RSSC01 Lot NM12
Guide catheter	5F Neuropath - right side 5F Cordis Envoy - left side
Guide wire	Radiofocus Glidewire Catheter Exchange Long Taper Angled Stiff Shaft Order GS3510 0.035" x 260cm Lot 120518

10-31-12

Comments

10-31-12

Recorded by: [illegible] **Date:** 10-31-12

Support Article Information

Procedure Date: 12-12-12 **Study Protocol:** TIPS-00612 **AUP:** 2011-254

Animal ID: T207 **Species:** Swine **PI:** Miller **Weight:** 31.5 Kg

Products used:

Product Type	Brand, Size, etc.
Introducer sheath	Terumo Pinnacle Fr 6 Ref RSS601 Lot PL12
Guide catheter	REF GMC510000-00 LOT C10999 (01)00878628009221 (17)160930(10)C10999 5F 100cm MPC NEUROPATH Guiding Catheter
Guide wire	Radiofocus Glidewire Catheter Exchange Long Taper Angled Order GS3510 Lot 120518 wrong box ~~Guidant~~ QS 12-12-12
Guidewire	Guidant Hi Torque HT FLOPPY® II 0.014" 190 cm REF 22339M LOT 4031052 GUIDANT
Micro catheter	LOT Lot Number ロット番号 5280224 REF Catalogue Number カタログ番号 103102 T-18 Tracker18 by Boston Scientific has only one radiopaque marker so not used REF MCC140000-00 LOT F13409 Concourse™ 14 Microcatheter

↑ 2 radiopaque markers used this microcatheters by Micrus

Comments

Boston → Scientific

LOT 15280625

REF 451102-4 Connecting Cables

~~QS 12-12-12~~

Recorded by: QS **Date:** 12-12-12

Sidewall Aneurysm Data

Procedure Date: 12-12-12 **Study Protocol:** IIS-00612 **AUP:** 2011-254

Animal ID: T207 **Species:** Swine **PI:** Miller

Measurements:

Right Side Wall Aneurysm: A N/A mm B N/A mm C N/A mm D N/A mm

E N/A mm F N/A mm G N/A mm H N/A mm I 4.31 mm J 5.38 mm

No Aneurysm ____

Left Side Wall Aneurysm: A 3.63 mm B 4.04 mm C N/A mm D N/A mm

E N/A mm F 3.48 mm G N/A mm H 2.66 mm I 5.44 mm J ~~5.58~~ 5.58 mm

unclear writing JD 12-12-12

No Aneurysm ____

AP Projection

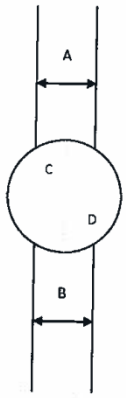

Lateral Projection

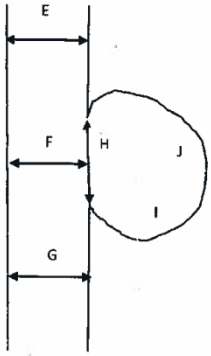

Comments right side is really faint and hard to measure, measured from 3D image

JD 12-12-12

Recorded by: [illegible] **Date:** 12-12-12

N/A = Not applicable

Texas A&M Institute for Preclinical Studies
TEXAS A&M UNIVERSITY

Page 1

Comments

Date: 12-12-12 **Study Protocol:** TIPS-00612 **AUP:** 2011-254 **PI:** Miller

Animal ID: T207 **Species:** Swine **Weight:** 31.5 kg **Sex:** Female

Dr. Miller and Dr Hartman are scrubbed in for deployments

Right side - SII Device number (new batch)

Sheath came off nice and smooth

device out of catheter - no resistance

first actuation at 5:50 on stopwatch - time since first blood touch

angiograms at stopwatch times 13:35 and 14:10

actuation at 16:38 on stopwatch (using additional actuations)

at 18:30 - still room in aneurysm (stopwatch time)

angiogram at 23:45 on stopwatch

deployment time 26:05 on stopwatch

a little foam was left on pusher wire end

Right Second device - 503 Device number (old batch)

measured 2D with first device - 8 mm × 6.5mm aneurysm

first actuation at 5:09 on stopwatch

angiogram at 9:49 on stopwatch

deployment time 13:30 on stopwatch - clock time 1320

angiogram at 14:50 on stopwatch ~~and 16:20 on stopwatch~~ left side angio JD 12-12-12

Left side - GDC devices JD 12-12-12 spelling

note - guide catheter micro has ~~cut~~ only one marker Tracker 18

Switched to Micrus Concourse microcatheter

con't on next page

Recorded by: JD **Date:** 12-12-12

TIPS-117, Rev0, 10/23/12

Texas A&M Institute for Preclinical Studies
TEXAS A&M UNIVERSITY

Comments

Date: 12-12-12 **Study Protocol:** TIPS-00612 **AUP:** 2011-254 **PI:** Miller

Animal ID: T207 **Species:** Swine **Weight:** 31.5 kg **Sex:** Female

1345 - microcatheter in aneurysm (left)

GDC™-18 2D 6mm x 20cm REF 352620-4 LOT 14804658 Detach time 0:06 + 0:38

① GDC™-18 SOFT 4mm x 10cm REF 351410-4 LOT 15279456 Detach time 0:07 + 0:21 ②

① Detached @ 1358 ② Detached @ 1405

GDC™-18 SOFT 2mm x 4cm REF 351204-4 LOT 15260739 Detach time 0:37 ③

③ Detached @ 1412 followed by angiogram

1421 - angiogram of right aneurysm

JS 12-12-12

Recorded by: JS **Date:** 12-12-12

TIPS-117, Rev0, 10/23/12

Support Article Information

Procedure Date: 12-13-12 **Study Protocol:** TIPS-00612 **AUP:** 2011-754

Animal ID: T208 **Species:** Swine **PI:** Miller **Weight:** 28 kg

Products used:

Product Type	Brand, Size, etc.
Introducer sheath	Terumo Pinnacle 6 Fr Order RS601 Lot PL12
Guide catheter	REF GMC610000-00 LOT C10999 (01)00878628009221 (17)160930(10)C10999 5F 100cm, MPC NEUROPATH Guiding Catheter
Guide wire	Radiofocus Glidewire Catheter Exchange Taper Long Order GS3510 Lot 120518
Micro Catheter	REF MCC140000-00 LOT F13409 Concourse™ 14 Microcatheter by Microus
Guide wire	HT WHISPER™ MS 0.014" 190 cm REF 1005357H LOT 5033152 GUIDANT

Comments

Boston → Scientific

LOT 15280625

REF 451102-4 Connecting Cables

12-13-12

Recorded by: JL DST **Date:** 12-13-12

Sidewall Aneurysm Data

Procedure Date: 12-13-17 **Study Protocol:** TIPS-00617 **AUP:** 2011-254

Animal ID: T208 **Species:** Swine **PI:** Miller

Measurements:

Right Side Wall Aneurysm: A N/A mm B N/A mm C N/A mm D N/A mm

E 4.35 3D mm F 2.88 3D mm G 4.02 3D mm H 3.57 3D mm 3.91(2D) I 6.43 2D mm 6.53(3D) J 6.74 2D mm 5.42(3D)

No Aneurysm ____

Left Side Wall Aneurysm: A N/A mm B N/A mm C 6.43 2D mm D 5.72 2D mm

E 3.89 3D mm F 2.34 3D mm G 3.76 3D mm H 2.89 3D mm I 6.29 3D mm J N/A mm

No Aneurysm ____

AP Projection

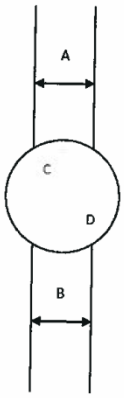

Lateral Projection

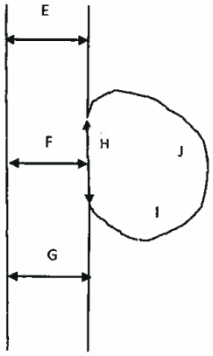

Comments Left side - clot in aneurysm / not completely filling from 3D angio - stroK first set of measurements - unable to get height, measurements also with 2D angio, Right side device = M19, Redid Right 3D angio 12-13-17

Recorded by: [illegible] **Date:** 12-13-17

N/A = Not applicable

Texas A&M Institute for Preclinical Studies
TEXAS A&M UNIVERSITY

Comments

Date: 12-13-12 **Study Protocol:** ~~T208~~ TIPS-00612 (wrong blank QD 12-13-12) **AUP:** 2011-254 **PI:** Miller

Animal ID: T208 **Species:** Swine **Weight:** 28 Kg **Sex:** Female

1107 - 2D angiogram

1112 - 3D angiogram

Left aneurysm - GDC

1135 - microcatheter in aneurysm

① GDC™-10 2D 5mm x 15cm REF 342515-4 LOT 15055098 Detach time 0:27

② GDC™-18 SOFT 4mm x 10cm REF 351410-4 LOT 15279456 Detach time 0:23

① Detached @ 1149

② Detached @ 1157

③ GDC™-10 SOFT 3mm x 6cm REF 341306-4 LOT 13962418 Detach time 0:25 + 0:12

④ GDC™-10 SOFT 3mm x 6cm REF 341306-4 LOT 13962418 Detach time 0:43

③ Detached @ 1201

④ Detached @ 1207

⑤ GDC™-18 SOFT 2mm x 4cm REF 351204-4 LOT 15260739 Detach time 0:32

⑤ Detached @ 1212

1216 - Moving to right side

Notes continued on next page

Recorded by: [signature] **Date:** 12-13-12

TIPS-117, Rev0, 10/23/12

Texas A&M Institute for Preclinical Studies
TEXAS A&M UNIVERSITY

Comments

Date: 12-13-12 **Study Protocol:** TIPS-00612 **AUP:** 2011-254 **PI:** Miller

Animal ID: T 208 **Species:** Swine **Weight:** 28 Kg **Sex:** Female

Right aneurysm

Device M19

1232 - device in catheter

Stopwatch 1:40 - at aneurysm with device

Stopwatch 4:08 - first actuation spelling QD 12-13-12 (power delivery)

~~Stopwatch 9:13 wrong time QD 12-13-12 Spelling QD 12-13-12 Second actuation actuation~~ unclear line - rewritten QD 12-13-12

Stopwatch 9:13 - second actuation

1246 - angiogram

Stopwatch 18:25 - third actuation

1252 - angiogram

Stopwatch 22:50 - fourth actuation

1259 - pulling back pusher wire - little resistance felt

1300 - Stopwatch 27:03 - removed pusher wire from catheter

1301 - angiogram - some foam in parent vessel

1306 - removed guiding catheter

QD 12-13-12

Recorded by: QL JJS **Date:** 12-13-12

TIPS-117, Rev0, 10/23/12

Support Article Information

Procedure Date: 1-28-13 **Study Protocol:** IIPS-00612 **AUP:** 2011-254

Animal ID: T225 **Species:** Swine **PI:** Miller **Weight:** 32.4 kg

Products used:

Product Type	Brand, Size, etc.
Introducer sheath	Terumo Pinnacle 6F Ref RSS601 Lot NM12
Guide catheter	 
Guide wire	Radiofocus Glidewire Order GS3510 Lot 091204 0.035"×260cm
Microcatheter	REF MCC140000-00 LOT F13409 Concourse™ 14 Microcatheter 
Guidewire	0.014"×300cm

Comments Microcatheter used for GDC placement

JL 1-28-13

Recorded by: JL JDS **Date:** 1-28-13

Sidewall Aneurysm Data

Procedure Date: 1-28-13 **Study Protocol:** IIPS-00612 **AUP:** 2011-254

Animal ID: T225 **Species:** Swine **PI:** Miller

Measurements:

Right Side Wall Aneurysm: A 4.50 mm B 4.42 mm C 8.06 mm D 5.21 mm

E 4.71 mm F 2.65 mm G 4.51 mm H 2.88 mm I 7.50 mm J 6.30 mm

All measured from 3D

No Aneurysm ____

Left Side Wall Aneurysm: A N/A mm B N/A mm C 6.07 mm D 4.22 mm

E 4.80 mm F 2.98 mm G 4.59 mm H 2.95 mm I 6.60 mm J 2.39 mm

measured by 3D angio

No Aneurysm ____

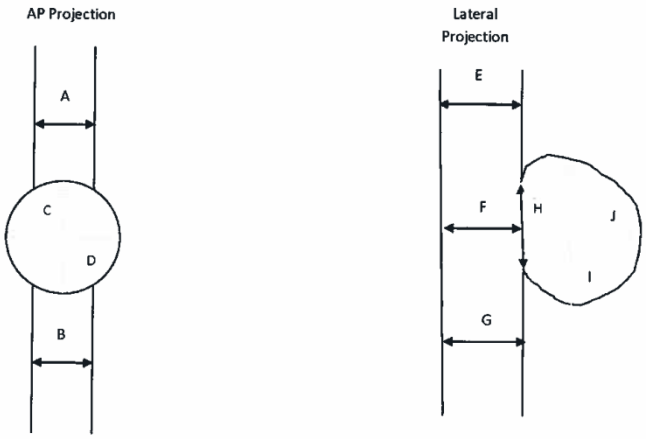

Comments All measurements were made from the 3D angiograms

JD 1-28-13

Recorded by: JD **Date:** 1-28-13

N/A = Not applicable

Texas A&M Institute for Preclinical Studies
TEXAS A&M UNIVERSITY

Comments

Date: 1-28-13 **Study Protocol:** TIPS-00612 **AUP:** 2011-254 **PI:** Miller

Animal ID: T225 **Species:** Swine **Weight:** 32.4 Kg **Sex:** Female

1258- Left aneurysm 3D - didn't fill completely on recreation

Neck = 2.95 Height = 2.39 Width = 6.60

GDC Coils:

Coil #2

② GDC™-10 2D 5mm x 15cm REF 342515-4 LOT 14852024 — 0:26

① GDC™-18 2D 8mm x 30cm REF 352830-4 LOT 14510995 — 2:00 + 1:45 replaced ground needle after both

LOT 15280625
REF 451102-4
Connecting Cables

③ GDC™-18 SOFT 4mm x 10cm REF 351410-4 LOT 15279456 — 0:45 not detached @ 0:13

④ GDC™-18 SOFT 4mm x 10cm REF 351410-4 LOT 15279456 — 0:42 - Complete

1418 Right aneurysm 3D - didn't fully fill on recreation

Device M20 8.51 x 6.94

Unable to get catheter MPD into aneurysm, switched to Mod Cerebral, Switched to MPC

1512 - device in catheter - NOTE - contrast in catheter/aneurysm is making it hard to see device stopwatch 4:06 - starting detachment sequences stopwatch 7:20 - angio stopwatch 7:40 detaching stopwatch 9:09 - angio - the pusher wire popped out 11:33 (Stopwatch) - removed pusher wire stopwatch 12:58 - angio

unclear writing 01-28-13

1528 ~~1528~~ - stopwatch 15:40 - complete

01-28-13

Recorded by: [signature] **Date:** 1-28-13

TIPS-117, Rev0, 10/23/12

Support Article Information

Procedure Date: 1-29-13 **Study Protocol:** TIPS-00612 **AUP:** 2011-254

Animal ID: T226 **Species:** Swine **PI:** Miller **Weight:** 31.5 kg

Products used:

Product Type	Brand, Size, etc.
Introducer sheath	Terumo Pinnacle 6F
Guide catheter	REF GMD610000-00 LOT C11035 (01)00878528009238 (17)151031(10)C11035 6F 100cm MPD NEUROPATH Guiding Catheter
Guide wire	Radiofocus Glidewire Order GR3504 Lot 100311 0.035" x260cm
Micro Catheter	Excelsior™ 1018™ 150cm x 6cm REF 144190 LOT 15278392 Boston Scientific
Guide wire	Cordis AGILITY ™10 614-178 LOT 13064511 +H7396141782K +08031130645111K8

Comments

LOT 15280625

REF 451102-4
Connecting Cables

QD 1-29-13

Recorded by: QD **Date:** 1-29-13

Sidewall Aneurysm Data

Procedure Date: 1-29-13 **Study Protocol:** TIPS-00612 **AUP:** 2011-254

Animal ID: T226 **Species:** Swine **PI:** Miller

Measurements:

Right Side Wall Aneurysm: A 4.56 mm B 4.54 mm C 8.21 mm D N/A mm

E 4.43 mm F 3.35 mm G 4.76 mm H 3.40 mm I 8.07 mm J 4.59 mm

No Aneurysm ____

Left Side Wall Aneurysm: A 3.93 mm B 4.20 mm C 8.17 mm D 5.02 mm

E 3.89 mm F 3.31 mm G 3.94 mm H 4.31 mm I 8.18 mm J 5.99 mm

No Aneurysm ____

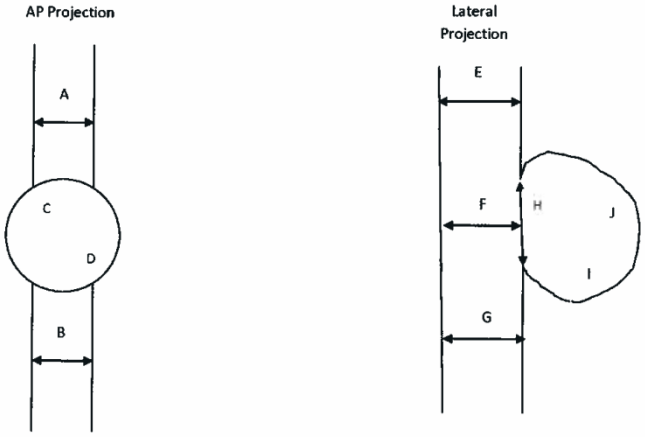

Comments Measurements made from 3D angiograms

RT 1-29-13

Recorded by: RT **Date:** 1-29-13

N/A = Not applicable

Texas A&M Institute for Preclinical Studies
TEXAS A&M UNIVERSITY

Comments

Date: 1-29-13 **Study Protocol:** TIPS-00612 **AUP:** 2011-254 **PI:** Miller

Animal ID: T226 **Species:** Swine **Weight:** 31.5kg **Sex:** Male

1137 - right 3D angiogram - partially filled on reconstruction

Device M12 7.96x 6.28

1147 - device in pig - sliding effortlessly Stopwatch 1:33 - device in aneurysm,

stopwatch 2:27 - detachment series starting

Stopwatch 4:45 - second detachment series starting

1159 - stopwatch 11:24 - releasing device - and 11:56 removed pusher wire

1213 - left 3D angiogram - partially filled on reconstruction

1230 - microcatheter in position in aneurysm

① GDC™-18 2D 8mm x 30cm REF 352830-4 LOT 15326412	② GDC™-10 2D 5mm x 15cm REF 342515-4 LOT 14809412	③ GDC™-18 2D 6mm x 20cm REF 352620-4 LOT 14487357	④ GDC™-10 SOFT 3mm x 6cm REF 341306-4 LOT 13962418
0:23	0:29	0:33	1:22

⑤ GDC™-10 SOFT 2mm x 3cm REF 341203-4 LOT 13855786	⑥ GDC™-10 SOFT 2mm x 3cm REF 341203-4 LOT 13959114
1:31	1:27

1330 - study complete for implanting

QS 1-29-13

Recorded by: QS **Date:** 1-29-13

TIPS-117, Rev0, 10/23/12

Support Article Information

Procedure Date: 2-5-13 **Study Protocol:** TIPS-00612 **AUP:** 2011-254

Animal ID: T228 **Species:** Swine **PI:** Miller **Weight:** 32.0 Kg

Products used:

Product Type	Brand, Size, etc.
Introducer sheath	Terumo Pinnacle 6F Ref R556O1 Lot NM12
Guide catheter	Neuropath - curved tip MPC resterilized
Guide wire	Radiofocus Glidewire Catheter Exchange Order GR3504 Lot 100311
Micro Catheter	Stryker Neurovascular Excelsior 1018 2tip resterilized
Wire	Boston Scientific Forte Guidewire Moderate Support Ref 34949-06 Lot 01975073 .014"x300cm

Comments GDC cables - resterilized

2-5-13

Recorded by: JL TLT **Date:** 2-5-13

Sidewall Aneurysm Data

Procedure Date: 2-5-13 **Study Protocol:** TIPS-00612 **AUP:** 2011-254

Animal ID: T228 **Species:** Swine **PI:** Miller

Measurements:

Right Side Wall Aneurysm: A 4.63 mm B 5.02 mm C 6.95 mm D 6.55 mm

E N/A mm F N/A mm G N/A mm H 4.01 mm I 7.19 mm J 5.67 mm measurement approximate due to not completely filling

No Aneurysm ____

Left Side Wall Aneurysm: A N/A mm B N/A mm C 8.11 mm D 7.18 mm

E 3.28 mm F 3.09 mm G 3.96 mm H 4.83 mm I 8.02 mm J 6.35 mm spelling JD 2-5-13 ~~measurement~~ measurement approximate due to not completely filling

No Aneurysm ____

AP Projection

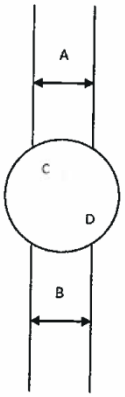

Lateral Projection

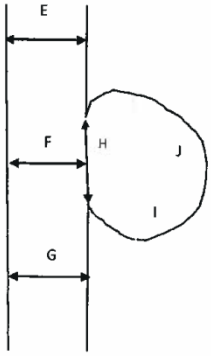

Comments

JD 2-5-13

Recorded by: QL JD **Date:** 2-5-13

N/A = Not applicable

Texas A&M Institute for Preclinical Studies
TEXAS A&M UNIVERSITY

Comments

Date: 2-5-13 **Study Protocol:** TIPS-00612 **AUP:** 2011-254 **PI:** Miller

Animal ID: T228 **Species:** Swine **Weight:** 32.0 Kg **Sex:** Male

Right side angiogram @ 1128

1138 - 3D angiogram - guide catheter in aneurysm

1155 - micro catheter in place in aneurysm

① GDC™-18 2D 6mm x 20cm REF 352620-4 LOT 14804658 — 0:45 detachment time

⑤ GDC™-18 2D 6mm x 20cm REF 352620-4 LOT 14804658 — 0:28

③ GDC™-10 2D 5mm x 15cm REF 342515-4 LOT 14809412 — 0:32

④ GDC™-10 2D 5mm x 15cm REF 342515-4 LOT 14852024 — 0:33

⑤ GDC™-10 SOFT 3mm x 6cm REF 341306-4 LOT 13949248 — 0:33

⑥ GDC™-10 SOFT 3mm x 6cm REF 341306-4 LOT 13962418 — 1:02

⑦ GDC™-10 SOFT 2mm x 3cm REF 341203-4 LOT 13959114 — 0:39

⑧ GDC™-10 SOFT 2mm x 3cm REF 341203-4 LOT 13855786 — 0:46

1242 - right side complete, angiograms

Left side angiogram @ 1247

1251 - 3D angiogram

Device M16 7.43 x 6.27

1300 - guide catheter in aneurysm in place

little ~~bit~~ bit of resistance then went easily spelling ✓ 2-5-13

Stopwatch 1:30 device is out of catheter, stopwatch 2:11 starting detachment

Stopwatch 4:07 - second detachment, stopwatch 11:20 - angiogram

Stopwatch 13:07 - "really want to pull" during detachment - Dr Miller is spinning core to attempt release 13:45 (Stopwatch) - pusher wire out - has foam attached to it

see next page

Recorded by: [signature] **Date:** 2-5-13

TIPS-117, Rev0, 10/23/12

Texas A&M Institute for Preclinical Studies
TEXAS A&M UNIVERSITY

Comments

Date: 2-5-13 **Study Protocol:** TIPS-00612 **AUP:** 2011-254 **PI:** Miller

Animal ID: T228 **Species:** Swine **Weight:** 32.0 Kg **Sex:** Male

1317 - angiogram of polymer in place
do not think able to get catheter and second foam polymer in place
to fill remaining cavity - stopping

QD 2-5-13

Recorded by: QC JDT **Date:** ~~2~~ 2-5-13
wrong month
QD 2-5-13

TIPS-117, Rev0, 10/23/12